USGS
science for a changing world

Prepared in cooperation with San Bernardino Valley Municipal Water District

Yucaipa Valley Integrated Hydrological Model

Chapter B in

Hydrology of the Yucaipa Groundwater Subbasin: Characterization and Integrated Numerical Model, San Bernardino and Riverside Counties, California

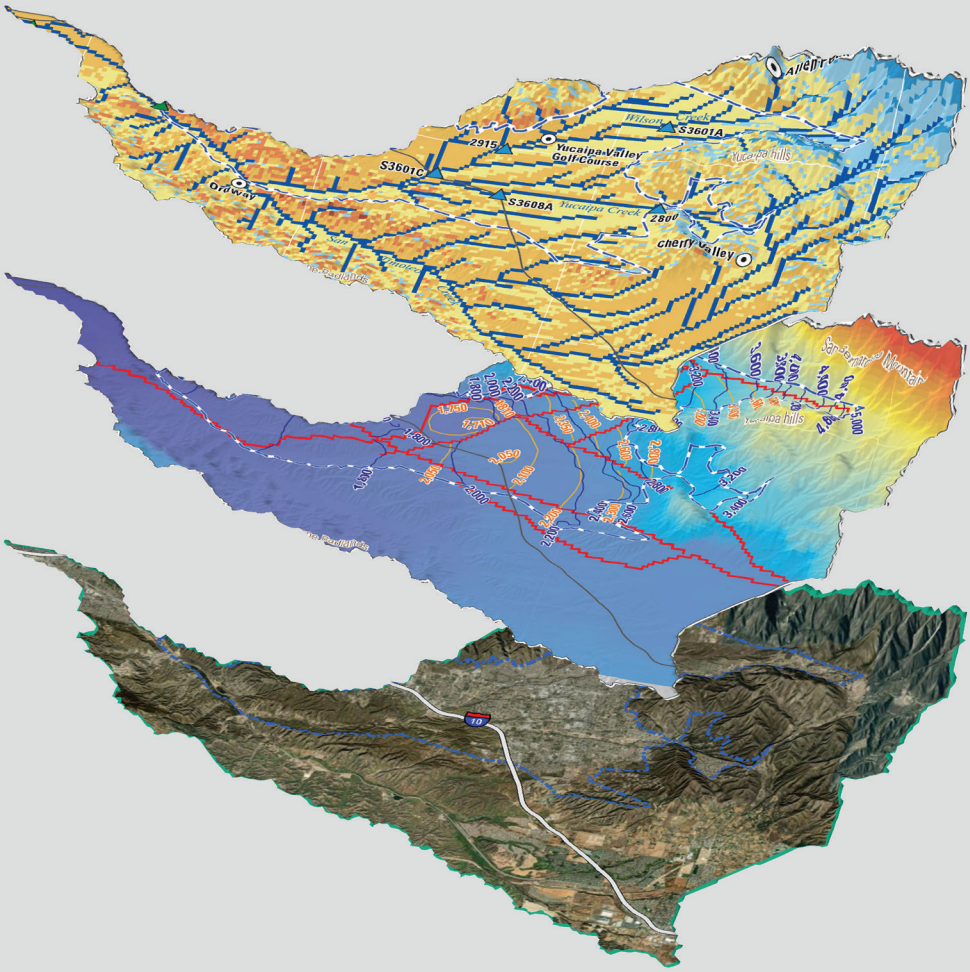

Scientific Investigations Report 2021–5118–B

U.S. Department of the Interior
U.S. Geological Survey

Cover: Visualization of the simulated domain and hydrologic components from the Yucaipa Integrated Hydrologic Model.

Yucaipa Valley Integrated Hydrological Model

By Ayman H. Alzraiee, John A. Engott, Geoffrey Cromwell, and Linda Woolfenden

Chapter B in

Hydrology of the Yucaipa Groundwater Subbasin: Characterization and Integrated Numerical Model, San Bernardino and Riverside Counties, California

Edited by Geoffrey Cromwell and Ayman H. Alzraiee

Prepared in cooperation with San Bernardino Valley Municipal Water District

Scientific Investigations Report 2021–5118-B

U.S. Geological Survey, Reston, Virginia: 2022

For more information on the USGS—the Federal source for science about the Earth, its natural and living resources, natural hazards, and the environment—visit https://www.usgs.gov or call 1–888–ASK–USGS.

For an overview of USGS information products, including maps, imagery, and publications, visit https://store.usgs.gov/.

Suggested citation:
Alzraiee, A.H., Engott, J.A., Cromwell, G., and Woolfenden, L., 2022, Yucaipa valley integrated hydrological model, chap. B *in* Cromwell, G., and Alzraiee, A.H., eds., Hydrology of the Yucaipa groundwater subbasin—Characterization and integrated numerical model, San Bernardino and Riverside Counties, California: U.S. Geological Survey Scientific Investigations Report 2021–5118-B, 76 p., https://doi.org/10.3133/sir20215118B.

Associated data for this publication:
Alzraiee, A.H., Cromwell, G., and Engott, J.A., 2022, GSFLOW model to evaluate the effect of groundwater pumpage and climate stresses on the integrated hydrologic system of the Yucaipa subbasin, Yucaipa Valley watershed, San Bernardino and Riverside Counties, California: U.S. Geological Survey data release, https://doi.org/10.5066/P9K540DV.

ISSN 2328-0328 (online)

Acknowledgments

The authors thank the San Bernardino Valley Municipal Water District for their cooperation on this project, including providing funding, expertise, and logistical support for data compilation and analysis. We also thank the respective staffs of the South Mesa Water Company, Western Heights Water Company, and the Yucaipa Valley Water District for providing hydrologic data and for their local and historical expertise about the area.

The authors thank U.S. Geological Survey colleagues for assistance in data compilation, analysis, and support, including: Claudia Faunt, Wes Danskin, Whitney Seymour, Jon Matti, Daniel Culling, Milissa Peterson, Sarah Roberts, and Lindsay Ellingson.

Contents

Figures

Tables

Conversion Factors

U.S. customary units to International System of Units

Multiply	By	To obtain
	Length	
inch (in.)	2.54	centimeter (cm)
inch (in.)	25.4	millimeter (mm)
foot (ft)	0.3048	meter (m)
mile (mi)	1.609	kilometer (km)
	Area	
Acre	4,047	square meter (m^2)
Acre	0.4047	hectare (ha)
Acre	0.4047	square hectometer (hm^2)
Acre	0.004047	square kilometer (km^2)
square mile (mi^2)	259.0	hectare (ha)
square mile (mi^2)	2.590	square kilometer (km^2)
	Volume	
cubic foot (ft^3)	28.32	cubic decimeter (dm^3)
cubic foot (ft^3)	0.02832	cubic meter (m^3)
acre-foot (acre-ft)	1,233	cubic meter (m^3)
acre-foot (acre-ft)	0.001233	cubic hectometer (hm^3)
	Flow rate	
acre-foot per year (acre-ft/yr)	1,233	cubic meter per year (m^3/yr)
acre-foot per year (acre-ft/yr)	0.001233	cubic hectometer per year (hm^3/yr)
foot per day (ft/d)	0.3048	meter per day (m/d)
inch per year (in/yr)	25.4	millimeter per year (mm/yr)
	Hydraulic conductivity	
foot per day (ft/d)	0.3048	meter per day (m/d)

International System of Units to U.S. customary units

Multiply	By	To obtain
	Length	
meter (m)	3.281	foot (ft)
kilometer (km)	0.6214	mile (mi)
kilometer (km)	0.5400	mile, nautical (nmi)
meter (m)	1.094	yard (yd)

Temperature in degrees Celsius (°C) may be converted to degrees Fahrenheit (°F) as follows:

$$°F = (1.8 \times °C) + 32.$$

Temperature in degrees Fahrenheit (°F) may be converted to degrees Celsius (°C) as follows:

$$°C = (°F - 32) / 1.8.$$

Datum

Vertical coordinate information is referenced to the North American Vertical Datum of 1988 (NAVD 88).

Horizontal coordinate information is referenced to the North American Datum of 1983 (NAD 83).

Elevation, as used in this report, refers to distance above the vertical datum.

Abbreviations

asl	above sea level
bls	below land surface
CIMIS	California Irrigation Management Irrigation System
CRT	Cascade Routing Tool
DEM	digital elevation model
ES	Ensemble Smoother
ET	evapotranspiration
GHB	general head boundary
GIRAS	Geographic Information Retrieval and Analysis System
GSFLOW	Groundwater and Surface-water FLOW model
HK	horizontal hydraulic conductivity
HRU	hydrologic response units
LANDFIRE	Landscape Fire and Resource Management Planning Tools
MAE	mean absolute error
MAR	Managed Aquifer Recharge

MODFLOW-NWT	Newton-Raphson formulation of the Modular Groundwater-Flow Model
NHD	National Hydrography Dataset
NLCD	National Land Cover Database
PEST	Parameter ESTimation
PET	potential evapotranspiration
PRISM	Parameter-Elevation Regressions on Independent Slopes Model
PRMS	Precipitation-Runoff Modeling System
RMSE	root mean square error
SBCFCD	San Bernardino County Flood Control District
SMWC	South Mesa Water Company
Ss	Specific storage
SSURGO	Soil Survey Geographic database
SURFK	surface conductivity
Sy	Specific yield
USGS	U.S. Geological Survey
UZ	unsaturated zone
VK	vertical hydraulic conductivity
VKS	unsaturated zone vertical hydraulic conductivity
WHWC	Western Heights Water Company
YIHM	Yucaipa Integrated Hydrologic Model
YVW	Yucaipa Valley watershed
YVWD	Yucaipa Valley Water District

Yucaipa Valley Integrated Hydrological Model

By Ayman H. Alzraiee, John A. Engott, Geoffrey Cromwell, and Linda Woolfenden

Introduction

The hydrologic system in the Yucaipa Valley watershed (YVW) was simulated using the coupled Groundwater and Surface-water FLOW model (GSFLOW; Markstrom and others, 2008). This study uses version 2.0 of GSFLOW, which is a combination of the Precipitation-Runoff Modeling System (PRMS; Markstrom and others, 2015), and the Newton-Raphson formulation of the Modular Groundwater-Flow Model (MODFLOW-NWT; hereafter referred to as MODFLOW; Harbaugh, 2005; Niswonger and others, 2011).

GSFLOW partitions the hydrologic system into three regions (fig. B1) that are linked by the exchange of unsaturated and saturated groundwater and surface water. The properties and processes within each region influence the flow of both groundwater and surface water into, out of, and within each region. The PRMS component of GSFLOW simulates Region 1, and the MODFLOW component simulates Regions 2 and 3. In the YVW, GSFLOW was applied as the simulation code and is referred to herein as the Yucaipa Integrated Hydrologic Model (YIHM; Alzraiee and others, 2022). In the YIHM, Region 1 includes the plant canopy, snowpack, and the soil zone; Region 2 includes the stream network; and Region 3 includes the subsurface beneath Regions 1 and 2 and consists of both the saturated and unsaturated zones. Soil-moisture conditions and head relations control the flow of both groundwater and surface water between regions. The maximum lateral extents of Regions 1 and 3 were defined using the surface-water drainage divides described in the "Description of Study Area" section of chapter A of this report. The boundaries for Region 2 are the lowest elevation of the streambeds, the stream channel widths, and the horizontal extent of the stream channels in the YVW. Flow across the unsaturated part of Region 3 is assumed to be vertical and does not cross the lateral boundary.

To simulate hydrologic processes occurring within the YVW using GSFLOW, a model domain was defined to match the surface watershed such that the domain includes each surficial hydrologic unit coinciding (at least partially) with the Yucaipa groundwater subbasin (hereafter referred to as "Yucaipa subbasin") as defined in California Bulletin 118 (California Department of Water Resources, 2016). The resulting simulated domain (fig. B2) includes the Yucaipa subbasin and intersects partially with parts of the San Bernardino and San Timoteo groundwater subbasins (fig. B2). The area of the active model domain in YIHM is about 121 square miles (mi^2). The developed YIHM can be used to improve understanding of the hydrologic processes in YVW and to simulate future management scenarios with different climatic and anthropogenic changes.

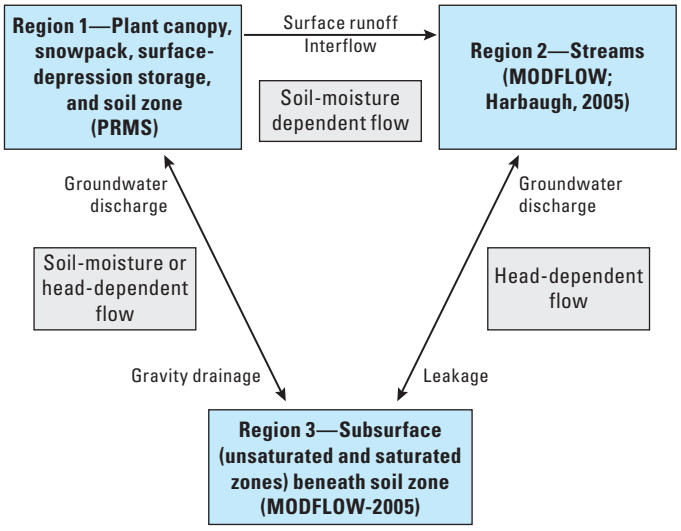

Figure B1. Conceptual diagram of the hydrologic system regions in Yucaipa Integrated Hydrologic Model that is simulated by Precipitation-Runoff Modeling System (PRMS; Markstrom and others, 2015) and MODFLOW (Harbaugh, 2005); Yucaipa Valley watershed, San Bernardino and Riverside Counties, California. Figure modified from Markstrom and others (2008).

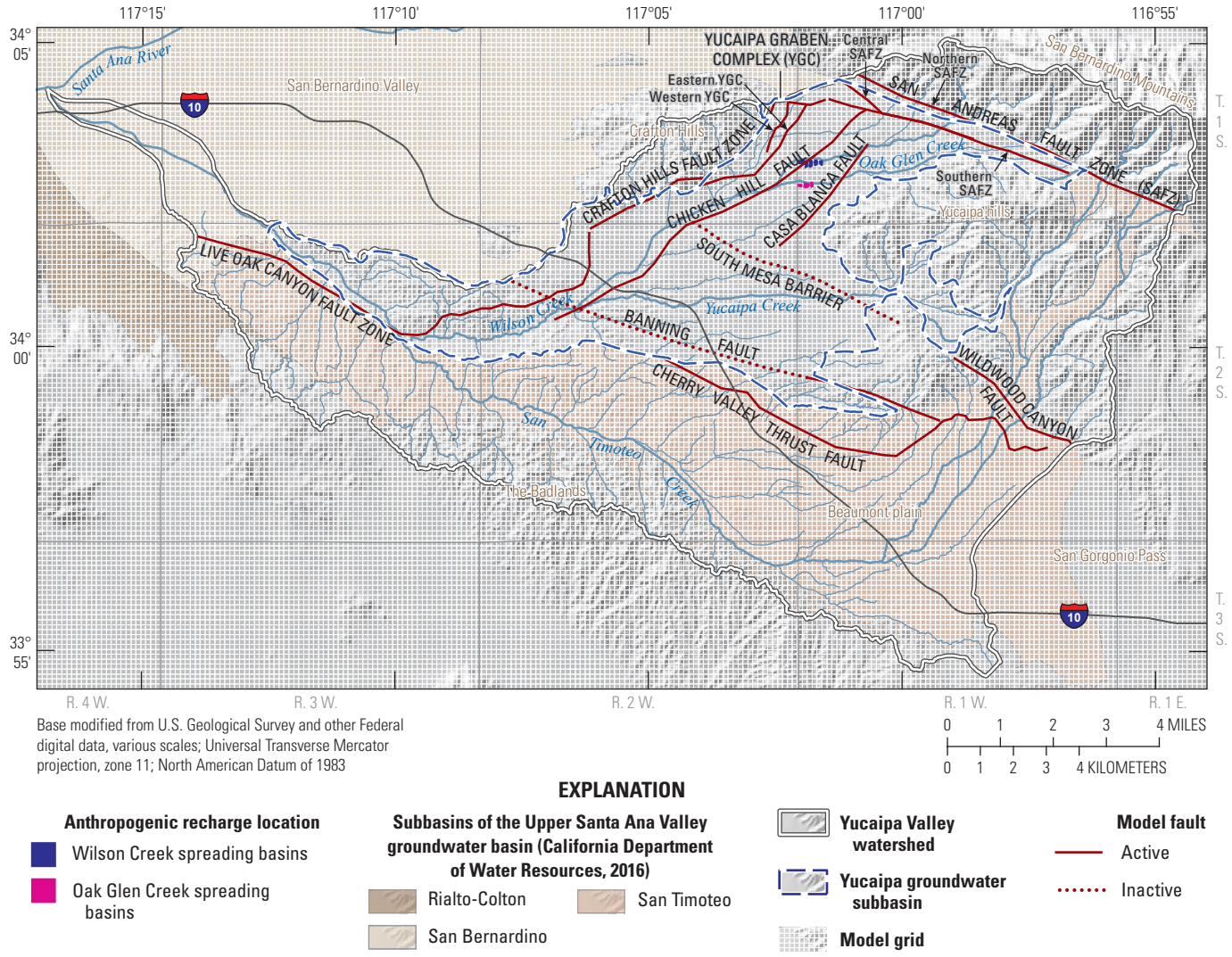

Figure B2. Yucaipa Hydrologic Integrated Model grid, Yucaipa groundwater subbasin, and adjacent San Timoteo, San Bernardino and Rialto-Colton groundwater subbasins, Yucaipa Valley watershed, San Bernardino and Riverside Counties, California.

Model Discretization

Application of GSFLOW to simulate water movement in surface-water and groundwater systems in the YVW requires the discretization of the model domain into smaller units. Climate and physical properties of the YVW are represented as being homogeneous within each discretized unit but are allowed to vary among discretized units. A gridded discretization approach was used for the YIHM, and the horizontal grid layout defining the PRMS discretized units is identical to the horizontal discretized units used to define model cells for MODFLOW. The discretized units are referred to as hydrologic response units (HRUs). Matching the PRMS HRU layout to the MODFLOW cell layout simplifies the connection between PRMS and MODFLOW, reduces the likelihood of water budget errors that can occur when mapping and intersection irregular HRUs with a MODFLOW grid, and allows for consistent parameterization between HRUs and MODFLOW cells with a more efficient and precise compilation of simulation results.

The YIHM was developed using a rectilinear grid with uniform grid spacing (fig. B2). The grid-cell size is about 492 feet (ft) by 492 ft with a total of 134 rows and 237 columns. There are 14,012 active HRUs in the PRMS model; these HRUs cover the entire area of the Yucaipa Valley watershed and overlie the uppermost active layer in the MODFLOW model. In the MODFLOW model, there are 32,084 active model cells in four layers, with 11,862 active cells in layer 1; 7,060 active cells in layer 2; 7,060 active cells in layer 3; and 6,102 active cells in layer 4.

The vertical discretization of the YIHM is based on the three-dimensional hydrogeologic framework model of the YVW (Cromwell and Matti, 2022). The elevation of the top of the uppermost active layers (layers 1 and 4) is the ground-surface elevation above the North American Vertical Datum of 1988 (NAVD 88). Model layer 1 represents primarily the surficial materials and the upper portion of the unconsolidated sediment unit, with some parts of the layer representing crystalline basement. The thickness of model layer 1 ranges from about 40 to 2,000 ft (fig. B3). Model layers 2 and 3 represent the middle and lower parts of the unconsolidated sediment unit, respectively. The thickness of model layer 2 ranges from about 16 to 360 ft, and the thickness of model layer 3 ranges from about 16 to 1,370 ft (fig. B3). Model layer 4 mostly represents the consolidated sedimentary materials unit, and ranges in thickness from about 100 to 1,970 ft (fig. B3). Crystalline basement underlies the active model layers and for the most part is not considered part of the groundwater-flow system because it likely does not contain large quantities of groundwater as a result of the relatively small hydraulic conductivity and porosity of the rock relative to overlying sedimentary aquifer materials (Cromwell and Matti, 2022). Model layer 1 and the southern part of layer 4 are simulated as an unconfined aquifer, and model layers 2, 3, and the northern part of model layer 4 are simulated as a confined or an unconfined aquifer (convertible aquifers).

The YIHM is a transient model that simulates hydrologic conditions for the period of January 1947 through December 2014. The temporal discretization of the YIHM model is daily time steps with monthly stress periods. GSFLOW requires 1-day time steps to synchronize with the PRMS model and to better simulate dynamic groundwater and surface-water interactions with MODFLOW. This temporal discretization results in 816 stress periods and 24,836 time steps. Within each monthly stress period, groundwater boundary conditions and hydraulic stresses, including groundwater pumping and anthropogenic recharge, are temporally invariant. The monthly stress periods are used to simulate the seasonal changes in water use; the daily time steps are used to simulate climate stresses that include precipitation, evapotranspiration, runoff, and recharge, as well as groundwater and surface-water interactions along active stream channels.

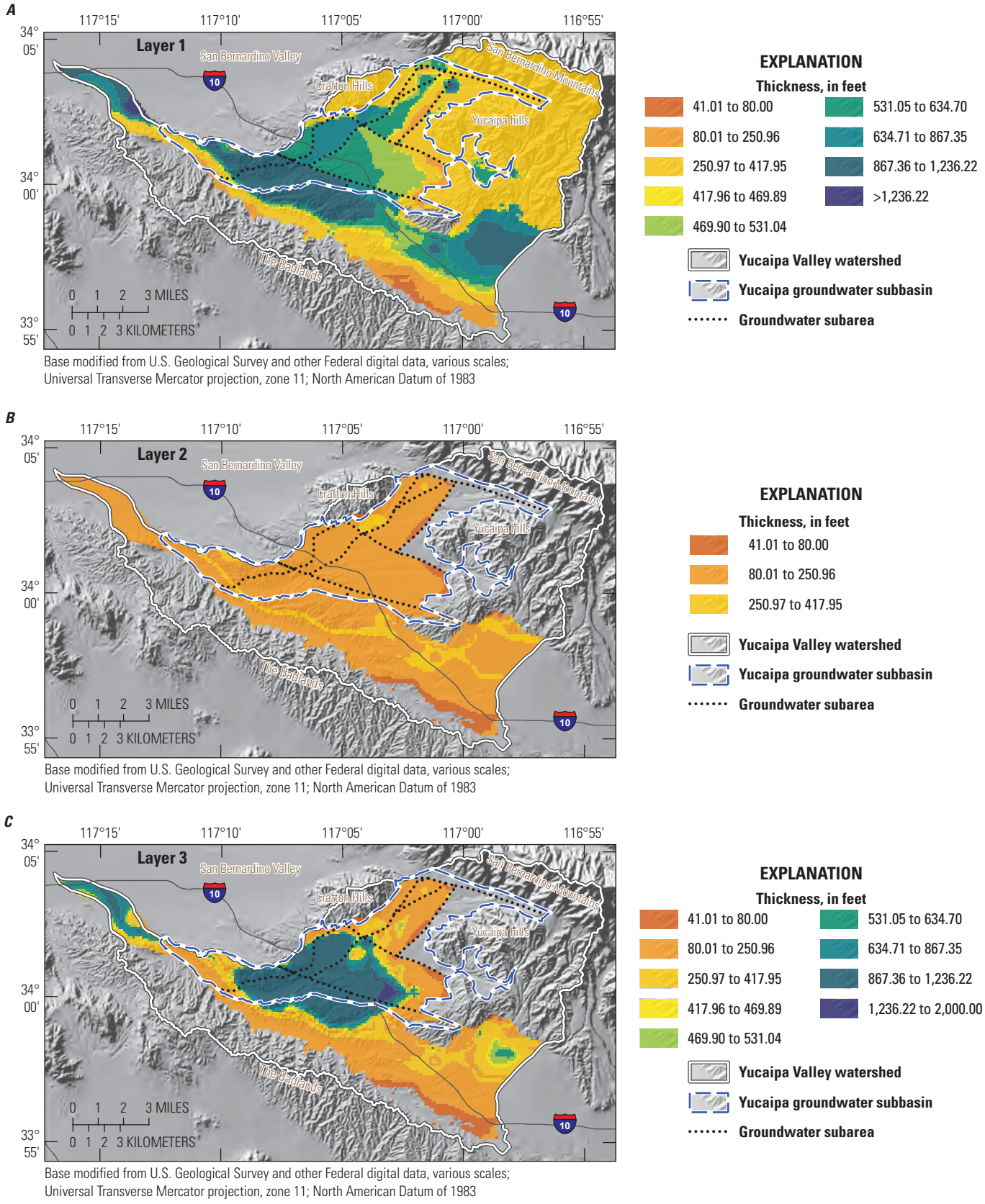

Figure B3. Thickness and extent of the Yucaipa Integrated Hydrologic Model layers, Yucaipa Valley watershed, San Bernardino and Riverside Counties, California. Panels A, B, C, and D show the thicknesses of layers 1, 2, 3, and 4; respectively.

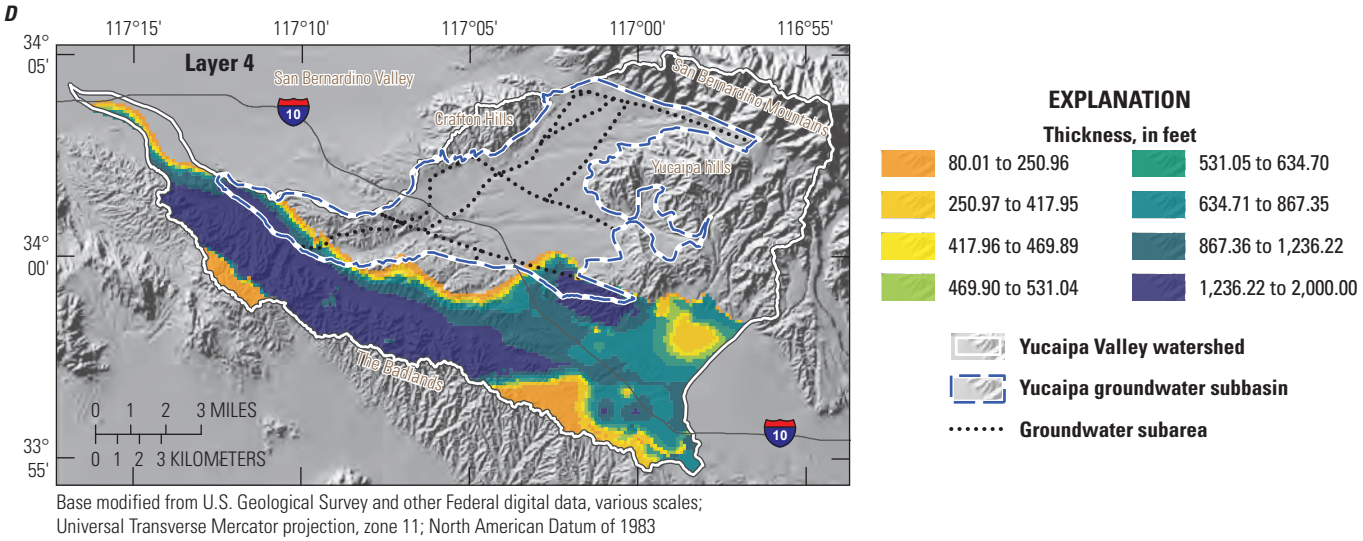

Base modified from U.S. Geological Survey and other Federal digital data, various scales; Universal Transverse Mercator projection, zone 11; North American Datum of 1983

Figure B3.—Continued

Initial Conditions

The initial conditions of the YIHM define the starting hydrological states of the model including (1) hydraulic heads in streams and groundwater, (2) moisture contents in the soil zone and underlying unsaturated zone, (3) water stored in stream channels, (4) water stored in the snowpack, and (5) water stored on vegetation canopy. Initial conditions for the groundwater model are estimated using a steady-state version of the MODFLOW model. Available data were insufficient for characterizing the predevelopment hydrologic states (for example, natural groundwater table elevations before the start of pumping and before land-use changes); therefore, the steady-state model was developed to represent the average hydrologic states during the period 1947–69. Steady-state groundwater stresses include average groundwater pumping during period 1947–69 and average recharge that is estimated via calibration as a fraction of the 30-year precipitation normal derived from the Parameter-Estimation Regressions on Independent Slopes Model (PRISM; PRISM Climate Group, 2013). The steady-state model was calibrated using average hydraulic heads data collected during the period 1947–69. In the transient and integrated model, the period from 1947 to 1969 was treated as a model initialization (spin-up) period to reduce uncertainties associated with the estimated initial conditions and to allow the YIHM to stabilize; the period 1970–2014 was simulated as the calibration period.

Precipitation-Runoff Modeling System Model Description

GSFLOW can simulate hydrologic flows using three different modes: PRMS-only, MODFLOW-only, or integrated simulations that include PRMS and MODFLOW. The PRMS is often run independently of MODFLOW as part of the initial calibration process because PRMS runs more efficiently than MODFLOW. The PRMS is a deterministic, distributed-parameter model that computes energy and water balances based on the climate, physical characteristics, and processes within a watershed. The watershed is conceptualized as a series of interconnected reservoirs that include the plant canopy, snowpack, impervious surfaces, soil zone, and streams (fig. B4). The PRMS includes a reservoir used to represent groundwater for PRMS-only simulations. Flow between and storage within these reservoirs is computed on a daily time step.

The climatologic, hydrologic, and physical characteristics distributed to the HRUs are land-surface elevation, slope, aspect, flow direction, precipitation, air temperature, land use, soil properties, surficial geology, vegetation type, and vegetation cover. Daily minimum and maximum air temperature and precipitation were used to simulate the following hydrologic responses in a watershed: potential evapotranspiration (PET), snow accumulation, snow melt, sublimation, actual evapotranspiration (ET), streamflow (surface runoff, interflow and base flow for decoupled PRMS), soil-moisture storage, and percolation through the root zone (groundwater recharge for decoupled PRMS model). A complete description of PRMS is available in Markstrom and others (2015), with subsequent updates to the model described in Regan and LaFontaine (2017). The following

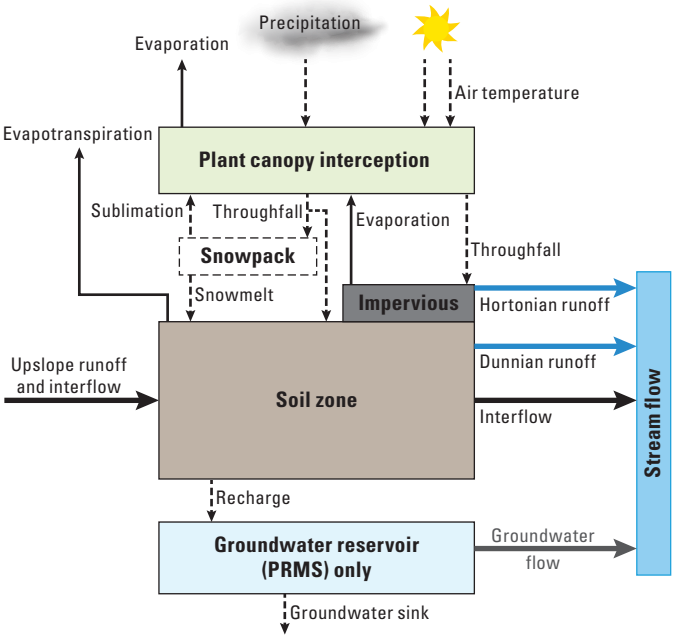

Figure B4. Conceptual diagram of the Precipitation-Runoff Modeling System (PRMS) model, including climate inputs, watershed components, and flow paths (modified from Markstrom and others, 2008). In Groundwater and Surface-water FLOW model mode, the groundwater reservoir is simulated by MODFLOW.

sections describe some of the key PRMS parameters for land-surface characteristics, land use, soils, topography and streams, and climate.

Land-Surface Characteristics

The PRMS parameters that describe land-surface characteristics were developed using the Gsflow-ArcPy Toolkit (Gardner and others, 2018) with geospatial datasets that include the National Elevation Dataset (NED) 10-meter (m) digital elevation model (DEM; U.S. Geological Survey, 2016), soil maps from the Soil Survey Geographic database (SSURGO; U.S. Department of Agriculture, 2016), a percent impervious map from the National Land Cover Database (NLCD; Vogelmann and others, 2001), and land-use maps from the Geographic Information and Analysis System (GIRAS; Mitchell and others, 1977), NLCD, and Landscape Fire and Resource Planning Tools (LANDFIRE; LANDFIRE, 2001, 2014) programs (Land-use maps and an analysis of changes in land-use through time are presented in chapter A). Initial PRMS parameter values were developed from geospatial datasets unique to this study; these values, along with default values, are listed in table B1. A full description of PRMS parameters and default parameter values are provided in Markstrom and others (2015).

Land Use

Lists of the 140 LANDFIRE vegetation codes (LANDFIRE, 2014) corresponding to PRMS parameters were developed by Gardner and others (2018) and used to reassign LANDFIRE codes for each land-use period (see the "Land-Use" section in chapter A) to the vegetation codes supported by PRMS. The HRU-specific parameters derived from the LANDFIRE codes were vegetation cover type (*cov_type*), summer and winter cover density (*covden_sum* and *covden_win*, respectively), snow interception (*snow_intcp*), summer and winter rain interception (*srain_intcp* and *wrain_intcp,* respectively), root depth, and short-wave radiation transmission coefficient (*rad_trncf*) through winter vegetation. For vegetation cover type (0=bare, 1=grass, 2=shrub, 3=trees), the predominant cover type within an HRU was assigned to that HRU. For the other vegetation-based parameters listed above, each HRU was assigned the area-weighted mean computed for the vegetation codes occurring within that HRU. For example, if 20 percent of the area of an HRU consisted of pasture and hay (*covden_sum* = 0.80) and the remaining 80 percent of the area consisted of low-intensity developed land cover (*covden_sum* = 0.10), then the value for *covden_sum* used for that HRU would be (0.20×0.80) + (0.80×0.10) = 0.24. Impervious land cover was held constant for the entire model simulation period, derived from the NLCD percent developed impervious map (Xian and others, 2011), and used to populate the PRMS *hru_percent_imperv* parameter for each active HRU.

Soils

The SSURGO database was used as input to Gsflow_ArcPy scripts to develop PRMS parameters that are based on soil properties. Soil texture (percent sand, clay, and silt), available water capacity, saturated hydraulic conductivity, and soil depth for each HRU were used to compute PRMS soil-zone parameters affecting storage, interflow, gravity drainage, and runoff. The PRMS parameter *soil_type* (1 = sand, 2 = loam, and 3 = clay) was assigned based on the predominant soil texture for each HRU. Initial values for other soil-zone parameters, including *soil_moist_max*, *soil_rechr_max*, *soil2gw_max*, and *slowcoef_lin*, were computed for each HRU using available water capacity, soil depth, slope, and porosity data from the SSURGO database and the Gsflow_ArcPy Toolkit (Gardner and others, 2018). These parameter values were adjusted during calibration of the YIHM using a scaling approach that preserved the relative spatial variabilities of each parameter.

Table B1. Initial Precipitation-Runoff Modeling System (PRMS; Markstrom and others, 2015) model parameter values determined from geospatial data, or otherwise not at default values, Yucaipa Valley watershed, San Bernardino and Riverside Counties, California.

Parameter[1]	Dimension	Minimum	Maximum	Units
fastcoef_lin	one	0.001	0.001	fraction/day
fastcoef_sq	one	0.001	0.001	none
gwstor_init	one	0.1	0.1	inches
hru_area	one	5.56	5.56	acres
imperv_stor_max	one	0.0	0.0	inches
melt_force	one	90	90	Julian day
potet_sublim	one	0.75	0.75	decimal fraction
pref_flow_den	one	0.2	0.2	decimal fraction
smidx_coef	one	0.001	0.001	decimal fraction
snarea_thresh	one	0	0	inches
slowcoef_sq	one	0.001	0.001	none
carea_max	nhru	0.05	1.0	decimal fraction
cov_type	nhru	0	4	none
covden_sum	nhru	0	0.85	decimal fraction
covden_win	nhru	0	0.78	decimal fraction
hru_aspect	nhru	0	315	angular degrees
hru_elev	nhru	301	2672	meters
hru_lat	nhru	34	34	angular degrees
hru_percent_imperv	nhru	0	0.95	decimal fraction
hru_psta	nhru	1	1	none
hru_slope	nhru	0	1.24	decimal fraction
hru_subbasin	nhru	0	8	none
hru_tlaps	nhru	2	4	none
hru_tsta	nhru	1	3	none
hru_type	nhru	0	1	none
jh_coef_hru	nhru	17	24	per degrees Fahrenheit
rad_trncf	nhru	0.21	0.99	decimal fraction
sat_threshold[2]	nhru	0	4.42	inches
slowcoef_lin	nhru	0	0.001	fraction/day
snow_intcp	nhru	0	0.04	inches
soil_moist_init_frac	nhru	0	1.000	decimal fraction
soil_moist_max[2]	nhru	0	4.92	inches
soil_rechr_init_frac	nhru	0	1.0	decimal fraction
soil_rechr_max_frac[2]	nhru	1.0	1.0	decimal fraction
soil_type	nhru	1	2	none
soil2gw_max[2]	nhru	2.76	2.76	inches
srain_intcp	nhru	0	0.04	inches
ssr2gw_rate[2]	nhru	0.40	168	fraction/day
tmax_adj	nhru	–1.8	1.8	degrees Celsius
tmin_adj	nhru	–1.8	1.8	degrees Celsius
wrain_intcp	nhru	0	0.04	inches
dday_intcp[2]	nmonths	–2.12	–1.95	degree day

Table B1. Initial Precipitation-Runoff Modeling System (PRMS; Markstrom and others, 2015) model parameter values determined from geospatial data, or otherwise not at default values, Yucaipa Valley watershed, San Bernardino and Riverside Counties, California.—Continued

Parameter[1]	Dimension	Minimum	Maximum	Units
dday_slope[2]	nmonths	0.28	0.44	degree day/degree Celsius
jh_coef[2]	nmonths	0.0104	0.0128	per degrees Fahrenheit
tmax_index	nmonths	16	34	degrees Celsius
rain_adj[2]	nmonths by nhru	0.64	8.33	decimal fraction
snow_adj	nmonths by nhru	0.64	8.3	decimal fraction
tsta_elev	ntemp	402	2,671	meters

[1]Parameter definitions can be found in Markstrom and others (2015).

[2]Parameters modified during the calibration of GSFLOW.

Topography and Stream Network

The mean elevation (*hru_elev*), mean aspect (*hru_aspect*), mean slope (*hru_slope*), and latitude of the centroid (*hru_lat*) were derived for each HRU from the 10-m DEM geospatial layer using the Gsflow_ArcPy Toolkit (Gardner and others, 2018). Except for *hru_lat*, these parameters were adjusted during the creation of the discretized stream network to ensure that individual stream segments in the model followed the natural-flow direction of the streams. Adjustment of the topographic parameters was an iterative process that required manual adjustment of HRU elevations, subsequent execution of the Cascade Routing Tool (CRT; Henson and others, 2013), and comparison of the generated stream network with streams from the NHD (National Hydrography Dataset) and satellite imagery from Google Earth (imagery date December 2018; Google, Maxar Technologies 2021).

During the initial stream network creation and revision process, two Gsflow_ArcPy parameters used to generate stream segments (flow-accumulation threshold and flow-length threshold) were also adjusted. The flow-accumulation threshold is the minimum number of upgradient cells required for water to flow to a particular cell for that cell to be designated a stream segment. The flow-length threshold is the minimum length (in number of cells) for all first order streams. The final values used for flow-accumulation threshold and flow-length threshold in CRT were 30 and 3, respectively. Figure B5 shows the final stream network used in the YIHM. Non-channelized overland flow was simulated using the *Srunoff* module. The CRT provides the direction of routing for all HRUs in the watershed, including many-to-many routing from HRU to HRU, and the *Srunoff* module routes overland flow along these pre-specified routing directions when overland flow is generated on an HRU during a simulation.

A major limitation of decoupled PRMS-only simulations is that once cascading flows are collected in the stream segments, flows cannot subsequently infiltrate to groundwater and are instead routed directly to the end of each segment; ultimately, all water collected in stream channels is discharged from the model domain. In other words, once flow reaches a stream segment, it accumulates (increases) as it moves downstream and neglects stream seepage losses to groundwater. The runoff computed by PRMS approximates the quantity of runoff that originates from the respective drainage areas and does not consider losses that occur as water moves through ephemeral channels (Allander and others, 2014). Accordingly, following initial PRMS-only calibration, additional calibration of PRMS parameters is often required during integrated simulations that represent both gaining and losing stream seepage conditions.

Precipitation and Air Temperature

Climate inputs to the PRMS model in the YIHM consisted of daily values of precipitation and minimum and maximum temperature (T_{min} and T_{max}, respectively) for the model simulation period 1947–2014. Precipitation data were distributed to each HRU using the PRMS precip_1sta module (Markstrom and others, 2015). The rain adjustment parameter (*rain_adj*) accounts for spatial variation in rainfall resulting from elevation and other factors and was computed as the ratio of mean monthly precipitation at the centroid of each HRU from PRISM (PRISM Climate Group, 2013) to the mean monthly precipitation calculated from measurements made at climate station 47306 Redlands (fig. B6) and supplemented with measurements made at climate stations 40609 Beaumont #2 and 50002 Beaumont (see chapter A for a description of the measured data and analysis).

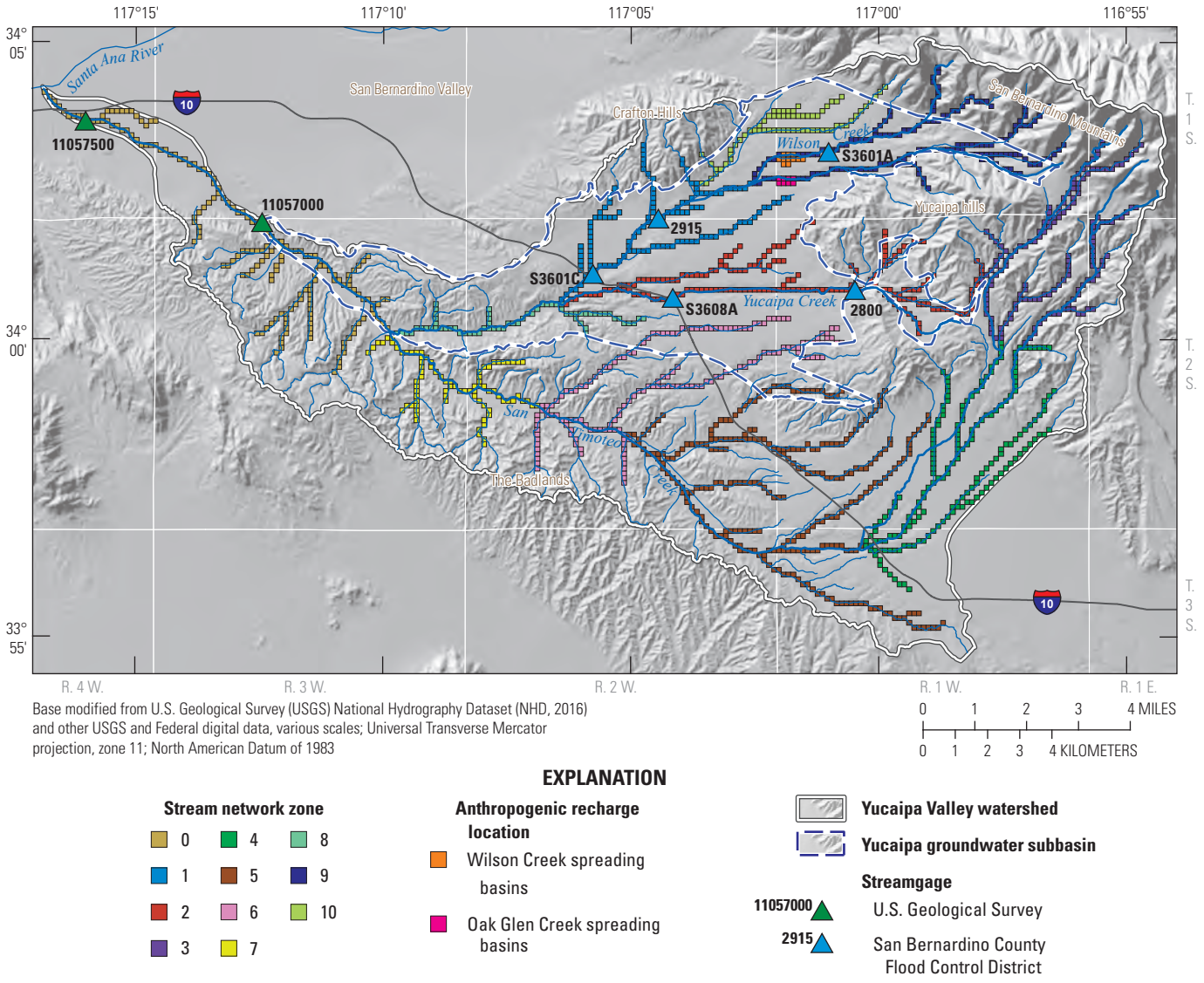

Figure B5. Discretized stream network, stream-segment groupings, and streamgage locations. Streams from National Hydrologic Dataset (NHD) are shown for reference, and the thick solid blue lines represent streams in the Yucaipa Integrated Hydrologic Model, Yucaipa Valley watershed, San Bernardino and Riverside Counties, California.

Temperature data were distributed to each HRU using the PRMS *temp_laps* module (Markstrom and others, 2015), which uses temperature data from multiple stations at different elevations. However, measured data from climate stations at different elevations were not available in the YVW; therefore, three virtual climate stations at elevations of 3,281, 5,906, and 8,763 ft were created. The elevations of the two lower virtual stations (3,281 and 5,906 ft) were chosen because they correspond generally to inflection points in the plots of mean monthly T_{min} (PRISM Climate Group, 2013) versus elevation (figs. B7, B8); the elevation of the highest virtual station (8,763 ft) was chosen because it corresponds to the centroid elevation of the highest HRU in the active model area.

Gridded mean monthly T_{min} data (PRISM Climate Group, 2013) were used to develop three linear regressions for T_{min} versus elevation for each calendar month to estimate daily T_{min} at each virtual station (table B2; Alzraiee and others, 2022). The first regression used data for all HRUs with centroid elevations between the elevation of the 47306 Redlands climate station (1,318 ft; fig. B6) and the lowest virtual climate station (3,281 ft). The second regression used data for all HRUs with centroid elevations between the elevation of the lowest virtual station (3,281 ft) and the second-highest virtual station (5,906 ft). The third regression used data for all HRUs with centroid elevations between the second-highest virtual station (5,906 ft) and the highest virtual station (8,763 ft).

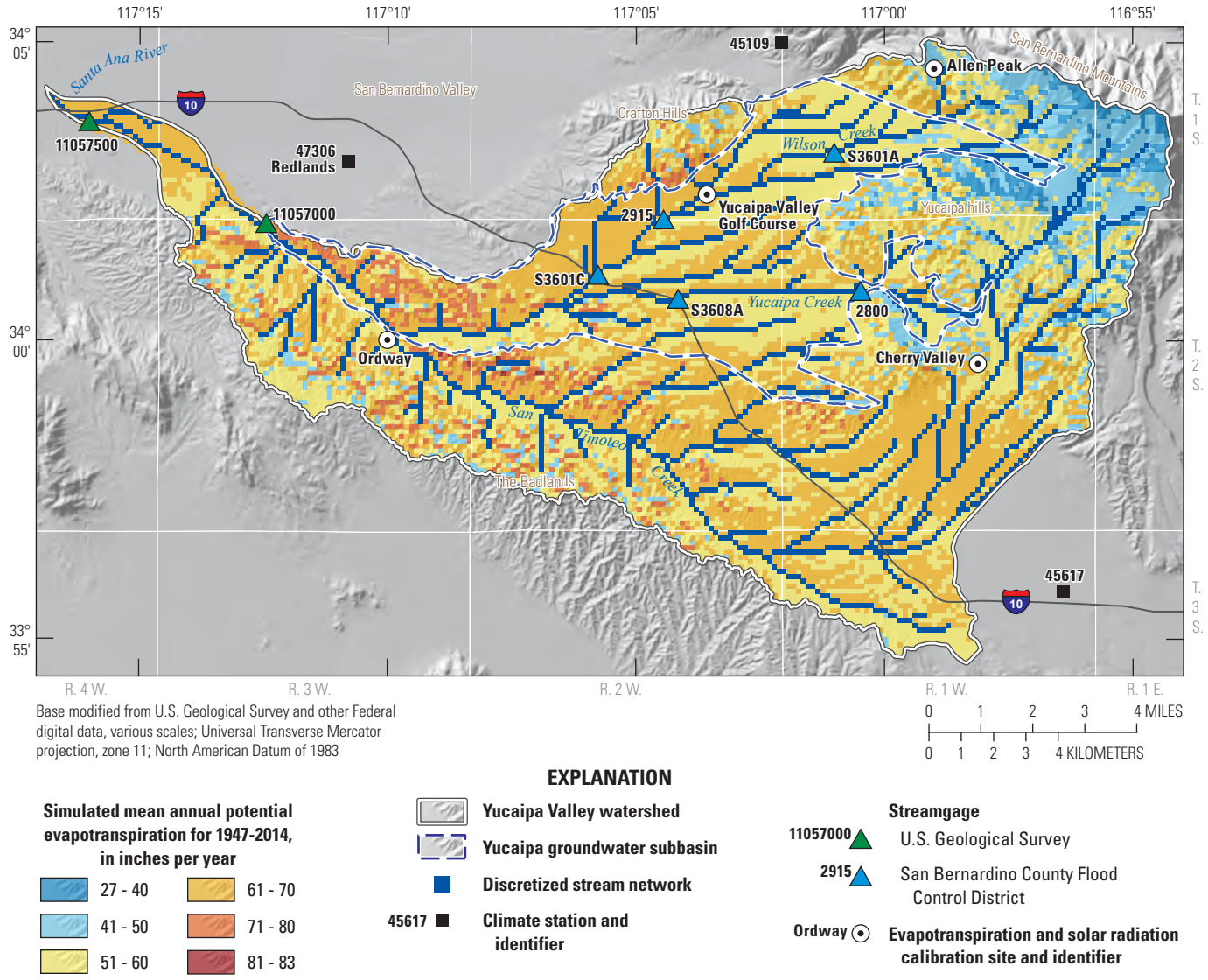

Figure B6. Mean annual evapotranspiration during 1947–2014, discretized stream network, and locations of sites used to estimate surface hydrologic parameters in the Yucaipa Valley watershed, San Bernardino and Riverside Counties, California.

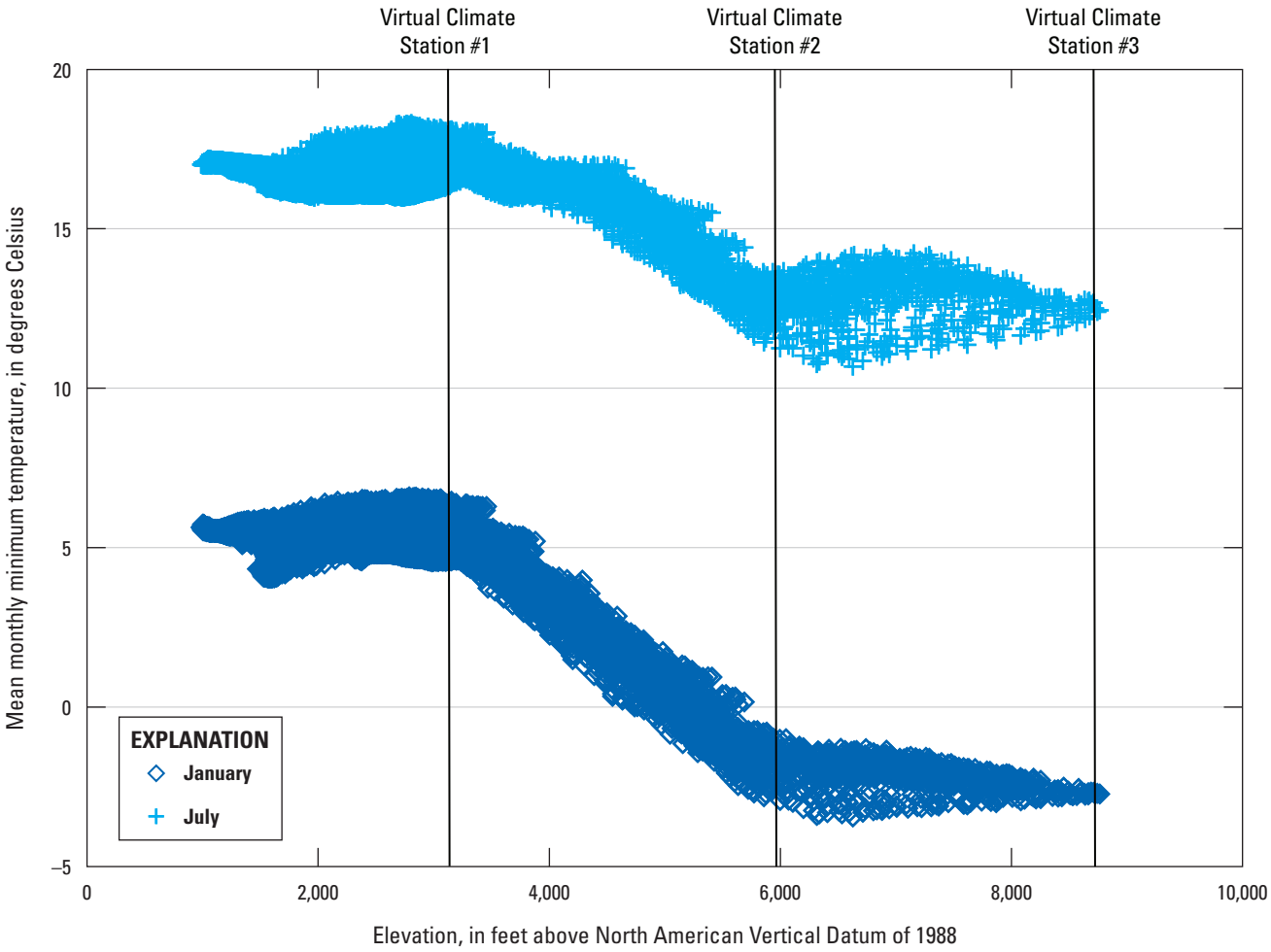

Figure B7. Mean monthly minimum temperature of each hydrologic response unit (HRU) versus elevation, Yucaipa Valley watershed, San Bernardino and Riverside Counties, California.

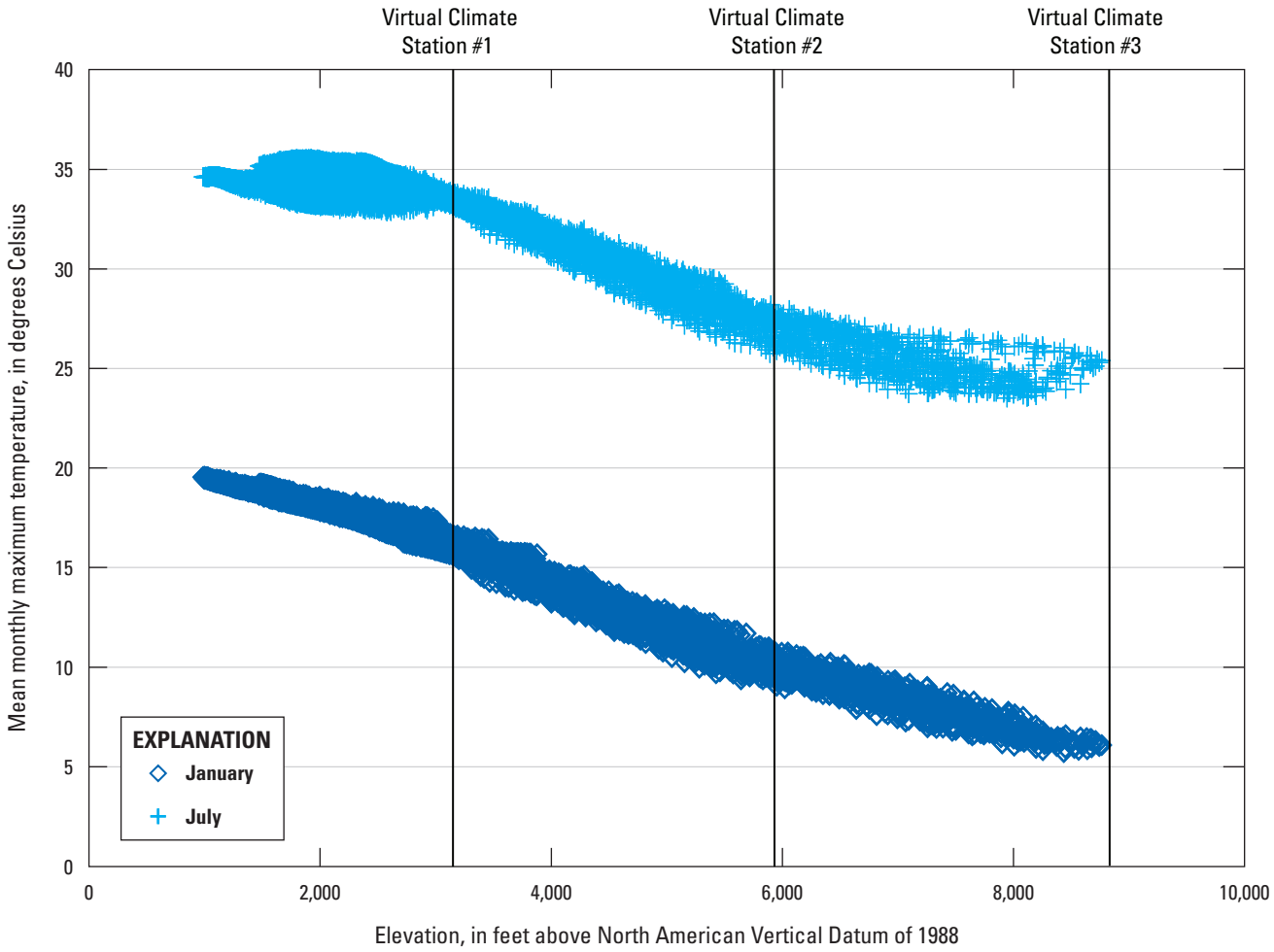

Figure B8. Mean monthly maximum temperature of each hydrologic response unit (HRU) versus elevation, Yucaipa Valley watershed, San Bernardino and Riverside Counties, California.

Monthly plots of T_{max} (PRISM Climate Group, 2013) versus elevation did not exhibit inflection points as pronounced as the T_{min} plots and were judged to be best fit by a single regression (figs. B7, B8; table B2). Therefore, gridded mean monthly T_{max} data were used to develop a single linear regression for T_{max} versus elevation for each calendar month to estimate daily T_{max} at each of the virtual stations (fig. B8); this regression used data for all the HRUs between the elevation of the 47306 Redlands climate station (1,318 ft) and 8,763 ft (table B2). Table B2 shows the coefficients of determination for each regression for monthly T_{min} and T_{max} along with the corresponding temperature lapse rates, which are the same as the slope of each regression.

Table B2. Monthly temperature lapse rates used to estimate daily minimum and maximum temperatures in the YIHM and the coefficients of determination (R^2) for the linear regressions used to estimate the temperature lapse rates from mean monthly temperature data (PRISM Climate Group, 2013).

[Low-elevation, below 3,281 ft.; Mid-elevation, between 3,281 and 5,906 ft.; High-elevation, above 5,906 ft. **Abbreviations**: °C, degrees Celsius; m, meter]

Month	Minimum temperature (T_{min})									Maximum temperature (T_{max})		
	Temperature lapse rate (°C/100 m)			Linear regression intercept (m)			Linear regression coefficient of determination			Temperature lapse rate (°C/100 m)	Linear regression intercept (m)	Linear regression coefficient of determination
	Low-elevation	Mid-elevation	High-elevation	Low-elevation	Mid-elevation	High-elevation	Low-elevation	Mid-elevation	High-elevation			
January	–0.03	–0.91	–0.11	5.30	14.45	0.17	0.38	0.95	0.25	–0.63	21.8	0.99
February	–0.21	–0.88	–0.24	6.85	14.2	2.77	0.41	0.95	0.25	–0.63	22.1	0.99
March	–0.29	–0.81	–0.25	8.24	14.2	4.06	0.61	0.94	0.62	–0.58	23.8	0.98
April	–0.35	–0.72	–0.24	10.1	14.3	5.75	0.73	0.94	0.56	–0.58	26.5	0.97
May	–0.44	–0.60	–0.13	13.3	15.5	7.13	0.83	0.94	0.23	–0.50	29.5	0.91
June	–0.27	–0.46	–0.10	14.8	17.4	10.5	0.64	0.80	0.10	–0.42	33.2	0.78
July	–0.05	–0.47	–0.00	16.9	22.0	12.8	0.039	0.79	0.00	–0.48	37.4	0.80
August	–0.07	–0.52	–0.08	17.4	22.6	14.4	0.08	0.79	0.07	–0.51	38.1	0.84
September	–0.04	–0.71	–0.16	15.6	23.4	13.2	0.02	0.89	0.21	–0.56	35.8	0.90
October	–0.12	–0.85	–0.06	12.3	20.4	6.37	0.13	0.94	0.05	–0.60	30.7	0.94
November	–0.05	–0.87	–0.18	7.89	16.6	4.53	0.03	0.94	0.34	–0.61	25.6	0.98
December	0.00	–0.90	–0.19	4.84	14.3	1.91	0.00	0.95	0.38	–0.60	21.5	0.99

MODFLOW Model Description

MODFLOW simulates streamflow and movement of water in the subsurface (the saturated and unsaturated zones beneath the base of the soil zone). The vertical area between the bottom of the soil zone and the groundwater table is the unsaturated zone, which is simulated using the Unsaturated-Zone Flow package (UZF1; Niswonger and others, 2006). Streamflow is simulated using the streamflow-routing package (SFR2; Niswonger and Prudic, 2005). This section includes a description of boundary conditions, hydrologic inflows and outflows, and aquifer hydraulic properties.

Boundary Conditions

Groundwater boundary conditions in MODFLOW represent how the YIHM groundwater-flow system interacts with groundwater and surface-water systems and features directly adjacent to the active model domain. In the YIHM, the bounding features includes topographic divides, crystalline basement, and adjacent groundwater subbasins not represented in the YIHM. The two types of boundary conditions that are used to simulate these interactions with adjacent systems and features are no-flow and head-dependent boundaries.

No-Flow Boundary

No-flow boundaries in the YIHM were assigned along the YVW boundary in the northwest, north, and east, where the border of the active model domain, as defined by the topographic divides of the YVW boundary, transgresses areas underlain by crystalline basement in Crafton Hills, San Bernardino Mountains, and the low hills just east of the City of Yucaipa (hereafter referred to as “Yucaipa hills”), respectively (fig. B9). Basement rocks have small hydraulic conductivity and likely do not transmit water to the overlying hydrogeologic units; therefore, a horizontal no-flow boundary was used to represent the underlying contact of the layers with this unit. A no-flow boundary also was assigned along the southwestern boundary of the YVW where the active model domain extends into The Badlands (fig. B9). In this part of the model domain, crystalline basement underlies parts of layers 1 and all of layer 4 (chapter A, fig. A11; Cromwell and Matti, 2022).

General-Head Boundary Conditions

Head-dependent boundaries are those across which flow entering or leaving the groundwater-flow system is simulated as a function of groundwater levels in the active model domain. The General-Head Boundary package (GHB; Harbaugh, 2005) is used to simulate groundwater flow between the model domain and adjacent groundwater systems. The exchange of water across the boundary is a product of the specified boundary conductance and the difference between the simulated head in the cell and the specified boundary head (reference boundary head). The boundary conductance regulates the rate of flow through the GHB.

In the YIHM, five GHBs were used to represent the hydraulic connections with adjacent aquifers (fig. B9): Redlands (1), Redlands (2), Beaumont, Mill Creek, and Crafton (fig. B9). The GHBs existed in all active layers. The specified heads at each GHB were estimated from available groundwater-level measurements at wells located across each GHB (fig. B9). The groundwater-level measurements for the period of record for each well were averaged and held constant for the simulation period. The heads in the cells along each GHB followed a linear slope. The conductance values at the five GHBs were estimated during model calibration.

Hydraulic Properties

The hydraulic properties for the MODFLOW model (vertical and horizontal hydraulic conductivity, specific yield, and specific storage) affect the rate at which groundwater moves through the model layers, and the rate and areal extent of changes in groundwater levels caused by groundwater pumping, boundary inflows and outflows, and recharge. The water-bearing hydrogeologic units in the YIHM include the surficial materials, unconsolidated sediment, and consolidated sedimentary materials (Moreland, 1970; California Department of Water Resources, 2016; Cromwell and Matti, 2022). The crystalline basement unit, which underlies the water-bearing formations and crops out in the San Bernardino Mountains, Crafton Hills, and Yucaipa hills, may contain fractures at shallow depths that transmit small quantities of water. A detailed description of the hydrogeologic properties of the crystalline basement and aquifer systems can be found in chapter A.

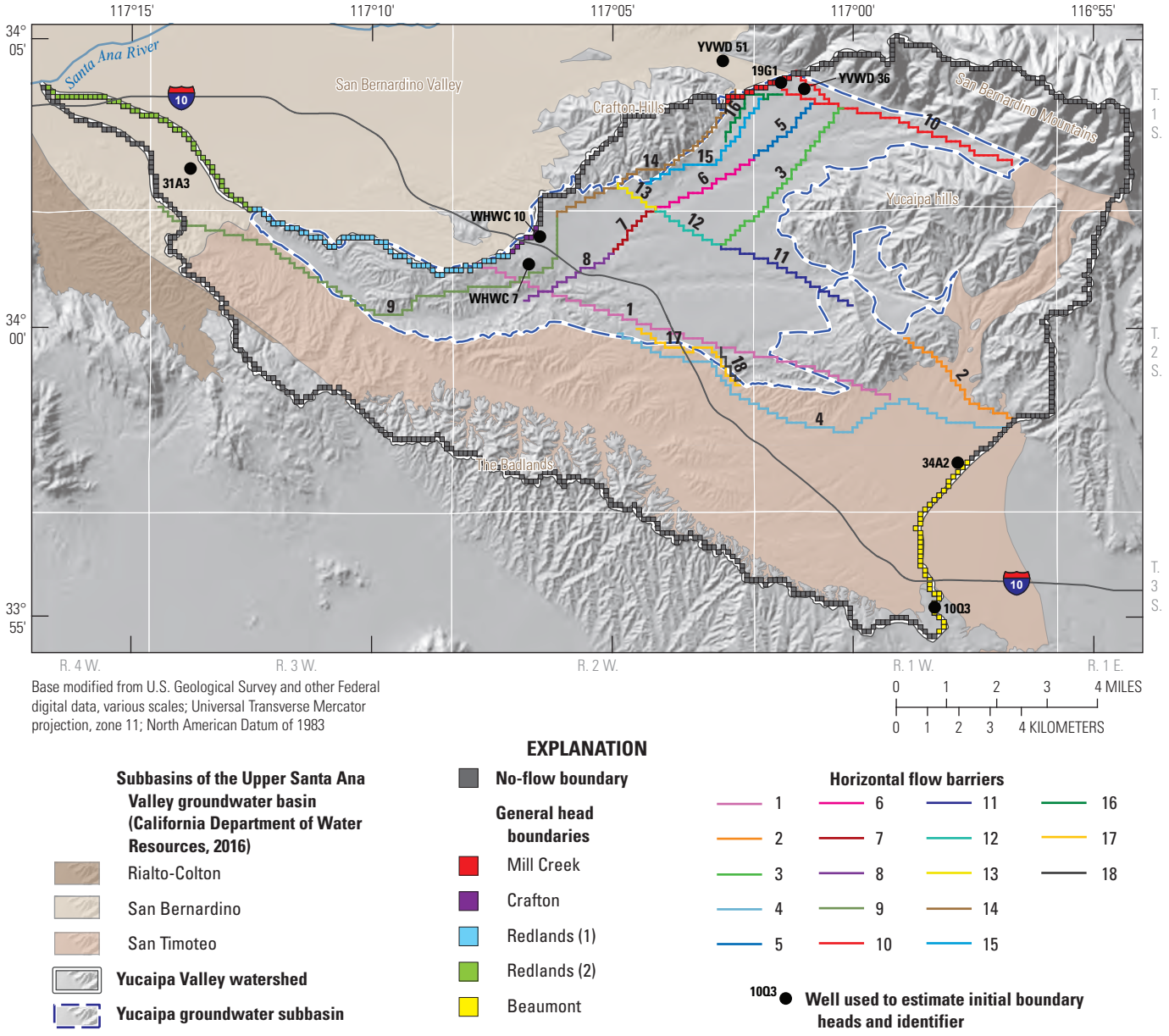

Figure B9. Simulated boundaries, faults and barriers, and their representation in the Yucaipa Integrated Hydrologic Model using the general-head boundary (GHB) and horizontal-flow barriers (HFB) packages (Harbaugh, 2005; Niswonger and others, 2011).

Hydraulic properties of the water-bearing formations in the YIHM were represented using the Upstream Weighting package (UPW; Niswonger and others, 2011). The initial estimation of the conductivity field assumed that hydraulic conductivity was correlated with sediment texture (Russo and Bouton, 1992). For this purpose, the texture of hydrogeologic units was represented using three end members: clay, sand, and gravel. The hydraulic conductivity was related to the percentage of each texture through the power equation (Phillips and Belitz, 1991),

$$K = \left[F_c K_c^p + F_s K_s^p + F_g K_g^p\right]^{1/p} \quad \text{(B1)}$$

where

F_c, F_s, and F_g are percentage of clay, sand, and gravel textures, respectively; and

K_c, K_s, and K_g are the reference conductivity of each texture. The power parameter p, controls the averaging scheme to be used. A p value of –1 produces a harmonic average, while a p value of 1 produces a weighted arithmetic mean.

Texture data provided valuable information about the hydraulic conductivity of geologic materials but also posed some issues for model calibration. First, the spatial variability of texture fields was constrained by the sparsity of texture data. Interpolation of such sparse data might result in unrealistically smooth texture fields. Second, using the texture data as a sole surrogate for the hydraulic conductivity might not be accurate because of the role other factors may play in determining the hydraulic conductivity (such as the degree of sediment compaction). Third, the use of the power equation to compute average hydraulic conductivity introduces a nonunique relation between the end-member conductivity values and the average value. For example, it is possible to produce any average value K using any positive values for K_c and K_s by solving equation B1 for K_g. As a result, infinite combinations for texture conductivities can produce the same average value. Finally, implicit in this method is that the reference hydraulic conductivity values (eq. B1) are constant in space, which might not be correct. To overcome the latest limitation, different reference conductivities could be used for different regions; however, doing so adds more complexity and uncertainty to the calibration. To further refine the estimation of the hydraulic conductivity field, the Ensemble Smoother (ES; Evensen, 1994) was used to improve the texture-based calibration by allowing the estimated hydraulic conductivity field to vary on a cell-by-cell basis (a unique hydraulic conductivity could be assigned to each grid cell) as part of the calibration procedure. Hydraulic storage properties, including specific yield and specific storage, were also calibrated using the ES.

Horizontal-Flow Barriers

Horizontal-flow barriers in the YVW can affect the connectivity of geologic units in the aquifer system (Cromwell and Matti, 2022). All faults and barriers included in the hydrologic characterization (chapter A, fig. A10) may impede groundwater flow and were simulated in the YIHM. The simulated faults and barriers (fig. B9) were assumed to extend vertically in all layers. The Horizontal-Flow Barrier (HFB) package (Hsieh and Freckleton, 1993) was used to simulate the faults and barriers. Some of these faults and barriers divided the basin into smaller groundwater subareas (hereafter called subareas; Moreland, 1970; Geoscience Support Services, Inc., 2014; see fig. A3 of chapter A). Flow across simulated horizontal-flow barriers was proportional to the hydraulic-head difference between cells. The constant of proportionality is the hydraulic characteristic (1/d) of the barrier, which is equal to the hydraulic conductivity of the horizontal-flow barrier divided by its width (the width was assumed to be 1 ft). Information about the hydraulic properties of the horizontal-flow barriers in the YVW were limited; therefore, the properties were estimated during model calibration.

Flow Processes

The MODFLOW model component of the YIHM includes processes that simulate one-dimensional unsaturated vertical flow below the soil zone, groundwater and surface-water interactions, and three-dimensional saturated flow. The UZF1 package (Niswonger and others, 2006) is used in GSFLOW to simulate flow through the unsaturated zone (UZ), groundwater recharge, and groundwater discharge to land surface (Markstrom and others, 2008). The streamflow-routing (SFR2) package (Niswonger and Prudic, 2005) is used to simulate groundwater and surface-water interactions and streamflow routing for the major streams and their tributaries. Various packages in MODFLOW (Niswonger and others, 2011) are used to simulate saturated flow, including groundwater inflow and outflow.

Unsaturated Zone

The UZ plays an important role in the interaction between the surface hydrological processes and the saturated groundwater system. The thickness and the hydraulic properties of the UZ controls the amount of water stored in the UZ, the rate of recharge, recharge arrival time, and the rate of groundwater ET. Available measured and reported groundwater-level data (chapter A; Rewis and others, 2006) indicated that seeping water through the unsaturated zone may locally perch because of intermittent low permeable sediment layers. The locations and the spatial extent of perched aquifers have not been fully determined in the YVW. Therefore, perched aquifers were not simulated explicitly in the YIHM.

The average thickness of the UZ was estimated from available groundwater-level measurements and was found to range from about 10 ft (in upstream areas such as in the San Bernardino Mountains and in the Triple Falls Creek subarea; fig. B2) to greater than 250 ft in Calimesa and Western Heights subareas (fig. A3). The spatial variability of the vertical hydraulic conductivity (VKS) of the UZ is represented by 20 zones that are based on soil properties from the SSURGO database (U.S. Department of Agriculture, 2016). A more detailed description of the VKS zonation will be presented in the "Model Parameterization" section. The VKS values were adjusted during model calibration but were defined as uniform values within each of the 20 zones. Other hydraulic properties that were used to simulate flow through the UZ were given spatially constant values. These properties, which were initially calibrated using a steady-state version of the YIHM (run as a decoupled MODFLOW-only simulation), include the saturated moisture content (0.18 cubic-feet [ft^3] of water per ft^3 of UZ material), surface leakage conductance (0.0019 feet per day [ft/d]), Brooks-Corey epsilon (3.5), average initial moisture content (0.11 ft^3 of water per ft^3 of UZ material), riparian extinction depth (5.74 ft below land surface [bls]), non-riparian extinction depth (2.87 ft bls), and the extinction-water contents (0.179 ft^3 of water per ft^3 of UZ material).

Aquifer-Stream Interaction

The major streams in the YVW (Wilson Creek, Oak Glen Creek, Yucaipa Creek, San Timoteo Creek, and their tributaries; figs. B2, B5) are simulated using the SFR2 package (Niswonger and Prudic, 2005). The SFR2 package accounts for the amount of water in the streams, routes the surface water through the stream network using the kinematic wave method, and simulates flow exchange between the subsurface and the stream network. The simulated quantity of flow between the streams and groundwater is a function of streambed conductance and the difference between the simulated stream stage and simulated hydraulic head in the underlying model layers. The streambed conductance is a function of the stream length and width, the streambed hydraulic conductivity, and the streambed thickness. In the condition when the simulated hydraulic head is above the simulated stream stage at a given stream reach, groundwater discharge (base flow) is added to the streamflow. In the condition when the simulated hydraulic head is below the simulated stream stage at a given stream reach, infiltration into the UZ is simulated, and streamflow is decreased.

In GSFLOW, the stream network is divided into segments and reaches (Markstrom and others, 2008). A segment includes one or more reaches and is divided by a confluence with another stream or by a diversionary segment. A reach is the length of the stream that is contained within a single model cell. In the YIHM, 170 segments were divided into 1,696 reaches. To simplify model calibration, the segments were grouped into 11 zones (fig. B5); within each zone the streambed conductivity was assumed to be constant. Stream segments routed streamflow to one point of outflow at the far-western boundary of the YIHM near USGS streamgage 11057500 (fig. B5). Values for streambed elevation were estimated to be 2 ft below the average DEM value of the cell. Streambed hydraulic conductivity values were determined in calibration. Stream segments were conceptualized as rectangular channels with a constant width for each segment; stream widths were estimated from Google Earth images (imagery date December 2018; Google, Maxar Technologies 2021) and ranged from about 7 to 100 ft. Streambed thickness can range from 1 ft to more than 5 ft (Niswonger and Prudic, 2005); in YIHM, a streambed thickness of 2 ft was assigned for all stream reaches.

Groundwater-Model Inflow

Groundwater inflow originates from natural and anthropogenic sources. Natural sources using GSFLOW are PRMS-simulated percolation through the soil zone, SFR2-simulated leakage from streamflow where and when the simulated water table is below the elevation of the streambed, and MODFLOW-simulated subsurface inflow from adjacent groundwater subbasins. If the groundwater head simulated by MODFLOW is below the elevation of the bottom of the PRMS soil layer, then percolation through the soil zone is simulated by PRMS as potential recharge when the water contents of soil zone storage components exceed threshold values. Potential recharge is applied to the top of the unsaturated zone, through which water percolates vertically and eventually may become actual recharge (inflow to the saturated zone), depending on how much additional ET is simulated by UZF1. As discussed in the previous section, surface-water leakage along stream channels (losing streams, or infiltrating streamflow) is simulated by SFR2 and is an additional source of potential recharge depending on the amount of riparian ET simulated by UZF1. The PRMS-simulated inflows to the SFR2 stream network are surface runoff, fast interflow, and slow interflow. Locations of potential subsurface inflows from adjacent subbasins depend on the boundary conditions (see previous section on boundary conditions) and hydraulic heads simulated by MODFLOW and were calibrated based on well data.

Anthropogenic recharge sources in the YIHM were (1) managed-aquifer recharge (MAR) at the Wilson Creek and Oak Glen Creek spreading basins (figs. B2, B5) using imported water from northern California (as part of the California State Water Project) and (2) return flow of wastewater effluent from septic tank leakage, municipal water system leakage, and irrigation-return flow from agriculture, lawns, golf courses, parks and residential landscaping. Irrigation-return flow agriculture was limited because agricultural lands decreased to less than 0.1 percent of the YVW since 2001. Amounts of MAR at the two spreading basins were reported by the San Bernardino Valley Municipal District and Yucaipa Valley Water District (A. Jones, San Bernardino Valley Municipal Water District, written commun., 2016; B. Brown, Yucaipa Valley Water District, written commun., 2016; see the "Anthropogenic Recharge" section in chapter A), while recharge from return flow was estimated during calibration of the YIHM. Recharge from return flow was estimated for each subarea. Return flow recharge rates were changed every 5 years to account for historical land-use changes and to capture the shift from using septic tanks to sewer systems (see the "Wastewater Effluent" section in chapter A).

MAR was simulated using the Multi-Node Well package (MNW2; Konikow and others, 2009), while recharge from return flow was simulated using the well package (WEL; Harbaugh, 2005). The recharge rates were assigned to the cell in the uppermost active layer.

Groundwater-Model Outflow

Groundwater outflow from the YIHM consists of groundwater ET, surface leakage, subsurface lateral outflow, and groundwater pumping. The amount of groundwater outflow from groundwater ET, surface leakage, and subsurface lateral outflow was simulated by the YIHM. The amount of groundwater pumping is reported by local water agencies (see the "Sources and Estimates of Discharge" section in chapter A) or estimated by Thomas Harder and Co. (2015).

Groundwater Evapotranspiration

GSFLOW simulates groundwater ET using PRMS and MODFLOW components. Initially, actual ET from the soil zone, plant canopy, and impervious surfaces is simulated by the PRMS model. The PRMS model also computes PET, which is the maximum rate of ET that can occur. The residual ET, which is the unused PET from the PRMS model that is available to the UZ and groundwater system (Markstrom and others, 2008), is the maximum rate of ET that MODFLOW can use to compute groundwater ET in the unsaturated and the saturated zones. The residual ET is used to remove water from the root zone in the UZ. If the root zone is deep enough to intersect the groundwater table, saturated-zone ET (phreatic evapotranspiration) can occur.

Surface Leakage

Surface leakage is groundwater discharge to the soil zone or land surface. Surface leakage can occur when the simulated groundwater heads are greater than the elevation of the land surface in model cells of the uppermost active layer in the MODFLOW model. This primarily occurs on steep hillslopes or when the moisture content exceeds the saturated moisture content in the UZ. Surface leakage is controlled by the vertical conductivity (VKS) of the unsaturated zone and by the surface conductivity (SURFK) value in the UZF1 package (Niswonger and others, 2006). Surface leakage is routed to streams segments specified in the UZF1 package for MODFLOW-only simulations, and surface leakage that occurs in integrated GSFLOW simulations flows into the PRMS soil zone.

Groundwater Pumping

Groundwater pumping is used to satisfy the needs of four water-use sectors: residential, landscape, industrial and commercial, and agricultural. The amount of groundwater pumping in the Yucaipa subbasin is reported by local water agencies (see chapter A), and the amount of groundwater pumping in the Beaumont plain is estimated by Thomas Harder and Co. (2015). Groundwater pumping is simulated in the model using the MNW2 package (Konikow and others, 2009). The MNW2 package simulates wells completed in multiple aquifers (fig. B10) and allows vertical groundwater movement through well bores. Most of the available pumping data within the 1947–2014 simulation period are reported as annual values (see the "Pumpage" section in chapter A). The quantities of monthly pumpage were estimated from these annual values on the basis of reported monthly data.

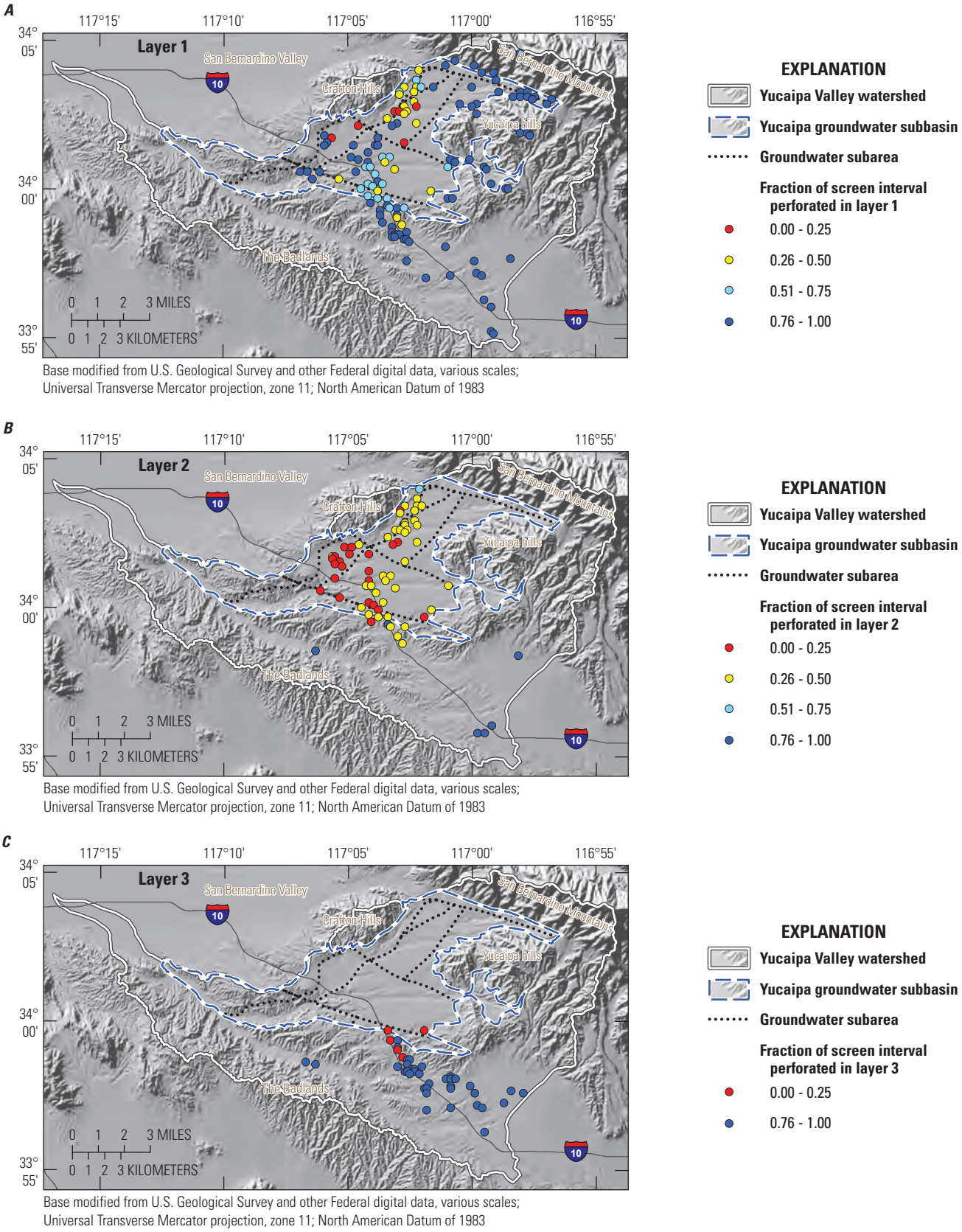

Figure B10. Location of groundwater pumping wells (assigned at the centroid of model cells) and the fraction of the perforated screen interval in *A*, layer 1; *B*, layer 2; *C*, layer 3; and *D*, layer 4 of the Yucaipa Integrated Hydrologic Model; Yucaipa Valley watershed, San Bernardino and Riverside Counties, California.

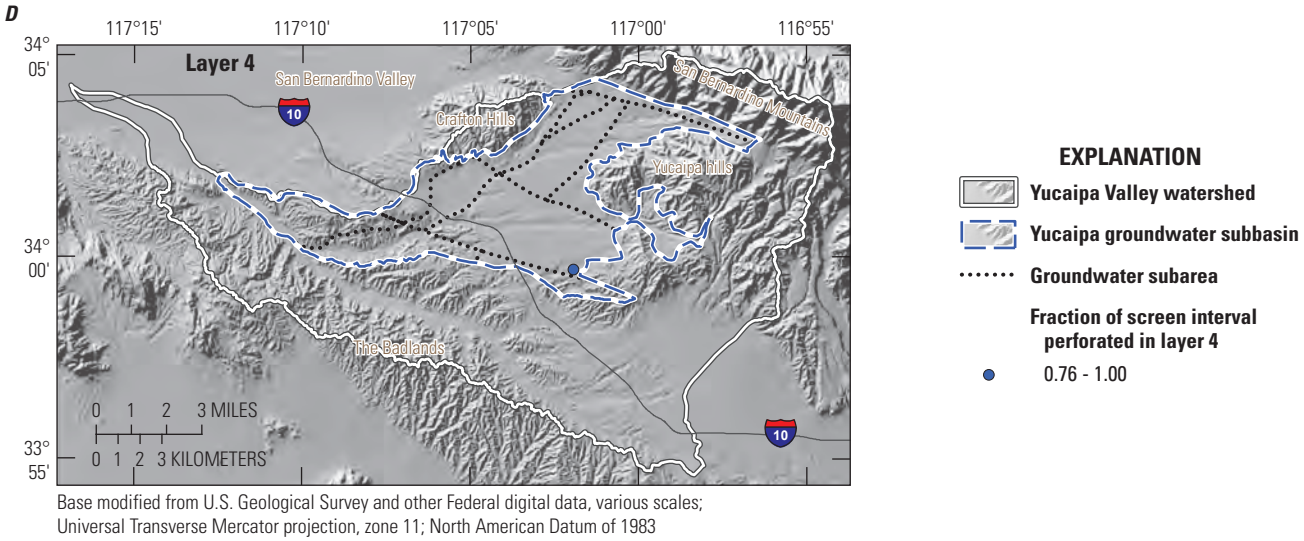

Base modified from U.S. Geological Survey and other Federal digital data, various scales; Universal Transverse Mercator projection, zone 11; North American Datum of 1983

Figure B10.—Continued

Integration of Precipitation-Runoff Modeling System and MODFLOW

Integration of PRMS and MODFLOW is completed by exchanging flow among the three regions of GSFLOW (fig. B1) on the basis of interdependent equations that calculate flow and storage of water throughout the simulated hydrologic system (Markstrom and others, 2008). Part of the water entering the watershed (region 1) infiltrates into the soil zone, flows to streams and lakes (region 2), and may drain into the groundwater systems (unsaturated and saturated zones in region 3). In a coupled GSFLOW model, the PRMS groundwater reservoirs are replaced with finite difference cells in MODFLOW. The soil zone in PRMS and MODFLOW exchanges water through the gravity reservoirs, which are used to transfer water between HRUs and finite-difference cells. The PRMS-simulated inflows to a stream segment include Hortonian and Dunnian runoff, slow interflow through the gravity reservoirs, and fast interflow through the preferential-flow reservoirs. These inflows are routed to stream segments specified in Streamflow-Routing (SFR2) Package in MODFLOW using a set of topologic parameters that define cascading flow among HRUs and the intersections among HRUs, stream segments, and stream reaches (Markstrom and others, 2008). Topologic parameters used to define cascading flow were derived for each HRU from the 10-m DEM geospatial layer using the Gsflow_ArcPy Toolkit (Gardner and others, 2018).

Integrated Model Calibration

Model calibration involved adjusting model input parameters to obtain a reasonable fit between simulated results and available measured data. During calibration of the PRMS-only model, estimated properties were constrained on the basis of measured parameters used in calculating solar radiation and PET. During calibration of the YIHM, estimated properties of the flow system were constrained on the basis of measured streamflows, groundwater levels, and pumpage. Calibration proceeded until the differences between simulated and measured data were acceptable for the intended use of the YIHM.

Calibration Process

Different calibration methods were used to calibrate the YIHM, including Ensemble Smoother (ES; Evensen, 1994), the automated parameter-estimation software PEST (Parameter ESTimation; Fienen and others, 2013; Doherty, 2015; Welter and others, 2015), and trial-and-error. The ES can estimate a large number of input parameters using a smaller number of model runs and was used to produce initial estimates of the unknown parameters. More details about ES theory and numerical implementation are presented in appendix B1. Parameters estimated using ES were further refined in PEST. PEST is a model-independent calibration tool that minimizes the sum of weighted squared deviation of simulated values from measured data (residual errors) by changing model input parameters. During automated calibration with PEST, insensitive model input parameters were identified and fixed at their initial values to improve subsequent calibration runtimes. The number of YIHM parameters estimated varied with calibration stage and with additional insight about the relative sensitivities of the estimated parameters.

Simulation of an integrated hydrological system using GSFLOW requires a large set of input parameters for both the PRMS model and the MODFLOW model. To simplify the estimation of these parameters, calibration is achieved in a two-stage process. In stage 1, watershed parameters are calibrated in PRMS-only mode using PEST to ensure that surface PET is being simulated properly. In stage 2, the PRMS and MODFLOW models are coupled to calibrate the YIHM using the three methods described previously.

Calibration Targets

Calibration targets are measured data that are compared with corresponding values simulated by the model. Observed data are compared with simulated values using various statistical assessments of the model's ability to reproduce the calibration targets. The objective of the calibration process is to reduce the differences between the calibration targets and corresponding simulated states by adjusting model input parameters. Calibration is completed to create a model that can reproduce the calibration targets to an acceptable level using physically reasonable parameter values. An acceptable calibration depends on the goals of the project, the amount of uncertainty in data used to develop the model, and the resources available to develop the model.

In stage-1 calibration, data used to calibrate the PRMS-only model to solar radiation and potential ET were obtained from the California Irrigation Management Irrigation System (CIMIS; 2017), which maintains 2-kilometers (km) grids of solar radiation and reference ET generated from remotely sensed satellite data. The CIMIS "grass reference" ET was used to represent "potential" or the maximum actual ET for well-watered conditions for all vegetation in the PRMS model. Four locations (named Allen Peak, Yucaipa Valley Golf Club, Cherry Valley, and Ordway for the purposes of this study; fig. B6) on the CIMIS 2-km grid within the YVW were selected for calibration of solar radiation and potential ET. These four locations represented a range of elevations, land-cover, and climatic variability. For each location, mean values of solar radiation and potential ET for each month of the year were computed from daily CIMIS data for the calendar period 2003–15.

During stage-2 calibration, four observation groups were defined in PEST to calibrate the coupled GSFLOW model: (1) streamflow, (2) transient groundwater levels, (3) drawdown, and (4) monthly pumping rates. Streamflow is measured at seven streamgages in the YVW (fig. B6). The five streamgages operated by the San Bernardino County Flood Control District (SBCFCD; S3601A, 2915, S3601C, 2800, and S3608A) were designed to measure high volumes of streamflow during flood conditions; therefore, measured rates of discharge during low streamflow conditions are less reliable (appendix B2). The two streamgages operated by the USGS (USGS stations 11057000 and 11057500) were designed to measure volumes of streamflow in both high- and low-flow conditions; however, measured streamflow were affected by several onstream retention ponds and by urban runoff generated from outside the YIHM study area (appendix B2). Observed monthly mean and annual mean streamflow values at all seven streamgages (fig. B6) were used in calibration of the YIHM; however, small weights were assigned to the streamflow values because of the uncertainties in the streamflow data. More details about the available streamflow measurements, evaluation of data quality and suitability for model calibration, and goodness-of-fit are discussed in appendix B2.

Groundwater-level data used in the PEST calibration were obtained from the USGS National Water Information System (NWIS; U.S. Geological Survey, 2018) and from local water agencies: Yucaipa Valley Water District (YVWD; B. Brown, Yucaipa Valley Water District, written commun., 2016), South Mesa Water Company (SMWC; D. Armstrong, South Mesa Water Company, written commun., 2016), Western Heights Water Company (WHWC; B. Brown, Western Heights Water Company, written commun., 2016; fig. B11). Drawdown is calculated as the difference between the first groundwater-level measurement and subsequent measurements for each well. A total of 18,945 transient groundwater-level and drawdown observations at 259 wells between 1970 and 2014 were used in the PEST calibration. Reported groundwater monthly pumping rates also were used as observations to avoid reductions in pumping caused by groundwater levels dropping below model cells that contain wells.

The contribution of each observation to the objective function was controlled by user-defined weights. Measurements with possible large uncertainties were given lower weights to limit their influence on the model calibration results. Low weights were assigned to observed period-of-record mean streamflow observations because some of the data were unreliable (appendix B2). Groundwater-levels measured when a well was being pumped or was recently pumped also were assigned low weights. Other factors that were used to assign low weights to groundwater-level measurements included wells located in areas where perched aquifers have been reported to be present, such as in the Western Heights subarea (fig. A3), and in the area between Cherry Valley thrust fault and the southern boundary of the Yucaipa subbasin (Rewis and others, 2006). These perched aquifers were not considered part of the regional simulated aquifer system.

Weights also were used to balance the contribution of wells with a different number of groundwater-level measurements. Wells with a large number of measurements contributed more to the PEST objective function compared with wells with a smaller number of measurements if equal weights were assigned. To ensure balanced contributions of differing number of groundwater-level measurements to the objective function, the assigned weights were scaled by the inverse of the number of measurements for each well.

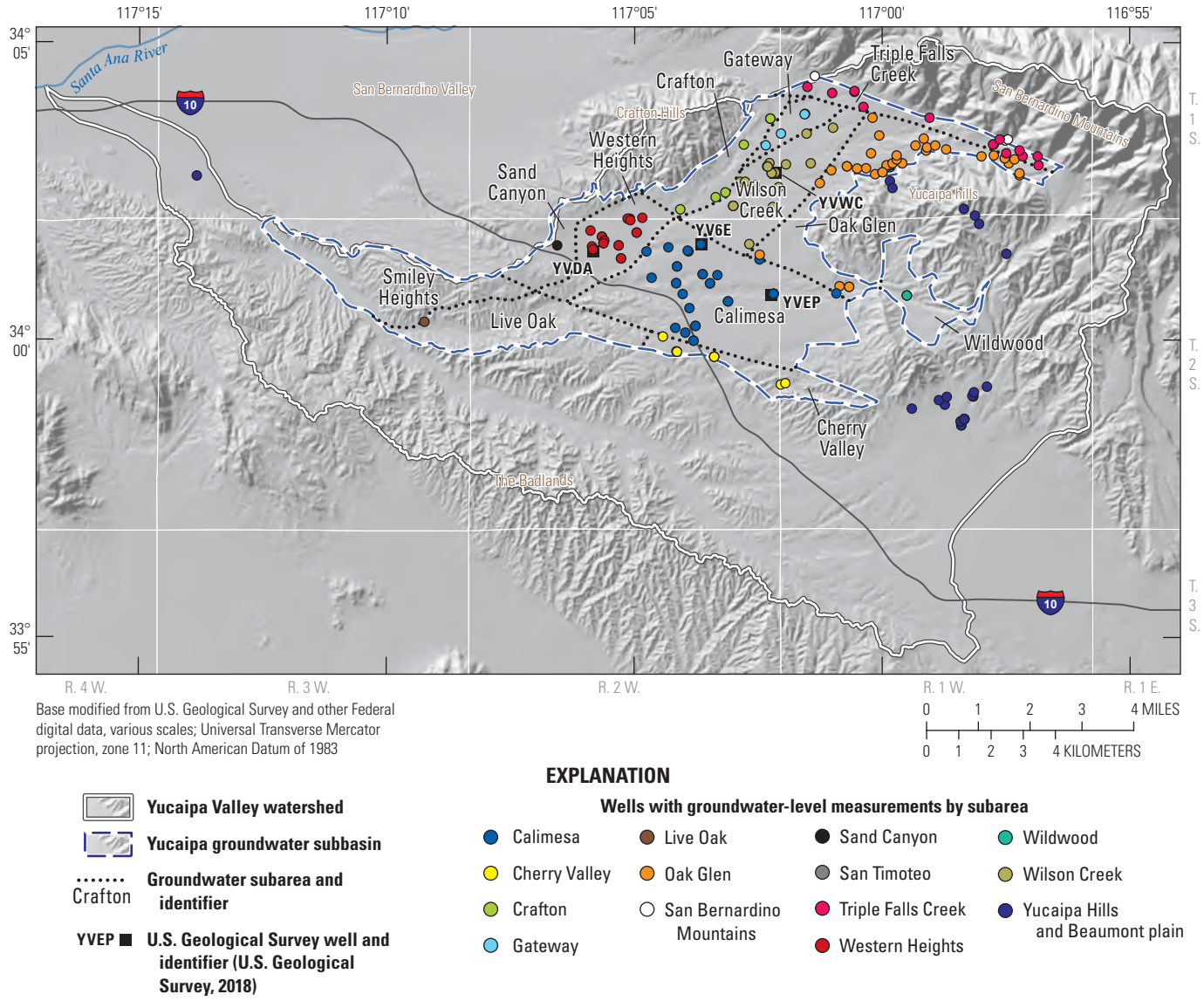

Figure B11. Wells with groundwater-level measurements (U.S. Geological Survey, 2018) during 1947–2014 used to calibrate the Yucaipa Integrated Hydrologic Model, Yucaipa Valley watershed, San Bernardino and Riverside Counties, California.

Model Parameterization

Calibration of all the YIHM input parameters is computationally intensive and requires at least as many separate simulations as there are parameters. Therefore, a smaller set of important (sensitive) parameters can be identified to limit the number of simulations needed for calibration and focus computational resources on the most relevant and identifiable parameters. When PEST is used, insensitive parameters can be identified during a calibration run, which greatly increases the efficiency of the calibration procedure.

Modifying model parameterization is another approach that was used in the calibration of YIHM to increase calibration efficiency. Model parameterization simplified the representation of spatially variable parameters in the model. In the YIHM, pilot points and zonation were used to simplify the distributions of horizontal and vertical hydraulic conductivity, specific storage, and specific yield. The parameters for the PRMS and MODFLOW models in the YIHM were divided into eight groups (table B3). Parameter groups and parameter initial values are discussed in this section.

In calibration stage 1, parameters used in the simulation of solar radiation and potential ET were estimated for the PRMS model. Following a stepwise calibration procedure (Hay and others, 2006), parameters controlling solar radiation and potential ET (Group A; table B3) were calibrated independently using PRMS-only mode. The YIHM used the modified degree-day (*ddsolrad*) module for simulating daily solar radiation and the Jensen-Haise (*potet_jh*) module for simulating potential ET (Markstrom and others, 2015). Two

Table B3. Summary of parameter groups, parameter descriptions, and calibrated components of the Precipitation Runoff Modeling System (PRMS; Markstrom and others, 2015) and MODFLOW (Harbaugh, 2005) in Yucaipa Integrated Hydrologic Model, Yucaipa Valley watershed, San Bernardino and Riverside Counties, California.

Group	Description	Model component
A	Parameters controlling the simulation of solar radiation and potential evapotranspiration.	PRMS
B	Parameters controlling natural recharge and anthropogenic recharge. This group consists of (1) scaling factors for spatially variable PRMS parameters, and (2) anthropogenic recharge rates for each groundwater subarea with residential and agricultural return flow.	PRMS, MODFLOW
C	Horizontal and vertical conductivity at each grid cell for Ensemble Smoother calibration and scaling factors at pilot points for calibration using Parameter Estimation software (PEST).	MODFLOW
D	Parameters specifying storage capacity of the saturated zone that include specific yield and specific storage fields.	MODFLOW
E	Parameters controlling boundary conditions. This group consists of five values for the hydraulic conductivities of the five different general head boundaries.	MODFLOW
F	The hydraulic characteristic of faults and barriers. Some of these faults and barriers were divided into smaller sections resulting in a total of 18 calibrated parameter values.	MODFLOW
G	Hydraulic conductivity of the streambed. The stream segments are grouped into 11 zones.	MODFLOW
H	Unsaturated Zone Flow (UZF) parameters controlling the unsaturated zone flow, which includes values for vertical hydraulic conductivities at 20 zones, evapotranspiration (ET) extinction depth in 2 zones (riparian and non-riparian), and the conductance controlling the surface leakage.	MODFLOW

sets of parameters (12 monthly values for each of *dday_intcp* and *dday_slope*) were adjusted to calibrate PRMS to the mean monthly values for solar radiation, and 12 parameters (monthly *jh_coef*) were adjusted to calibrate PRMS to the mean monthly values for potential ET.

Watershed parameters controlling natural and anthropogenic infiltration were estimated in calibration stage 2 (Group B; table B3). Parameters used to simulate natural infiltration were *sat_threshold, soil2gw_max, soil_moist_max, soil_rechr_max, rain_adj*, and *ssr2gw_rate*. These parameters were adjusted by using multipliers for the distribution of each parameter. The initial values of PRMS parameters were computed using Gsflow-ArcPy Toolkit (Gardner and others, 2018). Anthropogenic recharge was estimated for each subarea (chapter A, fig. A3*C*), and return flow was temporally changed to capture anthropogenic recharge changes with time (see the "Groundwater-Model Inflow" section). Initial values of anthropogenic recharge were estimated based on land-use maps and geospatial information about septic tank locations (for more details see the "Anthropogenic Recharge" section in chapter A and fig. A17*A*). A total of 70 recharge values were estimated (7 subareas multiplied by 10 time windows).

Groundwater parameters in table B3 include hydraulic conductivity (Group C), aquifer storage properties (Group D), the hydraulic conductivities of the general-head boundaries (Group E), the hydraulic characteristics of horizontal-flow barriers (Group F), the hydraulic conductivities of streambed zones (Group G), and the hydraulic properties of the unsaturated zones (Group H). The spatial representations of hydraulic conductivity and aquifer storage (Groups C and D, respectively; table B3) varied with calibration progress. Estimates of the aquifer hydraulic properties horizontal and vertical hydraulic conductivity, specific yield, and specific storage were based on borehole texture data (Cromwell and Matti, 2022) and used as initial values for the ES calibration, where parameters are estimated at the resolution of the grid. Resulting hydraulic properties fields are further modified using PEST to estimate spatially varying multipliers interpolated using pilot points to continuous cell values and parameter multipliers for crystalline basement zones shown in fig. B12. Areas with more groundwater-level data have more pilot points and more sensitivity in the YIHM. Areas with less groundwater-level data have fewer pilot points and less sensitivity in the YIHM. Pilot point locations in layer 1 and the unconfined part of layer 4 (fig. B12*A*) were also used to calibrate specific yield, while pilot points in layers 2, 3, and part of 4 are used to calibrate specific storage. The parameter zones are used to estimate a multiplier for fractured crystalline basement hydraulic conductivity (fig. B12).

Group E consisted of the GHB parameters (fig. B9; table B3). The unknown hydraulic conductivities at the five boundary conditions were estimated during calibration of the YIHM. The GHB conductivity was defined as the GHB conductance divided by aquifer thickness. Calibration of the hydraulic conductivity of the GHB instead of the boundary conductance allowed the representation of the spatial variability of the conductance to be consistent with the spatial variability of aquifer thickness along the GHB. Initial values of the GHB conductivities were chosen to be the same as the hydraulic conductivity of GHB cell.

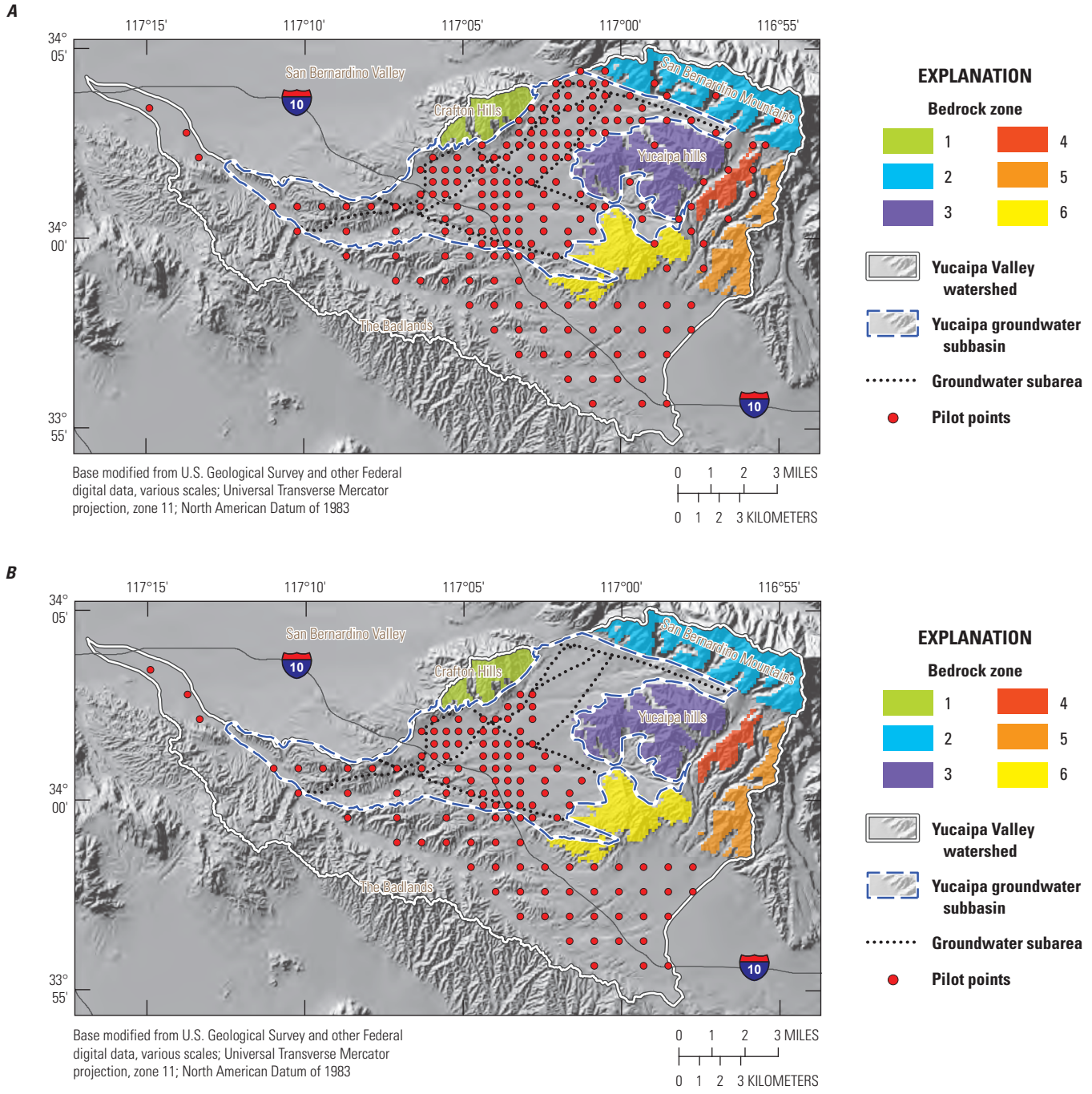

Figure B12. Pilot points used to calibrate horizontal and vertical conductivity fields within Yucaipa Integrated Hydrologic Model layers, and zonation of crystalline basement hydraulic conductivity. *A*, layer 1; *B*, layer 2 and 3; and *C*, layer 4. Pilot points in unconfined layer 1 and part of layer 4 are used to calibrate specific yield. Pilot points in layer 2, 3, and part of 4 are used to calibrate specific storage; Yucaipa Valley watershed, San Bernardino and Riverside Counties, California.

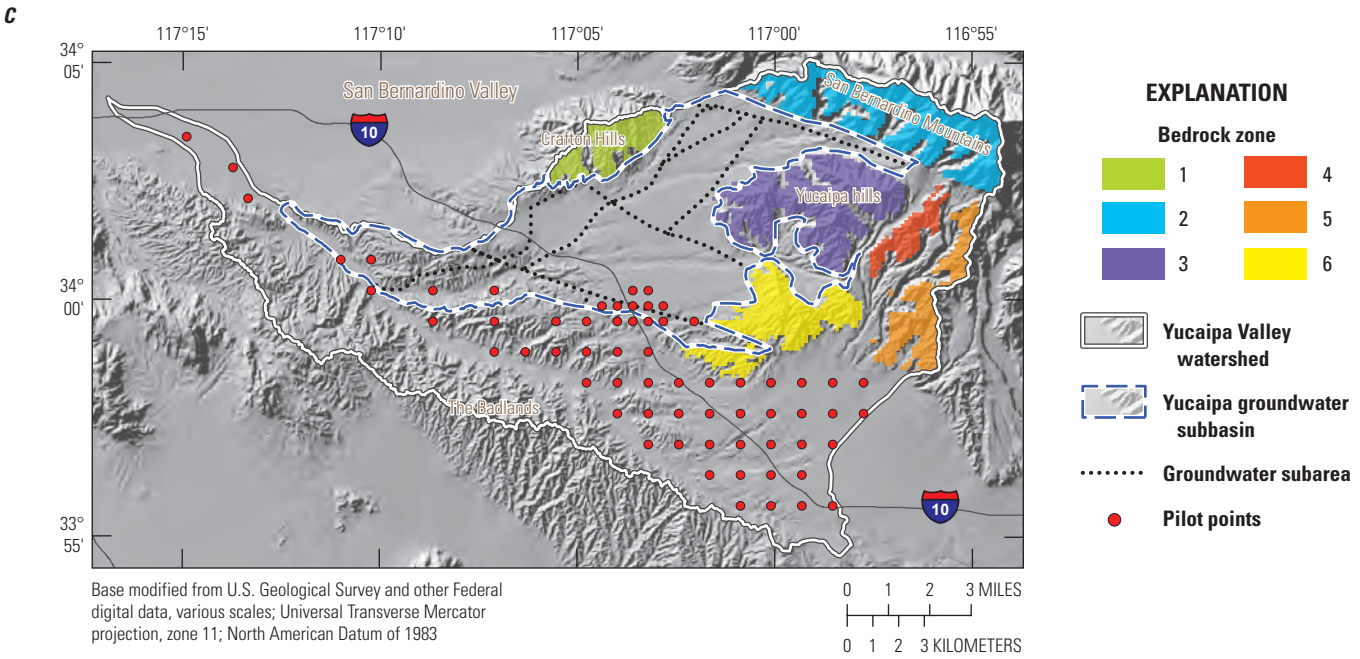

Figure B12.—Continued

Group F consisted of parameterized hydraulic characteristics for simulated the horizontal-flow barriers (HFB) that represented faults and barriers within the simulated domain (fig. B9). Some of the HFBs were divided into smaller sections to better represent the variability in their effectiveness at restricting groundwater flow across them. This resulted in a total of 18 parameter values (fig. B9). Limited information was available about the hydraulic characteristic of the faults and barriers. An initial value of 0.001 per day (1/d) was chosen for faults/barriers where head differences were evident from groundwater-level measurements on both sides of the faults/barriers; otherwise, an initial value of 1.0 (1/d) was used.

Group G consisted of streambed hydraulic conductivities parameterized into 11 stream network zones as shown in figure B5. Site-specific information about streambed hydraulic conductivity was not available, but literature reviews suggested that streambed conductivity can vary between 0.1 ft/d and more than 70 ft/d (Duwelius, 1996; Abimbola and others, 2020). An initial value of streambed conductivity of 1.0 ft/d was used for all stream zones.

Group H consisted of parameters related to the UZF1 package: the ET extinction depth that defines the depth of vertical zone where ET occurs, the vertical hydraulic conductivity, and the conductance controlling surface leakage. The ET extinction depth was parameterized into two zones: the riparian zone and non-riparian zone. The extinction depth for the riparian zones was assumed to be twice the depth of the non-riparian zones to reflect higher ET from riparian vegetation within the stream corridors. The spatial variability of the vertical hydraulic conductivity of the UZ was parameterized by zoning the soil conductivity map from SSURGO soil database (U.S. Department of Agriculture, 2016) into 20 zones. Initial UZF1 parameter values were estimated using the steady-state model (see section "Unsaturated Zone" in this report).

Calibration Results

Calibration results for the PRMS-only model include discussion of final values for input parameters and assessment of model fit. In addition to the residual analysis, literature values, including values estimated for the YVW (chapter A), were compared to simulated values for the quality and reasonableness of the calibration. Calibration results for the coupled GSFLOW model include discussion of final parameter values and parameter sensitivity.

Watershed Model Final Input and Model Fit

In the first step of the PRMS-only calibration process, two parameters (*dday_intcp* and *dday_slope*) were adjusted to calibrate the model to the mean monthly values for solar radiation (table B1). In the second step, one parameter (*jh_coef*) was adjusted to calibrate PRMS to the mean monthly values for potential ET (table B1). The third step is to adjust selected soil-zone and runoff parameters to calibrate PRMS to streamflow (Huntington and Niswonger, 2012). Selected soil-zone and runoff parameters were only adjusted during the integrated model calibration because available streamflow data were insufficient to complete this step in the PRMS-only calibration process. Additionally, anthropogenic changes to the natural stream network, which include numerous flood-control structures, reservoirs, and urban runoff generated from area outside the simulated domain, make streamflow simulation difficult in PRMS (see appendix B2 for more details about streamflow measurements).

Comparisons of simulated and measured solar radiation (fig. B13) and PET (fig. B14) data indicate how well the PRMS model represents the simulated energy balance of atmospheric conditions. For the PRMS-only model calibration, the calibrated parameter used in calculating mean monthly PET (*jh_coef*) resulted in an overall good fit of simulated values to observed data at the four PET and solar radiation calibration locations selected from the CIMIS 2-km grid (fig. B6). The simulated solar radiation and PET values at three of the locations (Allen Peak, Ordway, and Yucaipa Valley Golf Club) did not display pronounced bias (figs. B13, B14). However, at the Cherry Valley location, the model overestimates measured solar radiation for most months and underestimates measured PET for all months. The best model fit for solar radiation and PET was observed at the Yucaipa Valley Golf Club location. The calibrated parameters *jh_coef, dday_intcp,* and *dday_slope*, are fixed in the calibration of the coupled YIHM.

Coupled Groundwater and Surface-Water FLOW Model Final Input

The final MODFLOW parameters consisted of aquifer and fractured crystalline basement hydraulic properties, HFB hydraulic characteristics, streambed hydraulic conductivity, GHB conductivity, UZ parameters including ET extinction depth, surface hydraulic conductivity, vertical hydraulic conductivity, and PRMS parameters that controlled recharge simulation. The final parameter values in the YIHM are summarized in table B4 and were generally within the ranges of previously publish values. Final parameter values are discussed further in subsequent sections of chapter B.

MODFLOW Hydraulic Properties

Final hydraulic properties for the four MODFLOW layers consisted of horizontal (HK) and vertical (VK) hydraulic conductivity, specific yield (Sy), and specific storage (Ss). Figures B15 and B16 show the final spatial distribution of calibrated horizontal and vertical hydraulic conductivity, respectively. Final horizontal hydraulic conductivities ranged from 3.0×10^{-4} to 284 feet per day (ft/d), while the vertical hydraulic conductivities ranged between 3.4×10^{-5} and 36 ft/d. The HKs were generally low (3.0×10^{-3} to 0.1 ft/d) in the Yucaipa hills, Crafton Hills, and San Bernardino Mountains, where fractured crystalline basement appears at land surface (fig. B15). A similar pattern of spatial variability was observed for VKs (fig. B16). Low horizontal and vertical conductivities ($< 3.0\times10^{-3}$ ft/d) were used to represent the tilted Cherry Valley thrust fault (hfb-17, hfb-18, and part of hfb-4; table B4; fig. B9). In other areas in Yucaipa Valley, HKs were higher; HKs ranged from 1 to 10 ft/d in the area between Yucaipa hills and San Bernardino Mountains and reached about 284 ft/d at lower elevations in the Western Heights and Calimesa subareas and the Beaumont plain. The ranges of calibrated HKs and VKs in each layer are provided in table B4.

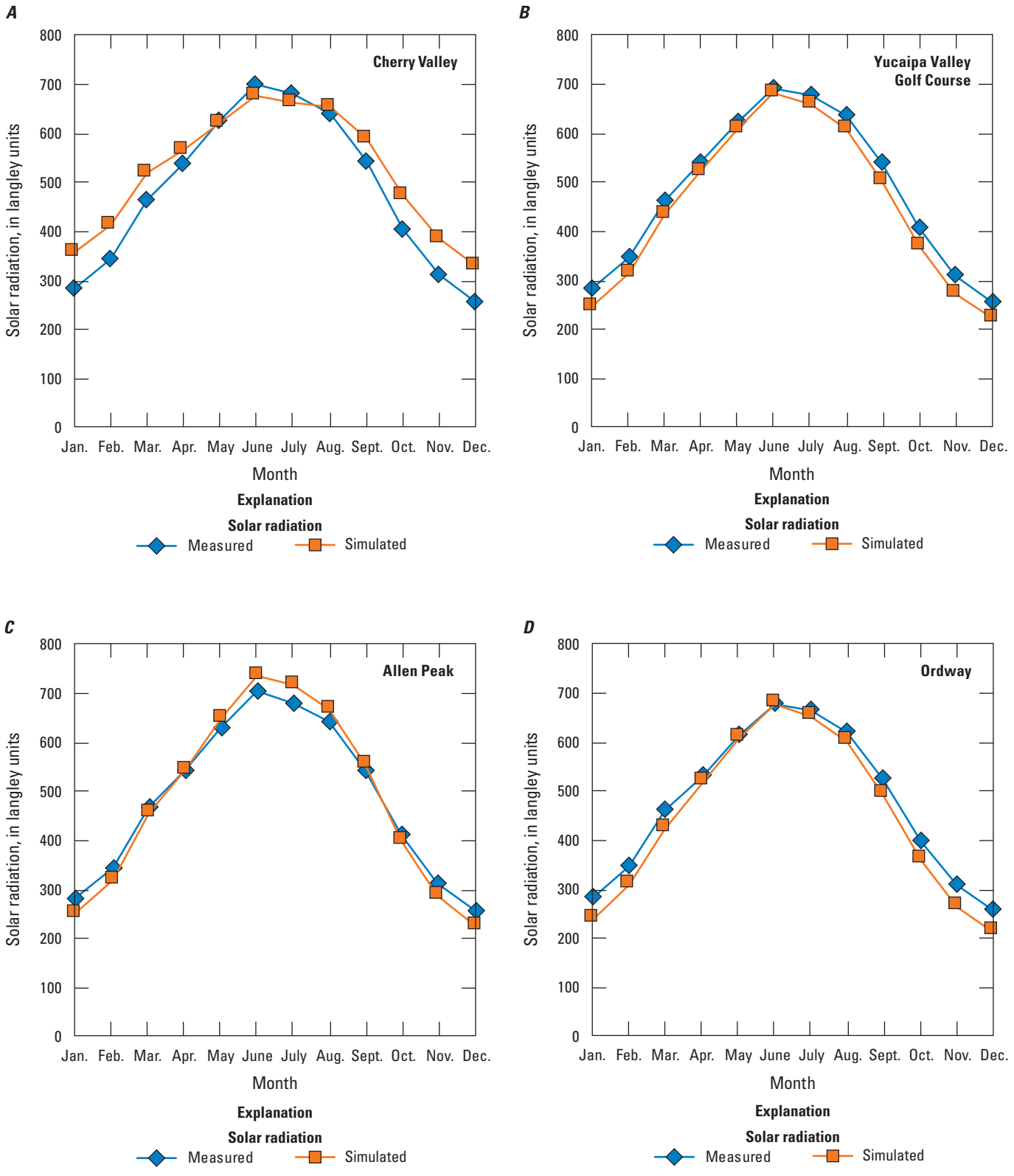

Figure B13. Precipitation Runoff Modeling System (PRMS; Markstrom and others, 2015) simulated mean monthly solar radiation versus measured data (CIMIS, 2017) for four locations: *A*, Cherry Valley; *B*, Yucaipa Valley; *C*, Allen Peak; and *D*, Ordway, in the Yucaipa Valley watershed, San Bernardino and Riverside Counties, California.

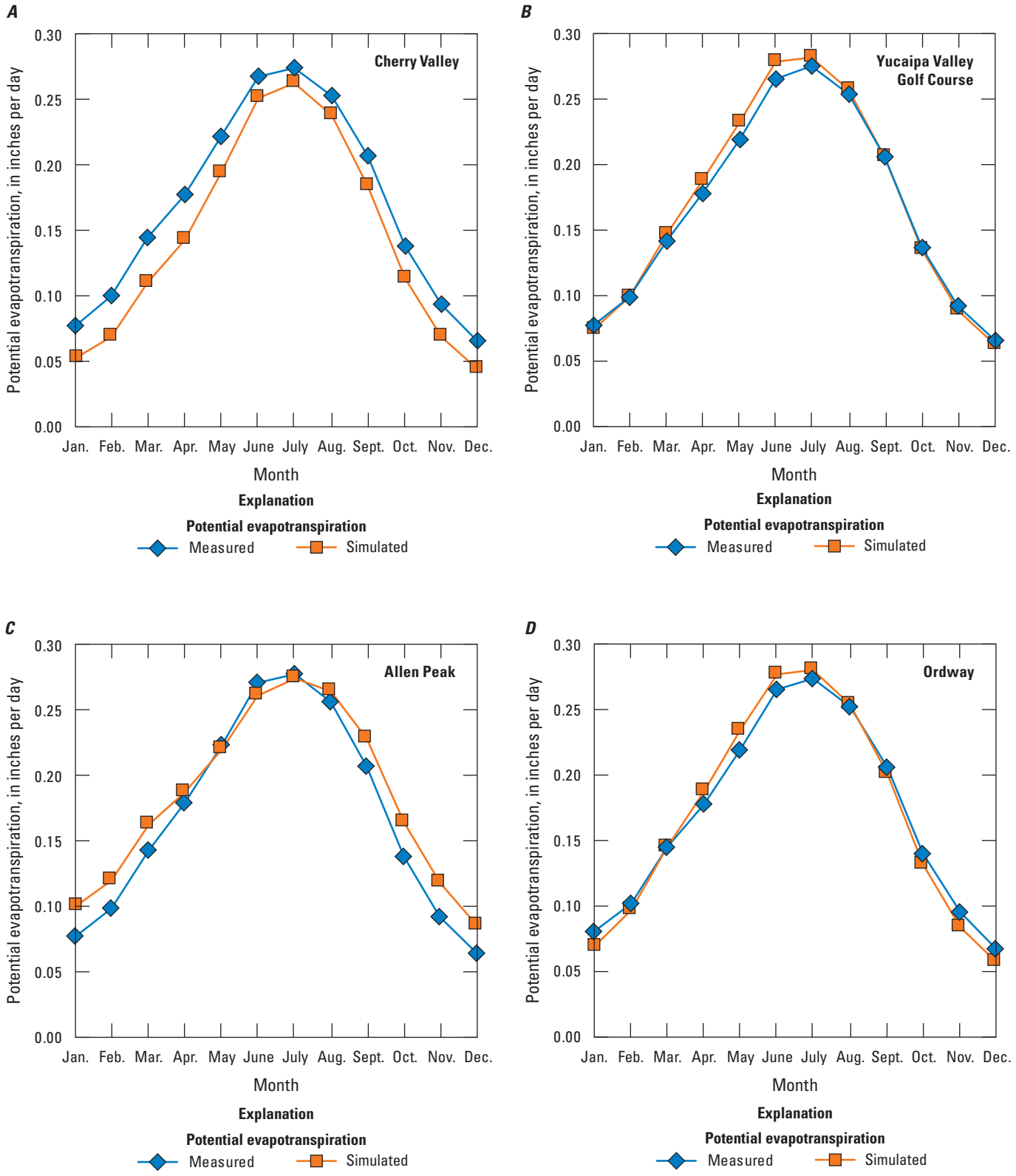

Figure B14. Precipitation Runoff Modeling System (PRMS; Markstrom and others, 2015) simulated mean monthly potential evapotranspiration versus measured data (CIMIS, 2017) for four locations: *A*, Cherry Valley; *B*, Yucaipa Valley; *C*, Allen Peak; and *D*, Ordway in the Yucaipa Valley watershed, San Bernardino and Riverside Counties, California.

Table B4. Summary of final parameter values in Yucaipa Integrated Hydrologic Model, Yucaipa Valley watershed, San Bernardino and Riverside Counties, California.

[ID, identification; ft/day, foot per day; —, not applicable]

Parameter ID	Parameter name	Units	Final value or range of values	Group
	Horizontal hydraulic conductivity (ft/day)			
Kh_1	Layer 1 (fig. B15*A*)	ft/day	3.0×10^{-4} –261	C
Kh_2	Layer 2 (fig. B15*B*)	ft/day	3.0×10^{-4} –265	C
Kh_3	Layer 3 (fig. B15*C*)	ft/day	3.0×10^{-4} –284	C
Kh_4	Layer 4 (fig. B15*D*)	ft/day	8.2×10^{-4} –261	C
	Vertical hydraulic conductivity (ft/day)			
Kv_1	Layer 1 (fig. B16*A*)	ft/day	3.4×10^{-5} –31	C
Kv_2	Layer 2 (fig. B16*B*)	ft/day	3.4×10^{-5} –36	C
Kv_3	Layer 3 (fig. B16*C*)	ft/day	1.3×10^{-4} –33	C
Kv_4	Layer 4 (fig. B16*D*)	ft/day	4.1×10^{-4} –28	C
	Specific yield (dimensionless)			
Sy_1	Layer 1 (fig. B18*A*)	—	0.06–0.085	D
Sy_4	Layer 4 (fig. B18*D*)	—	0.07–0.084	D
	Specific storage (1/ft)			
Ss_2	Layer 2 (fig. B18*C*)	1/ft	8.0×10^{-5} –8.0×10^{-6}	D
Ss_4	Layer 3 (fig. B18*A*)	1/ft	8.0×10^{-5} –8.0×10^{-6}	D
	Hydraulic characteristic (1/day)			
hfb_1	Banning fault (inactive)	1/day	1.02×10^{01}	F
hfb_2	Banning fault (active)	1/day	7.56×10^{-5}	F
hfb_3	Casa Blanca fault	1/day	3.38×10^{00}	F
hfb_4	Cherry Valley thrust fault	1/day	5.46×10^{-6}	F
hfb_5	Chicken Hill fault (segment 5)	1/day	1.53×10^{-2}	F
hfb_6	Chicken Hill fault (segment 6)	1/day	5.69×10^{-2}	F
hfb_7	Chicken Hill fault (segment 7)	1/day	4.71×10^{-06}	F
hfb_8	Chicken Hill fault (segment 8)	1/day	2.42×10^{-05}	F
hfb_9	Live Oak Canyon fault zone	1/day	1.02×10^{01}	F
hfb_10	San Andreas fault zone	1/day	6.66×10^{00}	F
hfb_11	South Mesa Barrier (segment 11)	1/day	7.71×10^{-01}	F
hfb_12	South Mesa Barrier (segment 12)	1/day	1.05×10^{00}	F
hfb_13	South Mesa Barrier (segment 13)	1/day	9.68×10^{-01}	F
hfb_14	Crafton Hills fault	1/day	2.68×10^{-01}	F
hfb_15	Yucaipa graben complex (segment 15)	1/day	1.74×10^{-02}	F
hfb_16	Yucaipa graben complex (segment 16)	1/day	8.16×10^{-01}	F
Hfb_17	Cherry Valley thrust fault (segment 17)	1/day	1.12×10^{-02}	F
Hfb_18	Cherry Valley thrust fault (segment 18)	1/day	1.12×10^{-02}	F
	Streambed hydraulic conductivity (ft/day)			
sfr_0	Streambed conductivity	ft/day	9.88×10^{00}	G
sfr_1	Streambed conductivity	ft/day	3.13×10^{-03}	G
sfr_2	Streambed conductivity	ft/day	1.38×10^{-01}	G
sfr_3	Streambed conductivity	ft/day	2.12×10^{00}	G
sfr_4	Streambed conductivity	ft/day	4.26×10^{-02}	G

Table B4. Summary of final parameter values in Yucaipa Integrated Hydrologic Model, Yucaipa Valley watershed, San Bernardino and Riverside Counties, California.—Continued

[ID, identification; ft/day, foot per day; —, not applicable]

Parameter ID	Parameter name	Units	Final value or range of values	Group
sfr_5	Streambed conductivity	ft/day	8.45×10^{00}	G
	Streambed hydraulic conductivity (ft/day)—Continued			
sfr_6	Streambed conductivity	ft/day	2.07×10^{01}	G
sfr_7	Streambed conductivity	ft/day	2.35×10^{01}	G
sfr_8	Streambed conductivity	ft/day	3.49×10^{00}	G
sfr_9	Streambed conductivity	ft/day	1.89×10^{01}	G
sfr_10	Streambed conductivity	ft/day	6.03×10^{00}	G
	Hydraulic conductivity of general head boundaries (ft/day)			
bc_0	Mill Creek	ft/day	4.18×10^{-01}	E
bc_1	Crafton	ft/day	1.79×10^{-07}	E
bc_2	Redlands (1)	ft/day	5.87×10^{-06}	E
bc_3	Redlands (2)	ft/day	5.00×10^{02}	E
bc_4	Beaumont	ft/day	1.08×10^{-06}	E
	Unsaturated Zone Flow and Evapotranspiration (ET)			
UZF_ET	ET extinction depth	ft	5.74	H
UZF_SURFK	Surface hydraulic conductivity	ft/day	1.9×10^{-03}	H
UZF_KVS	Vertical conductivity	ft/day	1.0×10^{-3}–0.51	H
	Precipitation Runoff Modeling System (PRMS) parameters			
sat_threshold_fac	sat_threshold multiplier	—	0.95	B
soil2gw_max_fac	soil2gw_max multiplier	—	0.96	B
soil_moist_max_fac	soil_moist_max multiplier	—	0.95	B
soil_rechr_max_fac	soil_rechr_max multiplier	—	1.04	B
ssr2gw_rate_fac	ssr2gw_rate multiplier	—	0.96	B
rain_adj_ave	Average rain adjustment factor	—	1.09	B
anth_rech_depth	Anthropogenic recharge	ft/day	Table B5	B

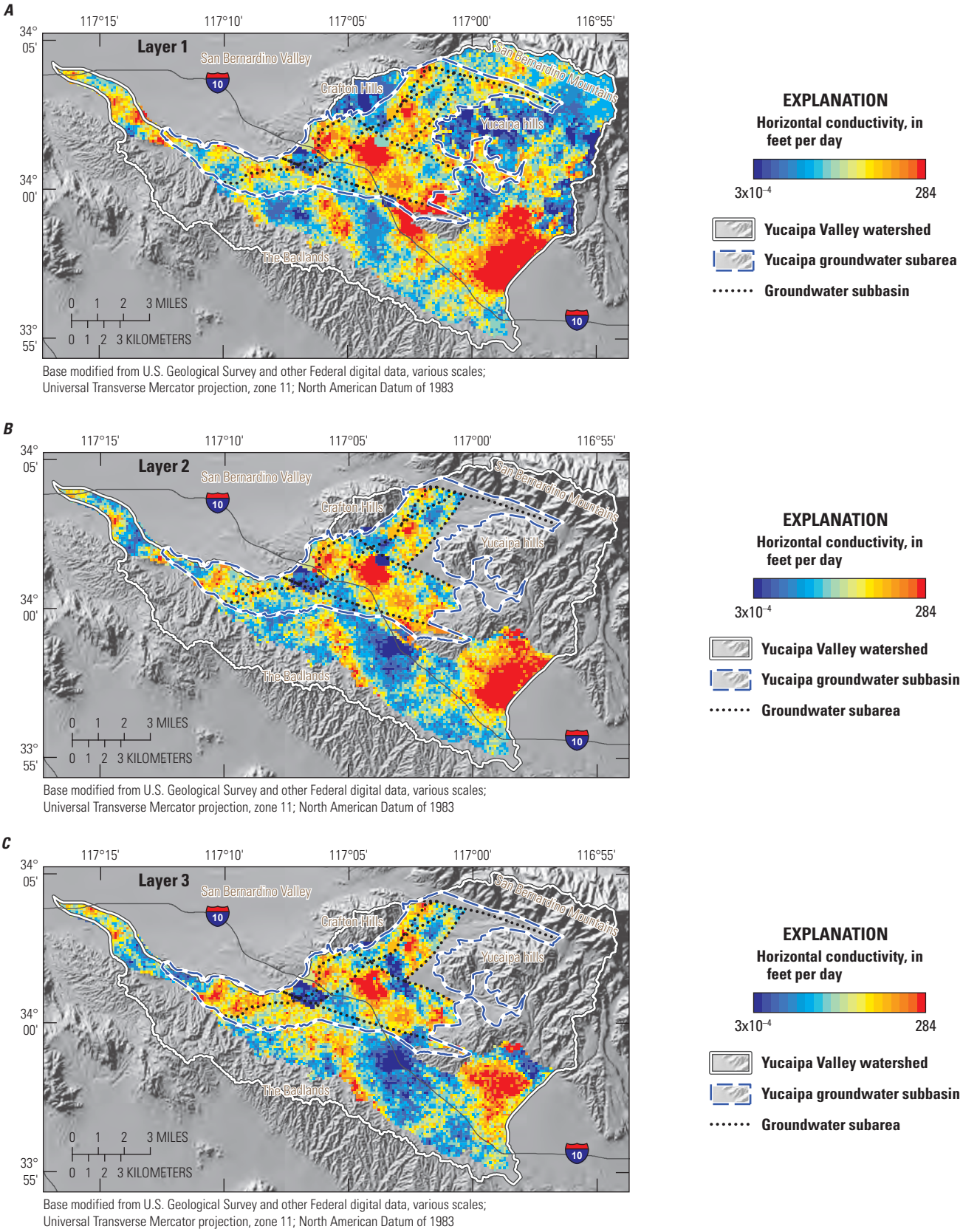

Figure B15. Estimated horizontal hydraulic conductivity for the Yucaipa Integrated Hydrologic Model, *A*, layer 1; *B*, layer 2; *C*, layer 3; and *D*, layer 4. Locations of pump test wells are shown in *D* (Geoscience Support Services, Inc., 2014), Yucaipa Valley watershed, San Bernardino and Riverside Counties, California.

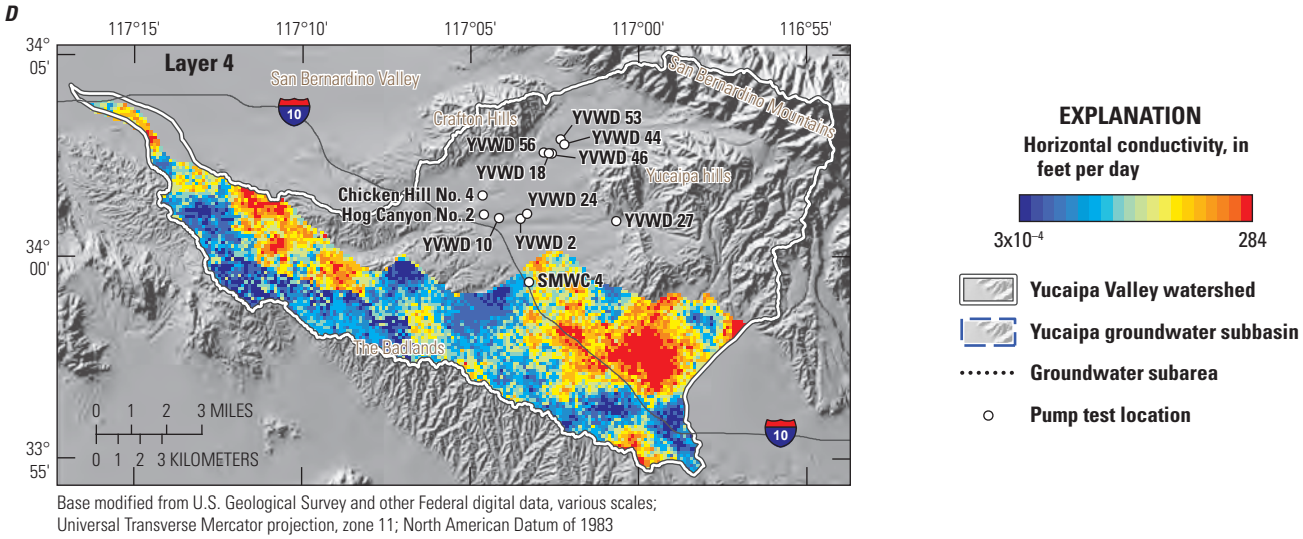

Base modified from U.S. Geological Survey and other Federal digital data, various scales; Universal Transverse Mercator projection, zone 11; North American Datum of 1983

Figure B15.—Continued

The HK values obtained from the calibrated YIHM were evaluated using reported HK values estimated from pumping tests at 12 well locations (Geoscience Support Services, Inc., 2014; figs. B15, B17); multiple tests were conducted for 10 of these wells. The calibrated HK is at the scale of the finite-difference cell size (492.13 ft), and the pumping tests can have a scale of several hundred feet; therefore, the average HK values from the pumping tests were compared with the calibrated HK values by averaging the calibrated HK values over the radius of influence (1,969 ft, equivalent to four finite difference cells; Cooper and Jacob, 1946). The calibrated HK values in layers 1 and 2 were averaged using (1) the harmonic mean, which provided the lowest effective value; (2) the geometric mean, which provided an intermediate value; and (3) the arithmetic mean which provided the highest effective value. Figure B17 shows the comparison between the average calibrated HK values and the average HK values from the pump tests. Figure B17 shows the general agreement between calibrated HK averages and reported HK values from pumping tests. The results show that HK values from pumping tests were generally bounded by the calibrated HK arithmetic and harmonic means and were often close to the calibrated geometric mean, indicating that the calibrated HK values reasonably agree with the pumping test data (fig. B17).

The distributions of calibrated specific-yield values (Sy) for layers 1 and 4 are shown in figure B18 and ranged between 0.06 and 0.085 (Sy is dimensionless); calibrated specific-storage (Ss) for layers 2 and 3 ranged from 8.0×10^{-6} to 8.0×10^{-5} 1/ft. Calibrated Sy values shown in figure B18 are similar to previous estimates of Sy from Eckis (1934; see fig. A13 in chapter A). The relatively low estimates of Sy in the Yucaipa subbasin are representative of semi-confined conditions and consistent with previous estimates (California Department of Water Resources, 1967).

Horizontal-Flow Barriers

The HFBs simulated in the YIHM are shown in figure B9 and their calibrated values for the hydraulic characteristic are listed in table B4. The calibrated hydraulic characteristic values ranged from 6.66 (1/day) for the San Andreas fault zone (table B4; fig. B9) to 4.71×10^{-6} (1/day) for the Chicken Hill fault (segment 7; table B4; fig. B9), indicating a range of barrier effectiveness from no barrier to restrictive barrier.

The measured groundwater-head difference across the Chicken Hill fault, which separates the Western Heights and Calimesa subareas along its southern extent, can be more than 300 ft (see fig. A23 in chapter A). To simulate this difference in groundwater levels, the calibrated hydraulic characteristics for the Chicken Hill fault (segment 7) was 4.71×10^{-6} (1/day) near the Western Heights subarea where the difference in groundwater levels is greatest; near the Wilson Creek subarea, the Chicken Hill fault (segment 6) is a less restrictive barrier with a calibrated value of 5.69×10^{-2} (1/day).

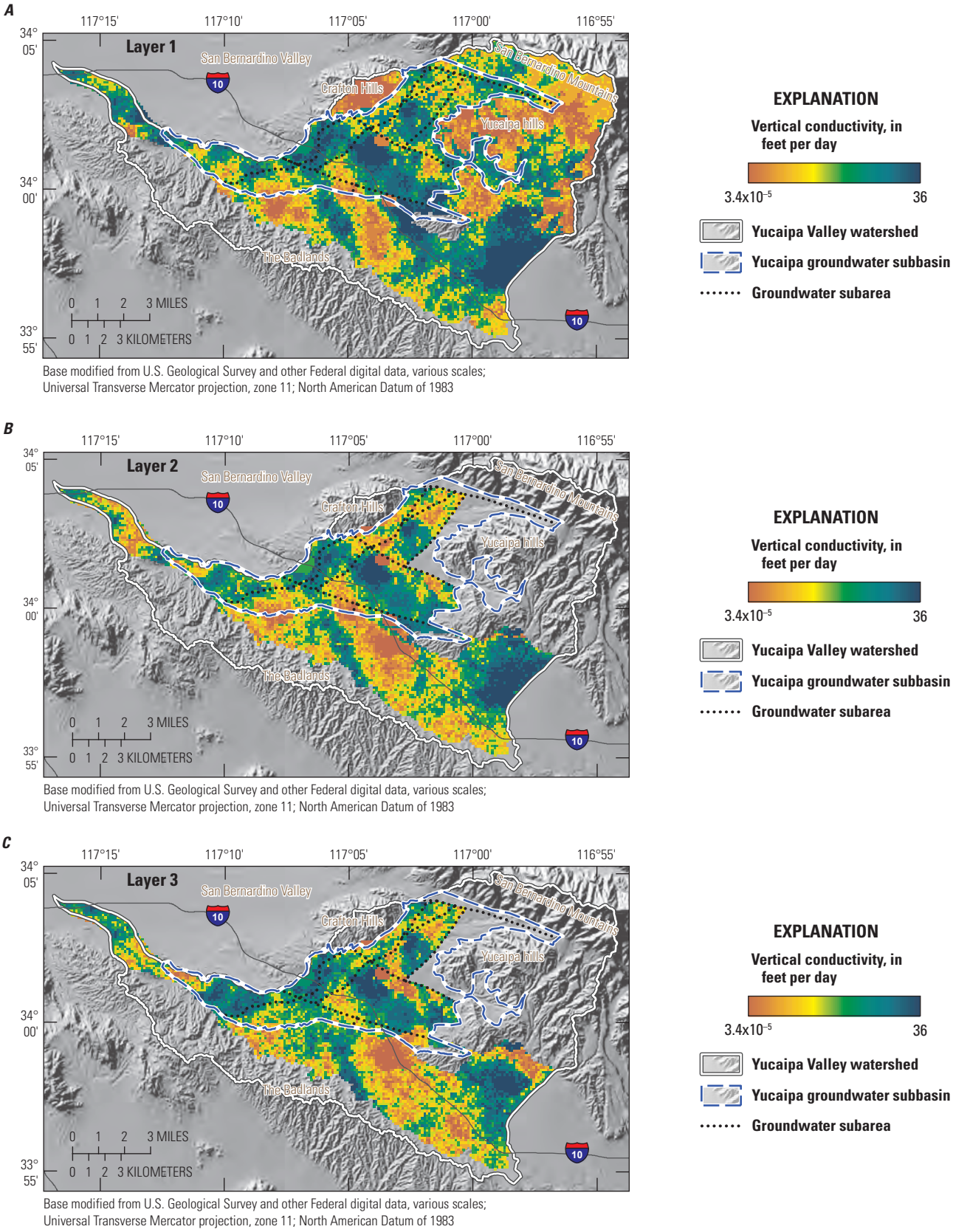

Figure B16. Estimated vertical hydraulic conductivity for the Yucaipa Integrated Hydrologic Model, *A*, layer 1; *B*, layer 2; *C*, layer 3; and *D*, layer 4, Yucaipa Valley watershed, San Bernardino and Riverside Counties, California.

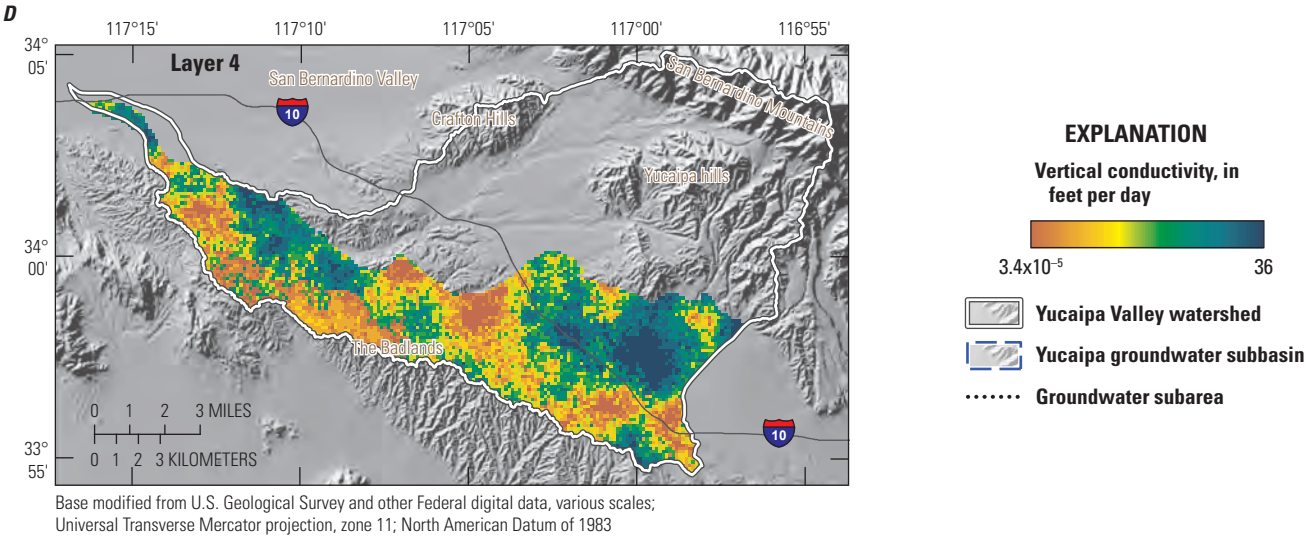

Figure B16.—Continued

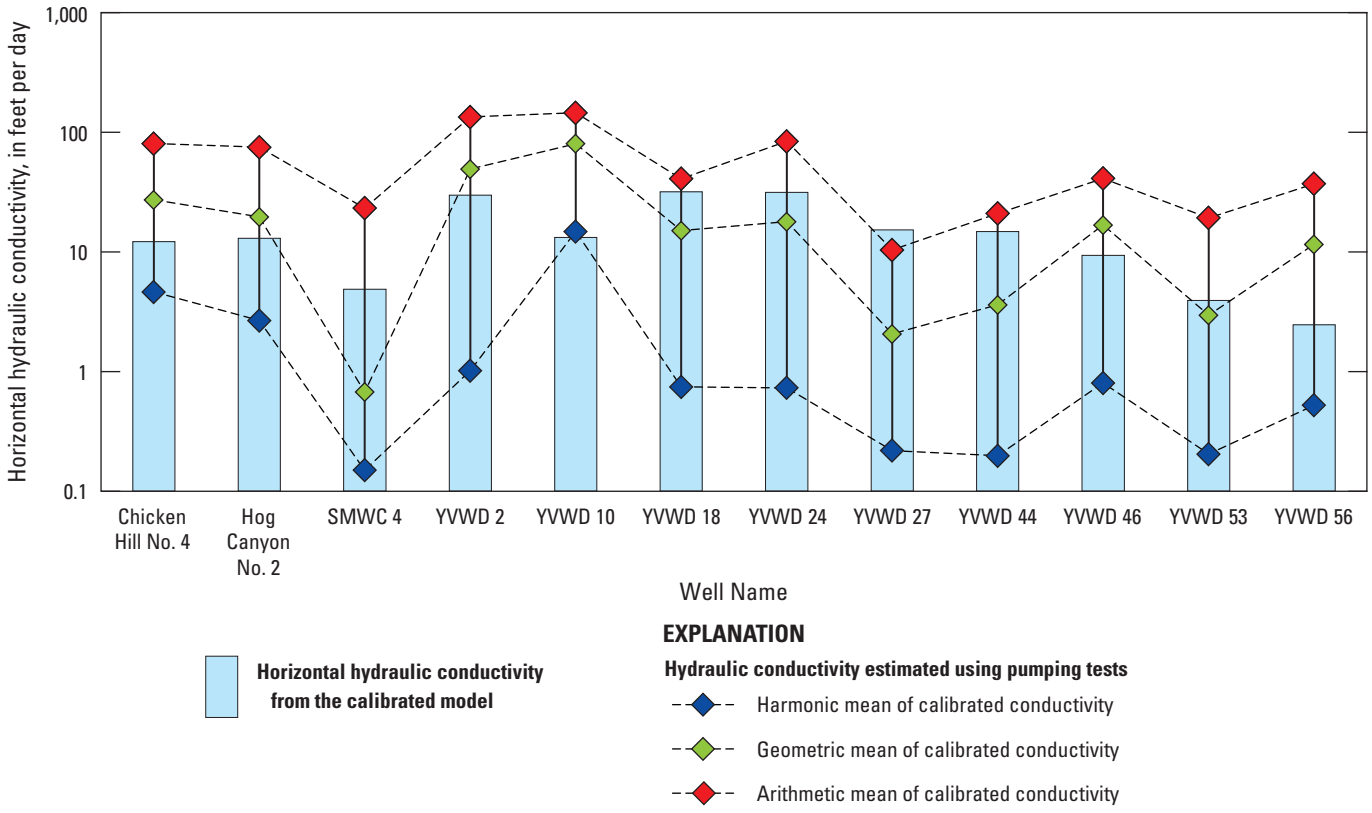

Figure B17. Comparison between calibrated horizontal hydraulic conductivity from the Yucaipa Integrated Hydrologic Model and reported horizontal hydraulic conductivity values from pumping tests (Geoscience Support Services, Inc., 2014), Yucaipa Valley watershed, San Bernardino and Riverside Counties, California. (SMWC, South Mesa Water Company; YVWD, Yucaipa Valley Water District)

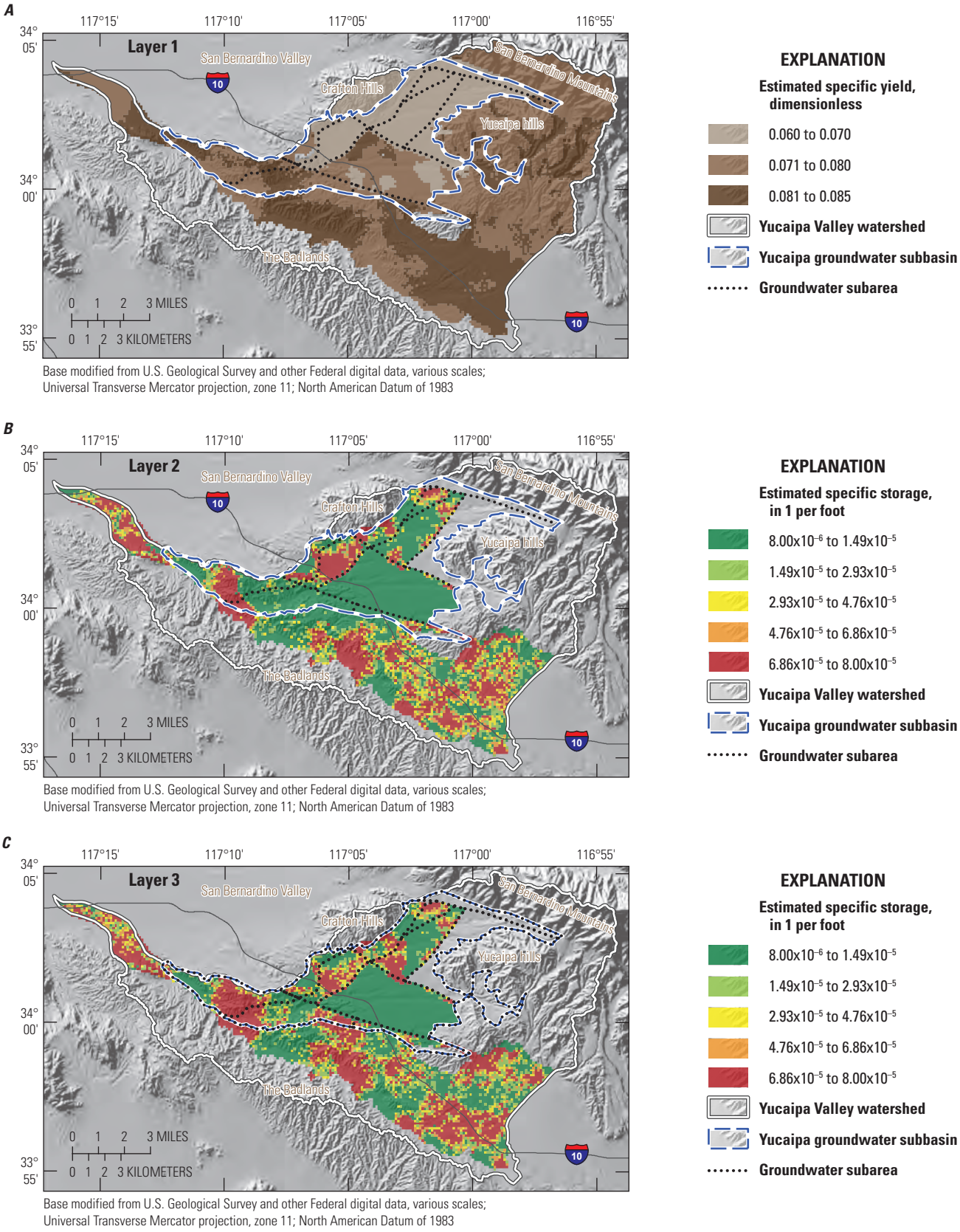

Figure B18. Calibrated specific yield for the unconfined parts of, *A*, layer 1 and, *D*, layer 4; and calibrated specific storage for, *B*, layer 2 and, *C*, layer 3 in Yucaipa Integrated Hydrologic Model, Yucaipa Valley watershed, San Bernardino and Riverside Counties, California.

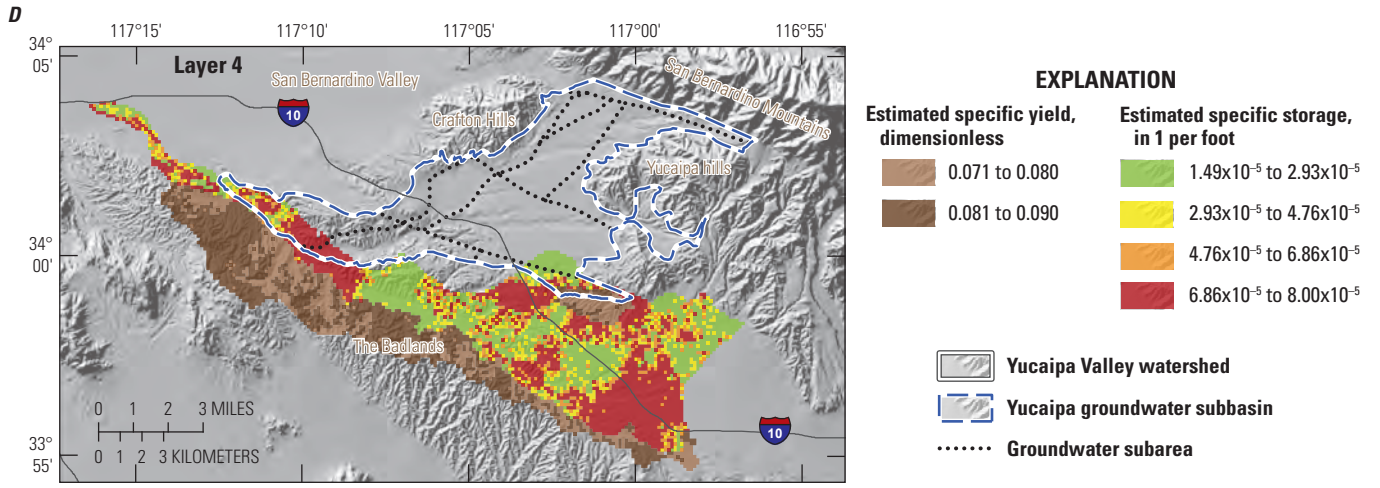

Base modified from U.S. Geological Survey and other Federal digital data, various scales; Universal Transverse Mercator projection, zone 11; North American Datum of 1983

Figure B18.—Continued

Streambed Hydraulic Conductivity

The estimated streambed conductivity ranged between 3.13×10^{-3} and 23.5 ft/d (table B4). The calibrated streambed conductivity value for stream network zone 9 (sfr_9; table B4; fig. B5), which includes Wilson Creek and parts of Oak Glen Creek, was comparatively high (18.9 ft/d; table B4). The presence of flood-control structures enhances stream seepage into the aquifer in this area. These structures are not explicitly represented in the model; however, the enhancement of stream seepage is simulated by a high streambed conductivity for the stream segments in sfr_9.

General-Head Boundary Parameters

The calibrated hydraulic conductivities of the five GHBs (fig. B9) are shown in table B4. These hydraulic conductivities were used to calculate the boundary conductance. Calibration results showed that the hydraulic conductivity values for the Crafton, Redlands (1) and Beaumont GHBs generally were relatively low (1.79×10^{-7}–5.87×10^{-6} ft/d) and indicated limited groundwater flow along these boundaries. The calibrated hydraulic conductivity for the Redlands (2) GHB was high (500 ft/d) and indicated groundwater may flow freely to the adjacent groundwater subbasin along this boundary.

Unsaturated Zone Parameters

The calibrated UZF1 parameters (table B4) consisted of ET extinction depth, ground-surface hydraulic conductivity, and VKS of the UZ. The calibrated riparian and non-riparian ET extinction depths were 5.74 and 2.87 ft, respectively. The ground-surface hydraulic conductivity (SURFK), along with the VKS of the UZ, control the rate of rejected infiltration and surface leakage outflow calculated by the YIHM. The calibrated value of SURFK was 1.90×10^{-3} ft/d. The distribution of VKS is shown in figure B19. The VKS also was important in the simulation of the rate and timing of groundwater deep percolation and the rate of groundwater ET. In zones with possible perched aquifers, low VKS values mimicked the average effect of low permeable sediments on the rate and timing of deep percolation. Calibrated VKS values for the unsaturated zone ranged from 1.6×10^{-3} to 0.51 ft/d (table B4).

Recharge Parameters

Recharge in the YIHM includes naturally occurring recharge from precipitation and anthropogenic recharge. The PRMS parameters controlling natural recharge were estimated in two phases. Parameters *dday_intcp, dday_slope,* and *jh_coef* were estimated in stage 1, and initial values are given in table B1. The PRMS parameters adjusted in stage 2 were *sat_threshold, soil2gw_max, soil_moist_max, soil_rechr_max,* and *ssr2gw_rate*. These spatially variable parameters were calibrated by adjusting multipliers for each parameter distribution. The calibrated values of the multipliers were close to 1.0, indicating that these parameter distributions were not changed substantially from their initial values.

The spatially variable rain-adjustment parameter (*rain_adj*) was calibrated by adjusting a multiplier for the mean of the parameter distributed to each PRMS HRU. The optimal average rain adjustment was 1.09 (table B4), which is 32 percent smaller than the initial rain adjustment factors computed using PRISM data (PRISM Climate Group, 2013). A possible reason for this reduction is that the estimated precipitation input in the YIHM was largely based on measured data from climate station 47306 Redlands, which is outside the study area (fig. A4); therefore, rain adjustment factors may not reflect the actual spatial variability

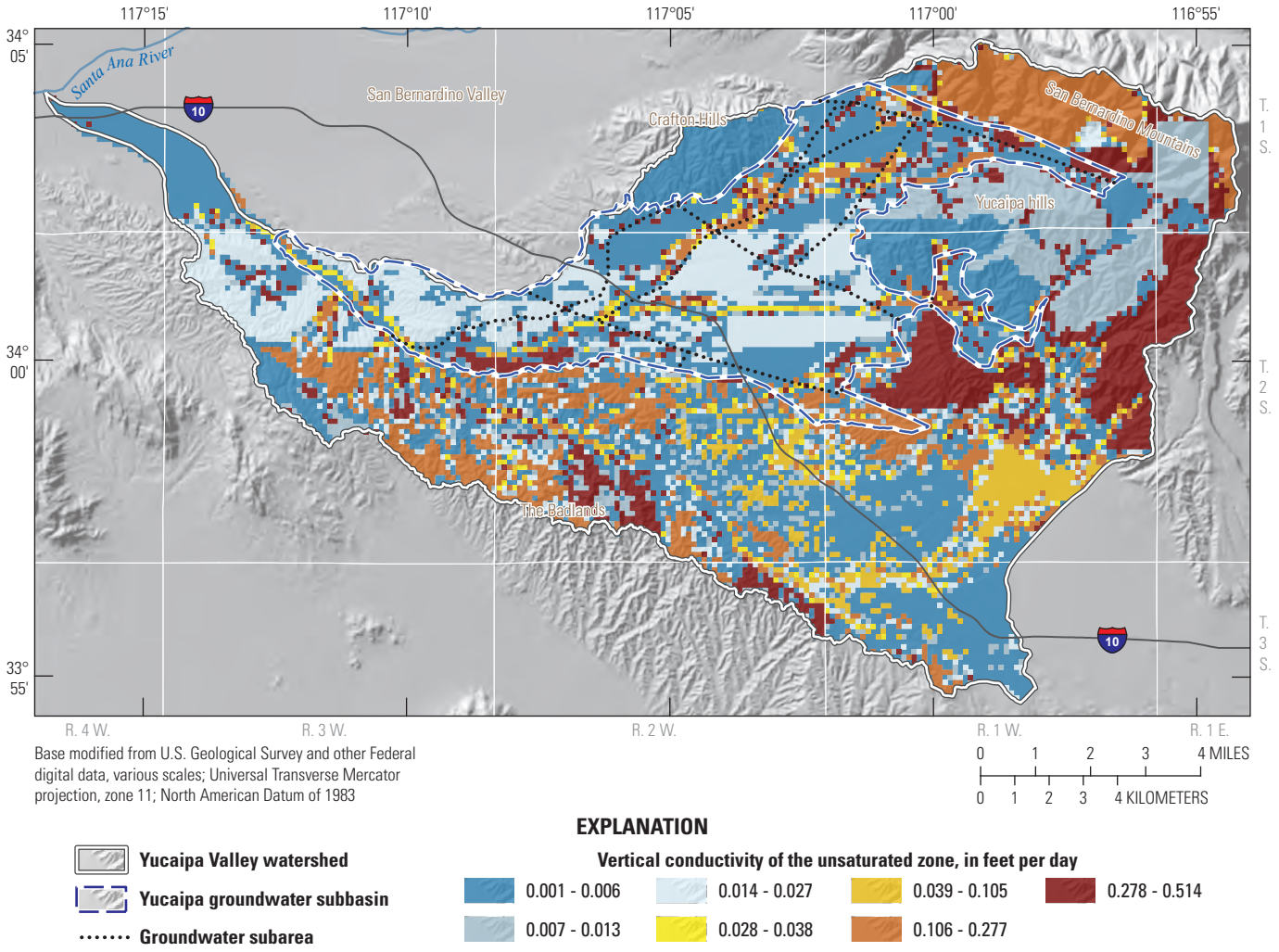

Figure B19. Calibrated vertical hydraulic conductivity field of the unsaturated zone in the Yucaipa Integrated Hydrologic Model, Yucaipa Valley watershed, San Bernardino and Riverside Counties, California.

of precipitation, particularly at locations far from the climate station. To test this possibility, data for the period 1998–2018 from two climate stations (45617 and 45109; fig. B6; Western Regional Climate Center, 2011) were used to evaluate the PRISM-based adjustment factors. The average PRISM-based adjustment factors at climate stations 45617 and 45109 were 1.36 and 1.63, respectively, while the actual average adjustment factors calculated from measured data were 1.03 and 1.26, respectively. These results indicate that PRISM-based calculations for the YIHM overestimate rain adjustment factors at both climate station locations by about 30 percent, which is consistent with the calibrated average rain adjustment factor.

The anthropogenic recharge rate was calibrated for each subarea (fig. A3*C*). The parameters were defined as constant rates for 10 different periods (table B5) to account for changes of anthropogenic recharge with time. The resulting anthropogenic recharge rates for each subarea are presented in table B5. The estimated anthropogenic recharge rates ranged from 3.1×10^{-8} ft/d in the Cherry Valley subarea to 2×10^{-3} ft/d in the Calimesa subarea.

Table B5. Estimated anthropogenic recharge rates (in feet per day) in each groundwater subarea (fig. A3*C*), Yucaipa Integrated Hydrologic Model, Yucaipa Valley watershed, San Bernardino and Riverside Counties, California.

Period	Cherry Valley	Calimesa	Live Oak	Wildwood	Western Heights	Oak Glen	Sand Canyon	Wilson Creek	Crafton	Triple Falls Creek	Gateway
1947–69	1.47×10^{-06}	2.60×10^{-05}	1.65×10^{-06}	7.05×10^{-05}	1.20×10^{-04}	6.63×10^{-04}	3.01×10^{-05}	8.09×10^{-04}	6.83×10^{-04}	2.24×10^{-04}	8.43×10^{-04}
1970–74	8.35×10^{-06}	1.28×10^{-04}	4.72×10^{-06}	5.29×10^{-05}	3.68×10^{-04}	5.86×10^{-04}	1.33×10^{-04}	9.99×10^{-04}	6.19×10^{-04}	1.82×10^{-04}	7.08×10^{-04}
1975–79	1.34×10^{-05}	2.22×10^{-04}	6.71×10^{-06}	5.24×10^{-05}	3.28×10^{-04}	5.93×10^{-04}	1.15×10^{-04}	1.02×10^{-03}	6.13×10^{-04}	1.80×10^{-04}	7.00×10^{-04}
1980–84	9.26×10^{-05}	1.40×10^{-03}	3.62×10^{-05}	2.45×10^{-05}	5.26×10^{-05}	2.41×10^{-04}	1.51×10^{-05}	4.00×10^{-04}	2.07×10^{-04}	6.29×10^{-05}	2.48×10^{-04}
1985–89	2.34×10^{-04}	2.44×10^{-03}	9.15×10^{-05}	3.11×10^{-05}	9.21×10^{-05}	3.79×10^{-04}	2.66×10^{-05}	6.37×10^{-04}	2.83×10^{-04}	8.80×10^{-05}	3.55×10^{-04}
1990–94	1.55×10^{-07}	1.14×10^{-05}	2.03×10^{-06}	4.55×10^{-05}	4.61×10^{-04}	2.35×10^{-04}	1.86×10^{-04}	3.54×10^{-04}	1.71×10^{-04}	7.83×10^{-05}	2.80×10^{-04}
1995–99	1.55×10^{-07}	1.37×10^{-05}	3.20×10^{-06}	4.60×10^{-05}	9.35×10^{-04}	2.80×10^{-04}	3.93×10^{-04}	4.26×10^{-04}	2.82×10^{-04}	8.48×10^{-05}	5.67×10^{-04}
2000–04	3.10×10^{-08}	1.44×10^{-05}	3.23×10^{-06}	5.65×10^{-05}	1.01×10^{-03}	3.11×10^{-04}	4.20×10^{-04}	5.85×10^{-04}	4.87×10^{-04}	9.43×10^{-05}	8.10×10^{-04}
2005–09	3.10×10^{-08}	1.84×10^{-05}	1.88×10^{-06}	5.76×10^{-05}	6.10×10^{-04}	4.25×10^{-04}	2.41×10^{-04}	1.56×10^{-03}	1.10×10^{-03}	1.08×10^{-04}	1.76×10^{-03}
2010–14	3.10×10^{-08}	2.43×10^{-05}	2.01×10^{-06}	6.43×10^{-05}	6.31×10^{-04}	6.80×10^{-04}	2.43×10^{-04}	1.92×10^{-03}	1.45×10^{-03}	1.89×10^{-04}	2.23×10^{-03}

Sensitivity and Identifiability of Estimated Parameters

Sensitivity analysis is an essential procedure to diagnose calibration results. A model sensitivity analysis evaluates the degree to which changes in model input parameters affect model responses. Sensitivity analysis is not limited to determining parameters with the greatest effect on model predictions. Sensitivity analysis also can be used to evaluate parameter identifiability (Doherty and Hunt, 2009) and uncertainties. During PEST calibration, the sensitivity (local gradient) of each observation-parameter combination is computed at each calibration iteration as follows,

$$\frac{\partial y_i}{\partial b_j} \tag{B2}$$

where

∂y_i is the infinitesimal change in model response,
∂b_j is the infinitesimal change in model parameter,
i and j are the indices of model response and model parameter, respectively.

In practice, the gradient is approximated using a finite difference scheme $\frac{\Delta y_i}{\Delta_{b_j}}$, which is evaluated by running the model using a perturbed parameter value (usually perturbation fraction is equal to 1 percent). The resulting combinations of all the sensitivities of simulated observations with respect to parameters constitutes the Jacobian matrix.

The need to assess the sensitivity of multiple model responses to a change in one parameter gives rise to the composite sensitivity (*cs*) statistic, which is the weighted average of a parameter's sensitivity. A drawback of the *cs* statistic is that its value depends on the units of the parameter and thus does not reflect the relative importance of the parameter; therefore, *cs* needs to be scaled by the parameter magnitude to produce the dimensionless composite scaled sensitivity (*css*) statistic, which is computed as follows:

$$css_j = \sqrt{\left(\sum_{i=1}^{ND}\left(\frac{\partial y_i}{\partial b_j}\right)|b_j|\sqrt{w_{ii}}\right)/ND} \tag{B3}$$

where

ND is the number of observations and
w_{ii} is the weight of observation i.

Several parameters were used to calibrate the YIHM; however, only the top 20 important (sensitive) parameters are presented in figure B20. The most sensitive parameter was the streambed conductivity of stream network zone 9 (sfr_9; table B4; figs. B5, B20), which represents streambed conductivity in Wilson Creek and in parts of Oak Glen Creek. The high sensitivity of this parameter demonstrated the important role that flood-control structures and MAR spreading basins in Wilson Creek play in restricting stream water outflow and enhancing stream water leakage into the YIHM aquifer. The second most sensitive parameter is the conductance of the Casa Blanca fault (hfb_3; fig. B9; table B4).

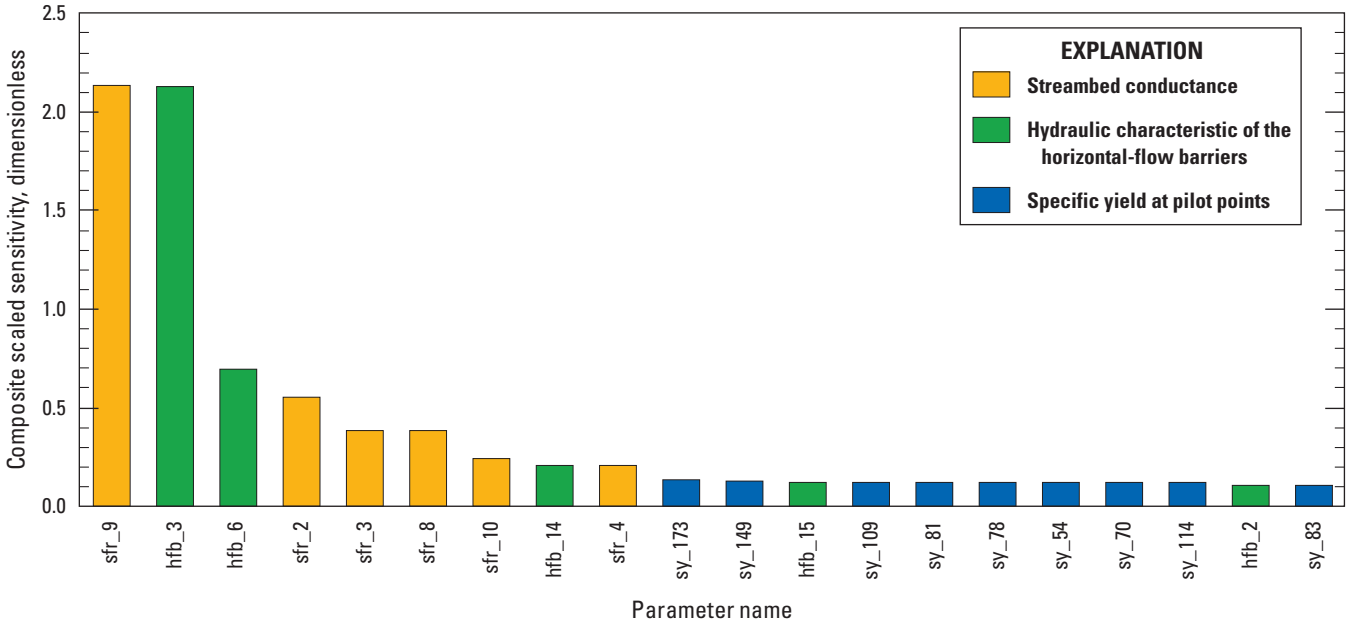

Figure B20. Composite scaled sensitivities for the top 20 sensitive model parameters estimated for the Yucaipa Integrated Hydrologic Model, Yucaipa Valley watershed, San Bernardino and Riverside Counties, California.

One limitation of using parameter sensitivities to assess calibration results is the issue of parameter correlation. When a pair of parameters is highly correlated, the *css* metric can be misleading and does not reflect the actual importance of the two parameters; therefore, evaluation of both *css* metric and correlation coefficients among important parameters is necessary. A pair of parameters that are perfectly correlated have an absolute value of correlation coefficient equal to 1.0, and a completely uncorrelated pair of parameters has a correlation coefficient that approaches 0.

The correlation matrix is computed by PEST at the end of calibration and provides the correlation coefficients between each pair of parameters. With hundreds of parameters, the number of correlation coefficients is large, making it impractical to assess both sensitivity and correlation for all pairs of parameters. The absolute value of correlation coefficients among the top 10 most sensitive parameters are shown in figure B21. High correlation coefficients of more than 0.9 occur among the most sensitive parameters, including streambed conductance (sfr_2, sfr_3, sfr_8; figs. B5, B20; table B4) and pilot points of the specific yield.

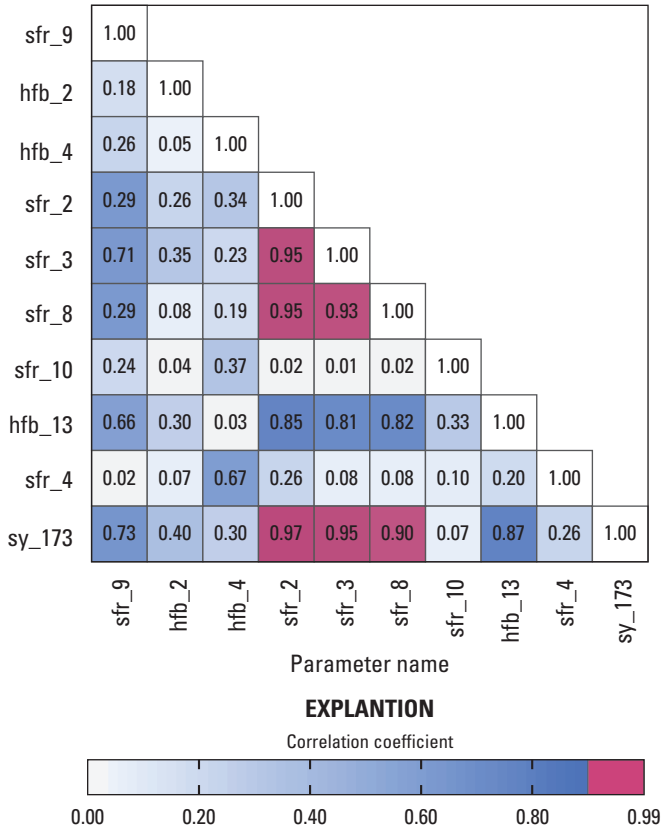

Figure B21. Correlation coefficient matrix among the top 10 sensitive parameters. Correlation coefficients close to 1.0 indicate highly correlated parameters, and correlation coefficients close to zero indicate uncorrelated parameters. Cross-correlation coefficients between different parameters that are greater than 0.9 are highlighted with red color. Yucaipa Integrated Hydrologic Model, Yucaipa Valley watershed, San Bernardino and Riverside Counties, California.

The parameter identifiability metric was computed to assess the sensitivity of correlated parameters (Doherty and Hunt, 2009). The parameter identifiability metric measures the amount of information from observations that is used to estimate a parameter. When computed, parameter identifiability metrics are normalized to have values ranging between 0 and 1.0. Parameters with a high identifiability value (about 1.0) are well informed by observations, while parameters with a low identifiability value (about 0.0) are not informed by the available observations and thus should be fixed at their initial values. Figure B22*A* and B22*B* show the 20 parameters with the highest and lowest computed indefinability metrics, respectively. The total height of each bar indicates the identifiability of the parameter.

Singular Value Decomposition (SVD) is used in the calculation of parameter identifiability to split the parameter space into a solution space (identifiable parameter space) and a null space (unidentifiable parameter space). On each bar of the identifiability graph (fig. B22*A*), the contribution to identifiability due to each singular value is displayed. Each bar is color-coded according to the contributions made to the identifiability by different singular values. Hotter colors indicate identifiability is attributed to the high singular values, whereas areas shaded in colors on the cool end of the color spectrum indicate identifiability is attributed to lower singular values.

Results in figure B22 show that the active strand of the Banning fault (hfb_2; fig. B9) and stream network zone 9 (sfr_9; fig. B5) are both highly identifiable by observations, whereas the VK pilot points (parameters beginning with "vk_" in fig. B22*B*) and the conductance values for all GHBs (bc_1–4), except for the Mill Creek boundary (bc_0), are all largely unidentifiable from the available observations (fig. B22*B*). Some parameters have relatively high composite sensitivities ranks (for example, streambed conductance at stream network zones 2, 3, and 8; sfr_2, sfr_3, sfr_8; fig. B20) but, they have lower identifiability metric ranks because of their high cross-correlations with other parameters. Parameters with low identifiability metrics are mostly dominated by VK pilot points and conductance of the general head boundaries (bc_1, bc_2, bc_3, bc_4; fig. B22*B*).

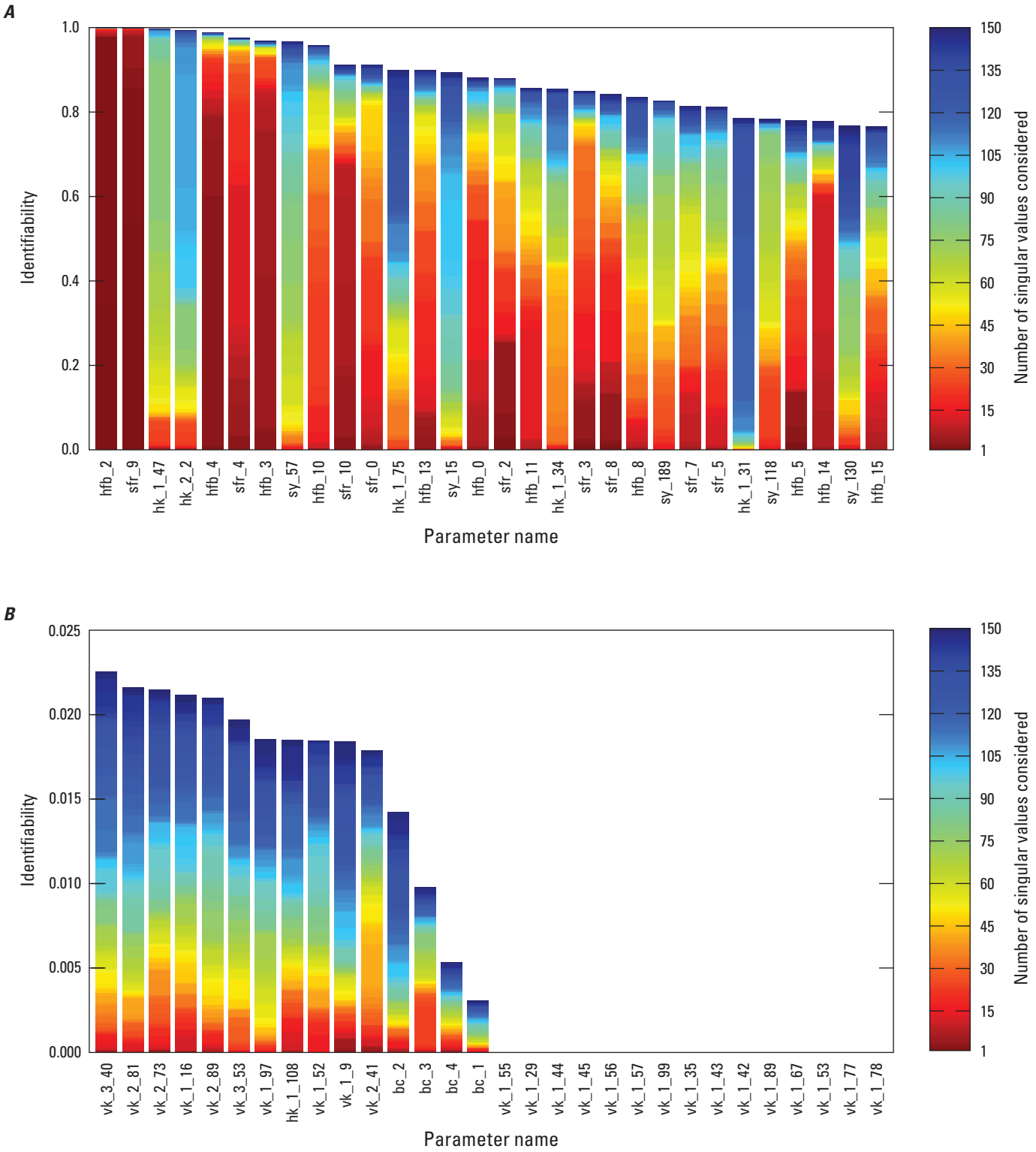

Figure B22. Identifiability of parameters in the Yucaipa Integrated Hydrologic Model, when the higher ranking singular-value parameters are considered; *A*, identifiability of the top 20 identifiable parameters; and *B*, identifiability of the lowest 20 identifiable parameters; red colors represent singular values of higher magnitude (and lower index), and blue colors represent singular values of lower magnitude (and higher index); Yucaipa Valley watershed, San Bernardino and Riverside Counties, California.

Groundwater and Surface-water FLOW Model Fit

Comparisons of simulated heads and measured groundwater-level elevations were used to indicate how well the YIHM replicates the groundwater-flow system for the calibration period 1970–2014 (figs. B23 and B24). Statistical measures of model fit were used in conjunction with graphical and descriptive comparison. Measures of model fit consisted of:

- Model-fit statistics for residuals (the difference between measured groundwater levels and simulated heads), including the mean bias error (MBE), root mean square error (RMSE), and mean absolute error (MAE). The number of groundwater level transient measurements is shown in figure B24*D*.
- Spatial distributions of simulated and measured groundwater-levels.
- Plotting measured groundwater levels against simulated hydraulic heads.

The MBE indicates the average amount of overestimation or underestimation of the model to the observed data. The RMSE is affected disproportionally by large errors. The MAE is the absolute value of the mean of the residuals and indicates the average magnitude of error. The percentages of these error statistics with respect to the range of water-level variability also were computed to evaluate the magnitude of the error. For the RMSE, this value is known as the normalized root mean square error (NRMSE; Anderson and Woessner, 1992). Measured groundwater level elevations within the YVW ranged from about 1,000 to 4,580 ft above sea level (asl), resulting in a variability range of about 3,580 ft.

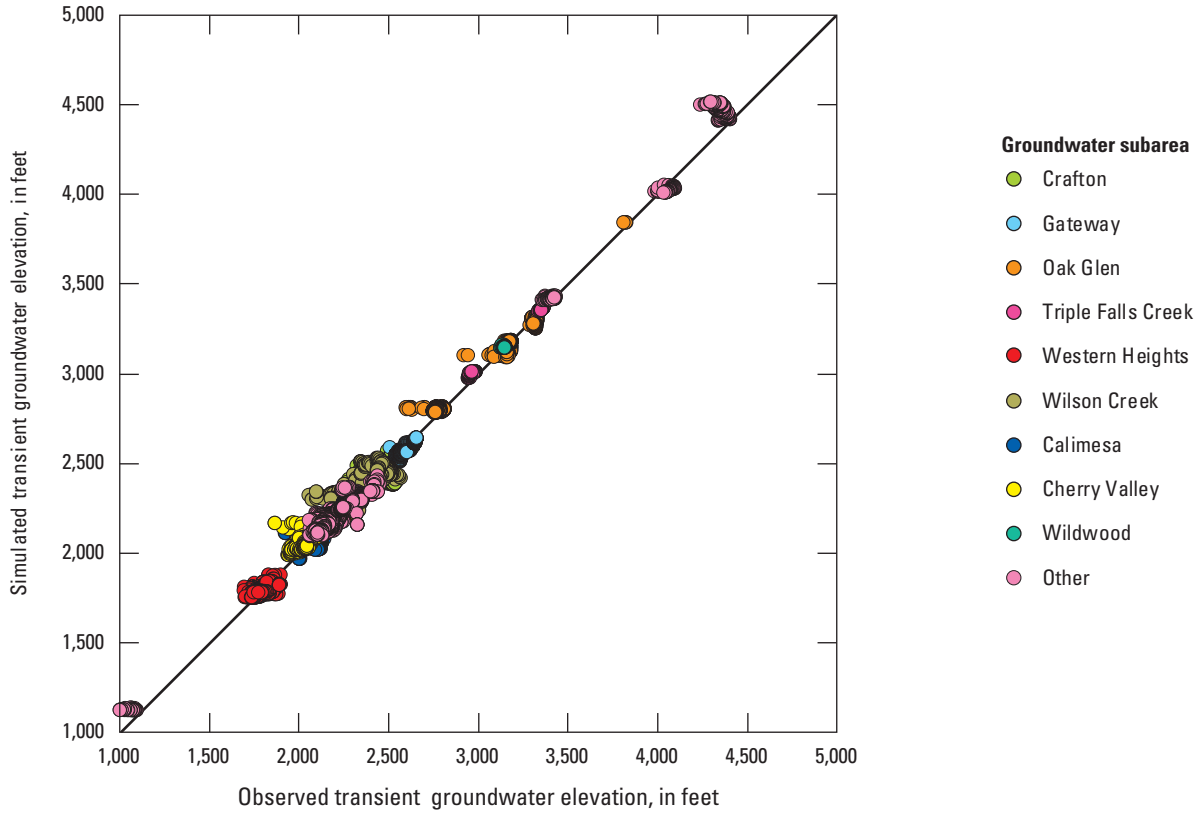

Figure B23. Simulated transient hydraulic heads in the Yucaipa Integrated Hydrologic Model compared with observed groundwater-level elevations for the calibration period 1970–2014 and the 1:1 line, Yucaipa Valley watershed, San Bernardino and Riverside Counties, California.

- Spatial distributions of model-fit statistics.

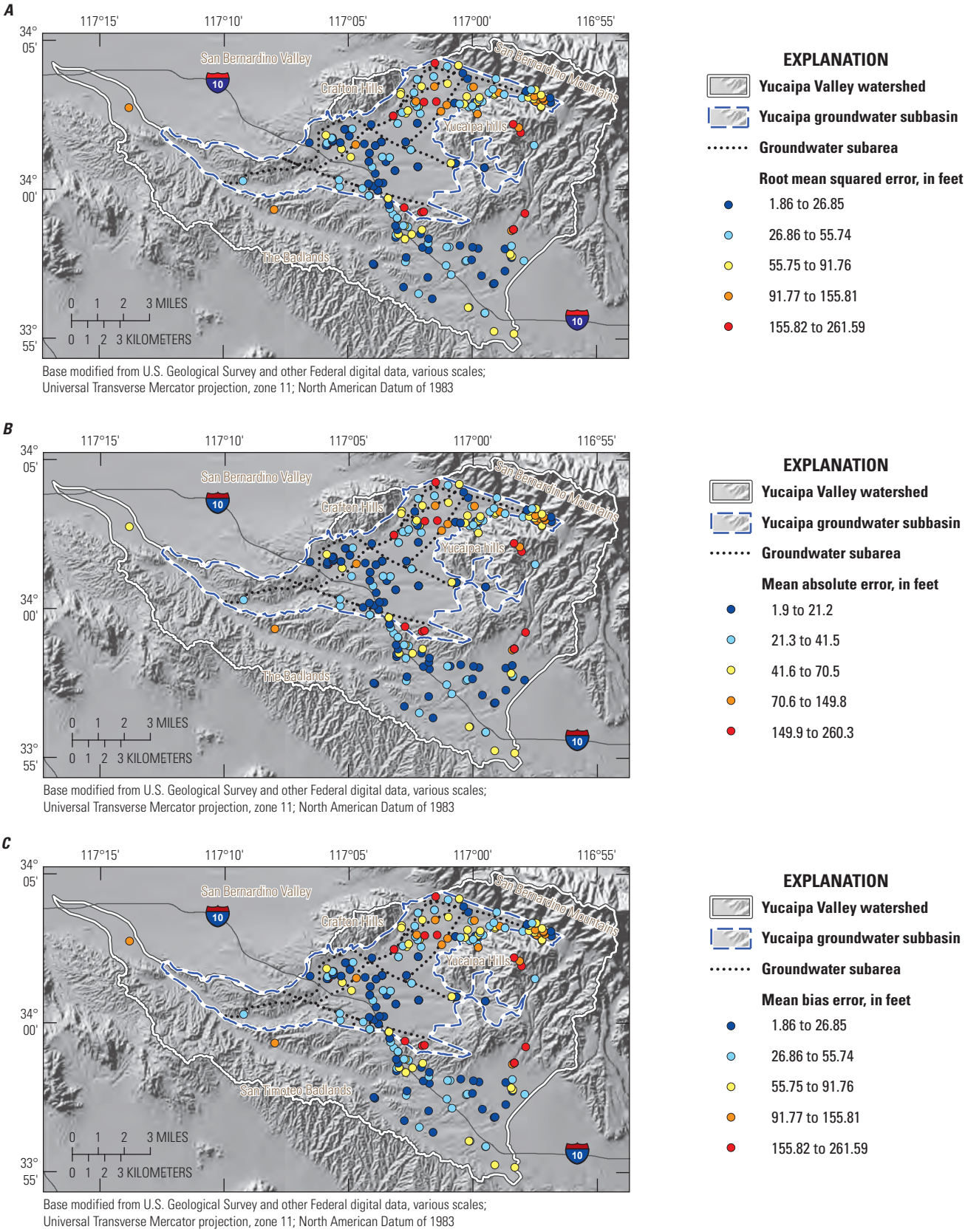

Figure B24. Statistical measures of model fit of the Yucaipa Integrated Hydrologic Model; *A*, root mean square error; *B*, mean absolute error; *C*, mean bias error; and *D*, the number of transient hydraulic head measurements at each well; Yucaipa Valley watershed, San Bernardino and Riverside Counties, California.

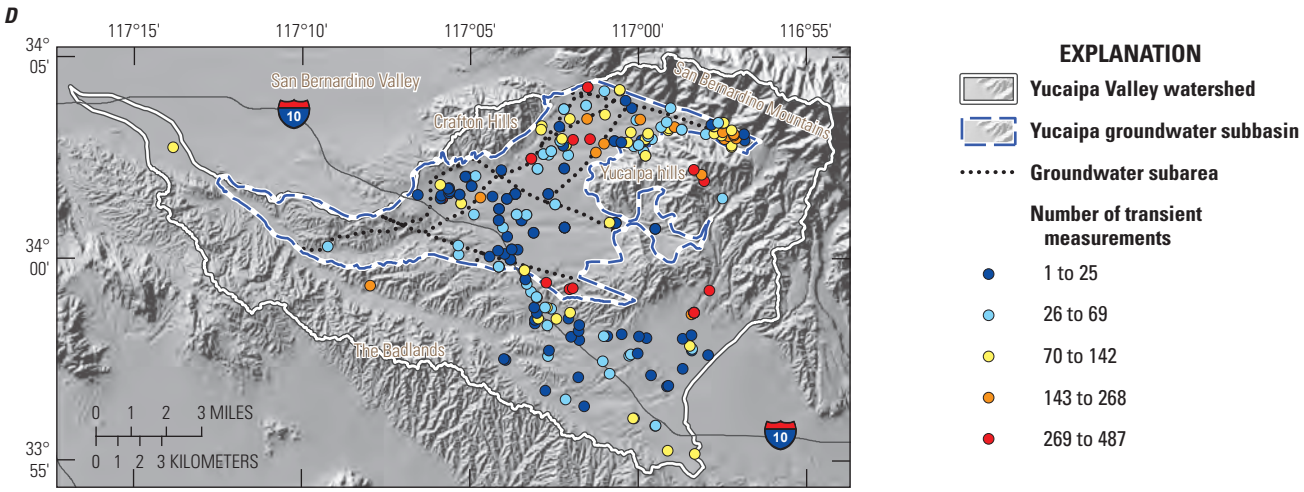

Base modified from U.S. Geological Survey and other Federal digital data, various scales; Universal Transverse Mercator projection, zone 11; North American Datum of 1983

Figure B24.—Continued

Comparison of Measured Groundwater Levels and Simulated Hydraulic Heads

Figure B23 shows the relation between simulated hydraulic heads and measured groundwater levels. All the points would plot on the 1:1 correlation line if the YIHM results matched the measured data perfectly. Overall, measured groundwater levels and simulated hydraulic heads generally followed the 1:1 correlation line. The residuals for the 1970–2014 calibration period showed that 56 percent of simulated heads exceeded the measured groundwater levels with a mean residual value of –23 ft; in contrast, 44 percent were less than measured groundwater levels with a median residual value of 22 ft.

For simulated heads to be acceptable, the distribution of simulated heads and gradients should approximate those measured. For this comparison, simulated and interpolated observed groundwater-level contours for June to November 2014 were used. The simulated groundwater-level elevation, computed by averaging heads in active layers, and groundwater-level elevation contours for June to November 2014 are shown in figure B25, which shows that YIHM reasonably approximates observed gradients. However, simulated elevations can deviate from observed groundwater-level elevations as a result of interpolation errors.

Spatial distributions of the model-fit statistics RMSE, MAE, and MBE for wells in the YIHM are shown in figures B24*A*, B24*B*, and B24*C*, respectively. Figure B24*D* shows the number of transient measurements at each well. The RMSE of the residuals for the YIHM was 35 ft and the NRMSE was 0.97 percent. Previous studies (Drost and others, 1999; Ely and Kahle, 2012) indicated that the NRMSE should be less than 10 percent to be acceptable. The RMSE value for the YIHM indicated that the overall fit to measured data was reasonable.

The MAE of the residuals gives equal weight to error values and is always smaller than RMSE. The MAE is highest when most of the error is from few values; ratios of MAE to RMSE (MAE:RMSE) approaching 1.0 indicate that most of the error in a model is caused by a few values. The MAE of the YIHM was 23.6 ft, which was about 0.66 percent of the range of groundwater level variability. The ratio MAE:RMSE of 0.67 indicates that a large part of the overall error comes from few locations. Figures B24*A* and B24*B* demonstrate that the wells with the largest errors represent a small proportion of study wells used to calibrate the YIHM.

The spatial distribution of the MBEs (average residuals) for wells used to calibrate the YIHM demonstrates the general bias in the model results (fig. B24*C*). The mean MBE for the YIHM of –5.7 ft (0.16 percent of the range of measured groundwater levels) indicated that overall, the simulated heads slightly overestimate the measured data. The largest negative residuals (simulated heads greater than measured groundwater-level elevations) were observed in the Yucaipa hills, in the Oak Glen and Crafton subareas (near the Chicken Hill and Casa Blanca faults, respectively), and south of the Live Oak subarea (fig. B24*C*). The largest positive residuals (simulated heads less than measured groundwater levels) were in the Cherry Valley subarea, in the Gateway subarea (near the Chicken Hill fault), and in the northeastern part of the Yucaipa subbasin in the Triple Falls Creek subarea (fig. B24*C*). However, residuals are generally distributed randomly throughout the modeled area. Therefore, simulated heads generally provided an acceptable representation of measured groundwater levels.

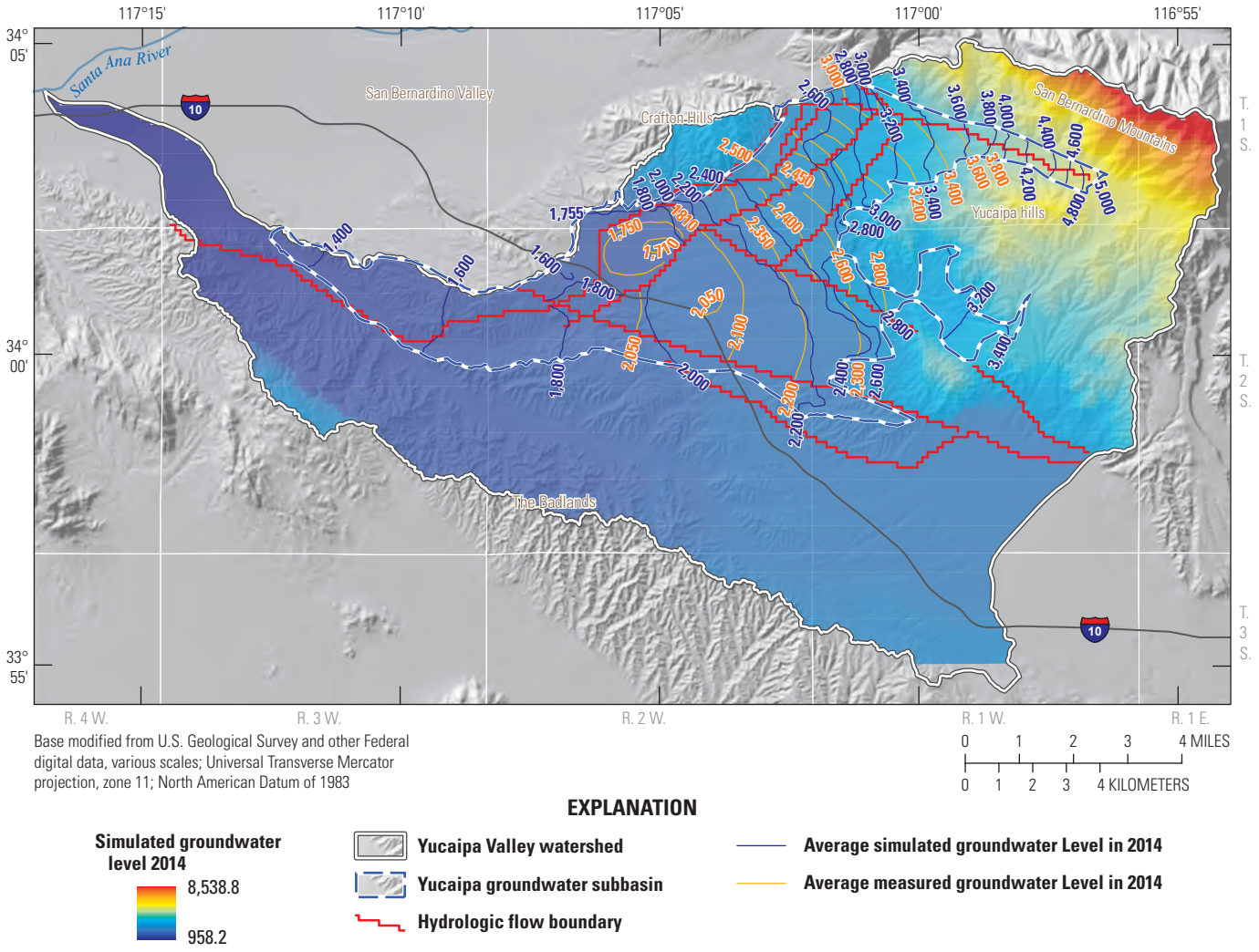

Figure B25. Average simulated groundwater-level elevations from the Yucaipa Integrated Hydrologic Model for June through November 2014, compared to groundwater-level elevation contour intervals for the same period (Geoscience Support Services, Inc., 2015), Yucaipa Valley watershed, San Bernardino and Riverside Counties, California.

Comparison of Measured Groundwater Levels and Simulated Hydraulic Heads by Groundwater Subarea

Residual error analysis and hydrograph comparison of simulated and measured groundwater levels were used to assess model fit by subarea. Hydrographs for selected wells are presented in figures B26–B31 to assess the ability of the YIHM to simulate temporal variations in groundwater levels. The wells were selected to represent temporal variations (groundwater-level patterns that extend through the calibration period), inter-annual variations, and seasonal fluctuations. The hydrographs are discussed by subarea in the following sections. While the YIHM generally simulates measured groundwater levels reasonably well, simulated hydraulic heads were both overestimated and underestimated in some parts of the study area. Mismatches between simulated heads and measured groundwater levels can be attributed to local variability in hydraulic properties that are not reflected in the model and uncertainty in the model input.

Calimesa Groundwater Subarea

Calimesa is the largest subarea within the YVW. The calibration results for the Calimesa subarea were evaluated using 7,133 measured groundwater levels. In general, the simulated and observed heads match reasonably well with an RMSE of 22.06 ft (table B6). The MBE of –0.49 ft indicates that the simulated heads generally are slightly higher than the measured groundwater levels. Figures B26 and B27 show the simulated heads and observed elevations of groundwater levels at select wells in northern and southern parts of the Calimesa subarea, respectively.

Table B6. Summary of hydraulic head residual error metrics (units in feet) for select groundwater subareas in the Yucaipa Integrated Hydrological Model, Yucaipa Valley watershed, San Bernardino and Riverside Counties, California.

[ft, foot]

Groundwater subarea	Number of observations	Mean biased error (MBE; ft)	Root mean square error (RMSE; ft)	Mean absolute error (MAE; ft)
Cherry Valley	815	–18.46	43.79	33.70
Live Oak	24	–27.24	29.91	27.24
Calimesa	7,133	–0.49	22.06	15.09
Wildwood	183	–0.78	7.02	5.10
Oak Glen	1,309	–6.52	36.80	25.89
Western Heights	1,514	–2.96	26.15	18.23
Wilson Creek	3,782	–10.49	49.37	29.63
Crafton	973	10.80	55.36	39.29
Gateway	605	19.40	23.71	21.47
Triple Falls Creek	101	–22.28	27.04	22.28
Other and Beaumont	2,332	0.12	18.49	51.33

Wet seasons during 1978–83 (fig. A5) affected groundwater-level elevations and demonstrate the importance of climate on the groundwater system. From the early 1970s through about 1986, groundwater-level elevations steadily increased. From 1987 to about the mid-2000s, groundwater-level elevations declined as a result of the combined impacts of increases in groundwater pumping and decreases in groundwater recharge caused by less precipitation during the 1984–90 period (fig. A5). From about 2009 through 2014, a slight increase in the groundwater-level elevations was observed in the simulated heads and in the measured groundwater levels despite the precipitation being below normal. This increase in groundwater-level elevations likely is explained by the delayed effects of imported water being added to the municipal water system and applied as MAR at the Wilson Creek and Oak Glen Creek spreading basins, along with the corresponding decrease in pumping associated with this added source of water to the overall water supply.

The hydraulic heads at USGS multiple-depth monitoring-well site YV6E (fig. B26*B*) show a substantial downward head difference of about 40 ft along a vertical distance of 580 ft. The downward vertical gradient at well site YV6E may be caused by a combination of localized recharge from nearby irrigation return flow and a shallow low-conductivity zone.

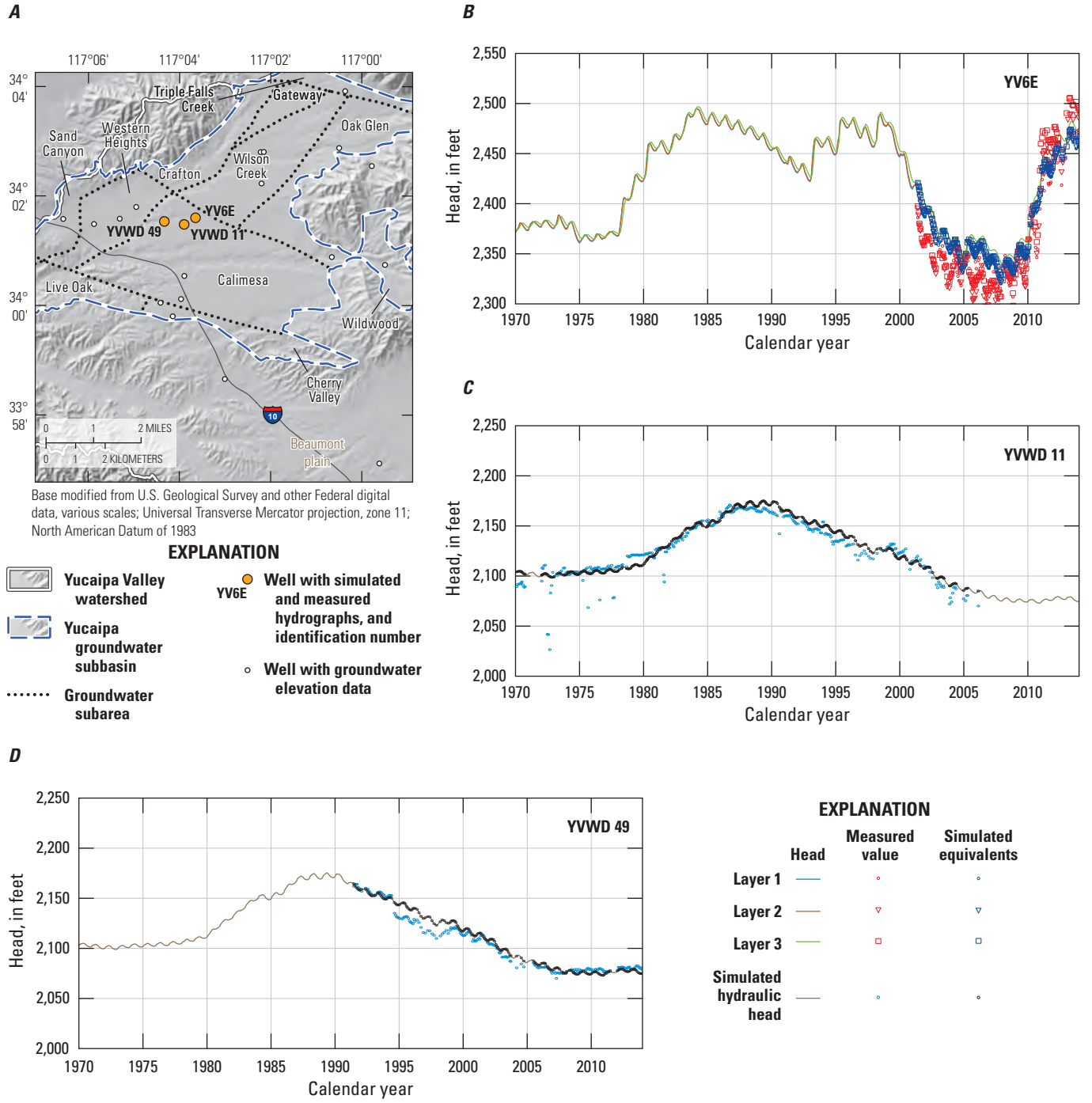

Figure B26. Comparisons of simulated hydraulic heads and measured groundwater-level elevations at select wells in the northern part of the Calimesa groundwater subarea for the Yucaipa Integrated Hydrologic Model, Yucaipa Valley watershed, San Bernardino and Riverside Counties, California. *A*, Well locations; *B*, YV6E; *C*, YVWD 11; and *D*, YVWD 49.

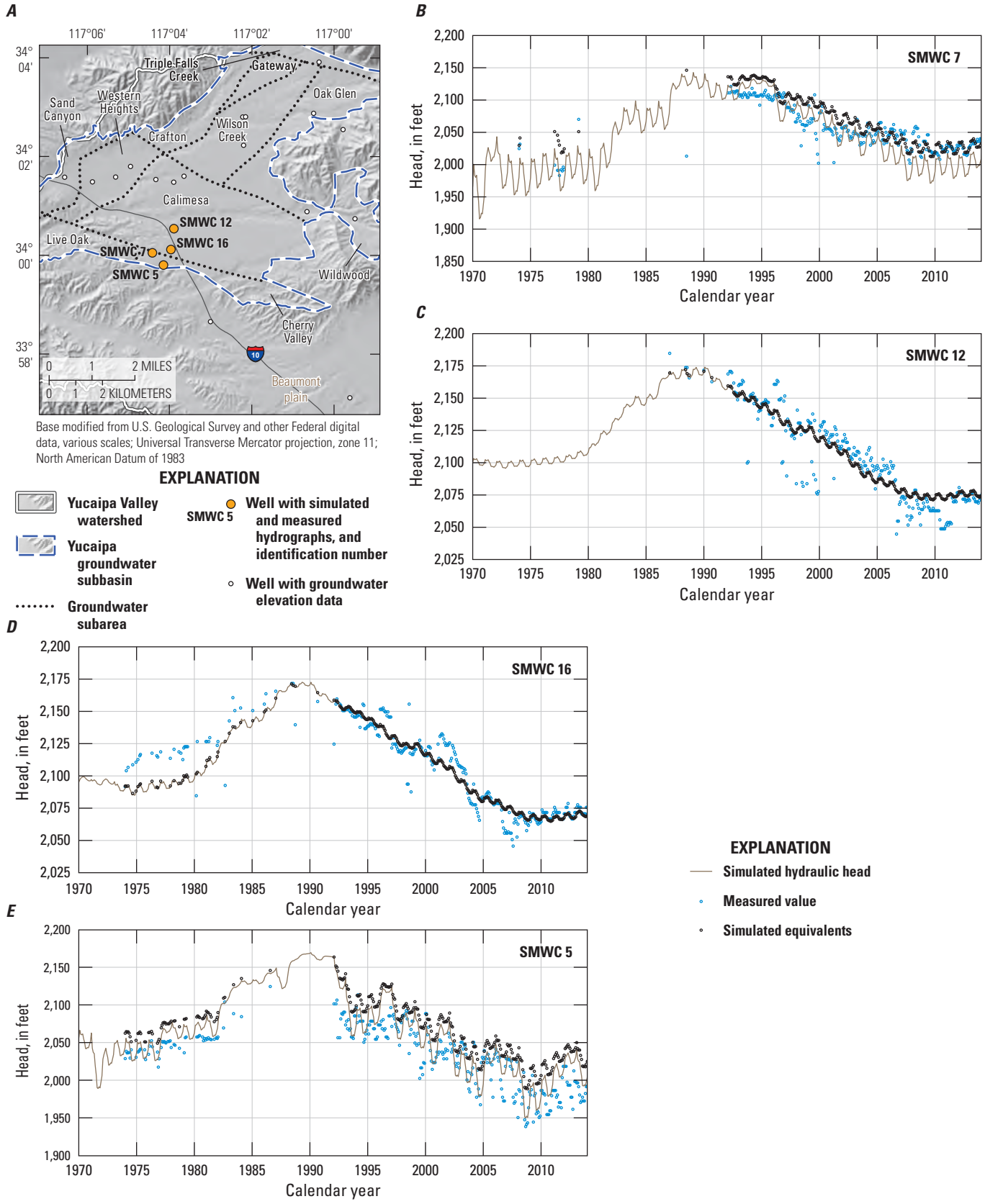

Figure B27. Comparisons of simulated hydraulic heads and measured groundwater-level elevations at select wells in the southern part of the Calimesa groundwater subarea, Yucaipa Integrated Hydrologic Model, Yucaipa Valley watershed, San Bernardino and Riverside Counties, California. *A*, Well locations; *B*, SMWC 7; *C*, SMWC 12; *D*, SMWC 16; and *E*, SMWC 5.

Western Heights and Sand Canyon Groundwater Subareas

The spatial variability of the water table in the Western Heights and Sand Canyon subareas is small (between 1,800 and 1,900 ft asl) compared to other subareas (fig. B28). Simulated heads and measured groundwater-level elevation data showed a steady decline in groundwater-level elevations during the simulation period. For example, simulated and measured groundwater level at well WHWC 6 (fig. B28*B*) experienced decline of about 60 ft between about 1980 and about 2000 because of pumping during this period and minimal recharge to the subarea. Evaluation of head residual errors indicated RMSE of 26.1 ft and an average residual error of –2.96 ft (table B6), indicating that the YIHM generally slightly overestimates measured groundwater-level elevations in the subarea.

Upgradient Groundwater Subareas

Upgradient subareas consist of the Oak Glen, Triple Falls Creek, Gateway, Wilson Creek and Crafton subareas (figs. B29, B30); the Oak Glen subarea (fig. B30) is the largest upstream subarea. The Oak Glen subareas receives recharge (1) from mountain-front runoff infiltration of streamflow and precipitation, (2) from lateral underflow through fractured crystalline basement in the Yucaipa hills to the south and east, and (3) through basin-fill aquifer materials in Triple Falls Creek to the north. Elevations of groundwater levels ranged from about 2,000 ft at the southwest portion of the subarea to about 4,800 ft in the eastern part of the subarea (fig. B25). The average residual error was –6.52 ft, and the RMSE was 36.8 ft. In general, the groundwater-level elevations at wells in the Oak Glen subarea experienced some fluctuations without substantial long-term trends (YVWD 13, YVWD 27, and YVWD 16; YVWD 16 is just outside of the Oak Glen subarea boundary; fig. B30). Some of the fluctuations likely are caused by seasonal climate stresses, but large fluctuations (for example, YVWD 13 in the period 1970–93 ; fig. B30*C*) likely are caused by groundwater pumping.

North of the Oak Glen subarea is the Triple Falls Creek subarea, which is bounded by the San Bernardino Mountains along the north and east. The San Bernardino Mountains receive a larger amount of precipitation compared to lower elevation areas and drain into Triple Falls Creek subarea as mountain-front runoff, infiltration from streamflow, and lateral groundwater flow through fractured crystalline basement. The general direction of groundwater flow (fig. B25) in Triple Fall Creek subarea is from the southeast, where groundwater-level elevations were as high as about 4,800 ft asl, to the northwest toward the boundary of the YVW with the San Bernardino Subbasin, where groundwater-level elevations were about 3,000 ft. Generally, groundwater levels in the Triple Falls Creek subarea experienced relatively small seasonal fluctuations (for example, well 20Q1; fig. B29*D*). Evaluation of head residual errors produced an RMSE of 27.04 ft.

The area between the Crafton Hills and the Oak Glen subarea consists of three small subareas: Crafton, Gateway, and Wilson Creek, that have root mean square errors of 55.36, 23.71, and 49.37 ft, respectively. Groundwater sources include natural recharge, MAR, stream depletion, and lateral underflow from the Triple Falls Creek and Oak Glen subareas. Since 2002, part of the imported water was applied as MAR at the Wilson Creek and Oak Glen Creek spreading basins in the Wilson Creek subarea. The combined effects of pumping reduction and MAR resulted in an increase in the groundwater levels from about 2008–14. For example, simulated heads at wells YVWD 7 and YVWD 44 (figs. B29*B*, B29*E*), and measured groundwater levels in USGS multiple-depth monitoring-well site YVWC 1 (fig. B29*C*) show an increase of more than 150 ft.

Beaumont Plain and Wildwood Groundwater Subarea

The general groundwater-flow direction in the Beaumont plain is from the east, where groundwater-level elevations were about 2,200–2,400 ft asl along the southeastern boundary of the YVW, to the west along San Timoteo Canyon, where the groundwater-level elevations drop to less than 2,000 ft asl at the western-most boundary of the YVW (fig. B25). Some groundwater lateral underflow comes from the Yucaipa hills to the north through the Cherry Valley subarea and from the east across the Beaumont plain general head boundary (fig. B9). Simulated heads and observed groundwater-level elevations showed a decline in wells 24N2 (fig. B31*C*) and 33L1 (fig. B31*B*) starting in the years 1998 and 2005, respectively. The RMSE in the area is 18.49 ft with a positive bias of 0.12 ft.

The Wildwood subarea receives groundwater inflows from natural recharge, stream leakage, and lateral underflow from the Yucaipa hills. The Wildwood subarea discharges groundwater through Wildwood Canyon into the Calimesa subarea. The Wildwood subarea has small groundwater level fluctuations (YVWD 28; fig. B31*D*), and the RMSE is 7.02 ft.

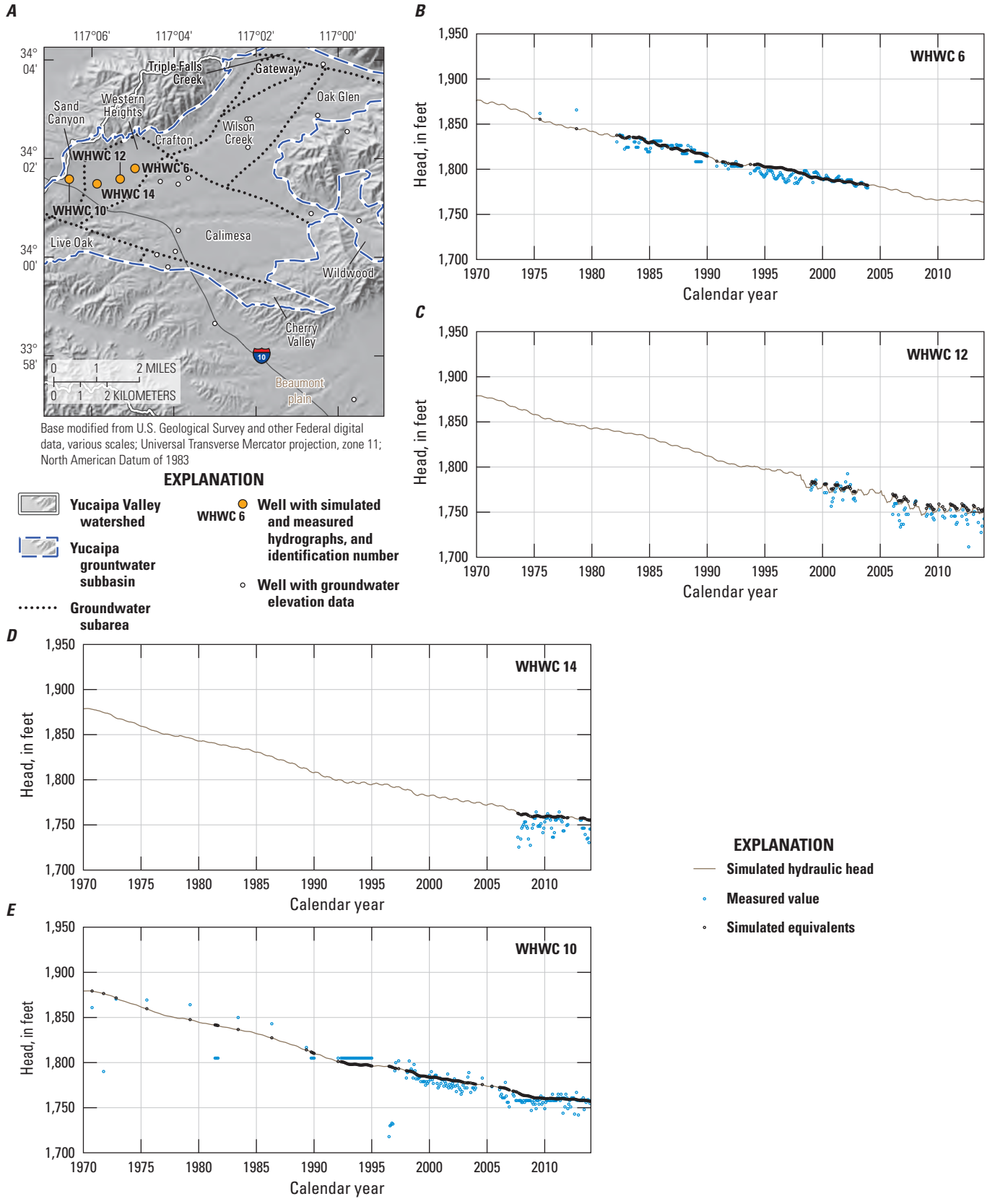

Figure B28. Comparisons of simulated hydraulic heads and measured groundwater-level elevations at select wells in the Western Heights and Sand Canyon groundwater subareas, Yucaipa Integrated Hydrologic Model, Yucaipa Valley watershed, San Bernardino and Riverside Counties, California. *A*, Well locations; *B*, WHWC 6; *C*, WHWC 12; *D*, WHWC 14; and *E*, WHWC 10.

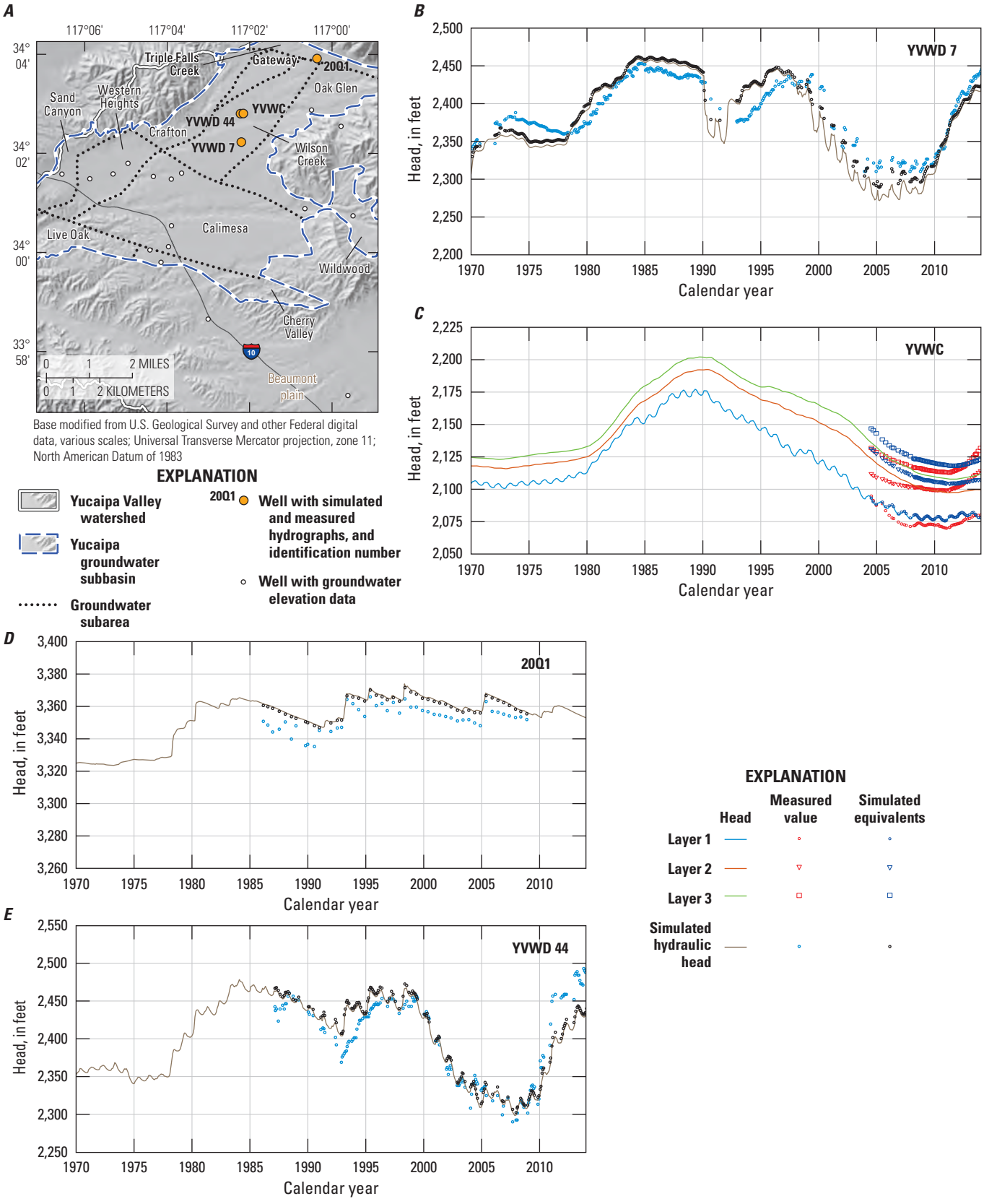

Figure B29. Comparisons of simulated hydraulic heads and measured groundwater-level elevations at select wells in the Triple Falls Creek and Wilson Creek groundwater subareas, Yucaipa Integrated Hydrologic Model, Yucaipa Valley watershed, San Bernardino and Riverside Counties, California. *A*, Well locations; *B*, YVWD 7; *C*, YVWC; *D*, 20Q1; and *E*, YVWD 44.

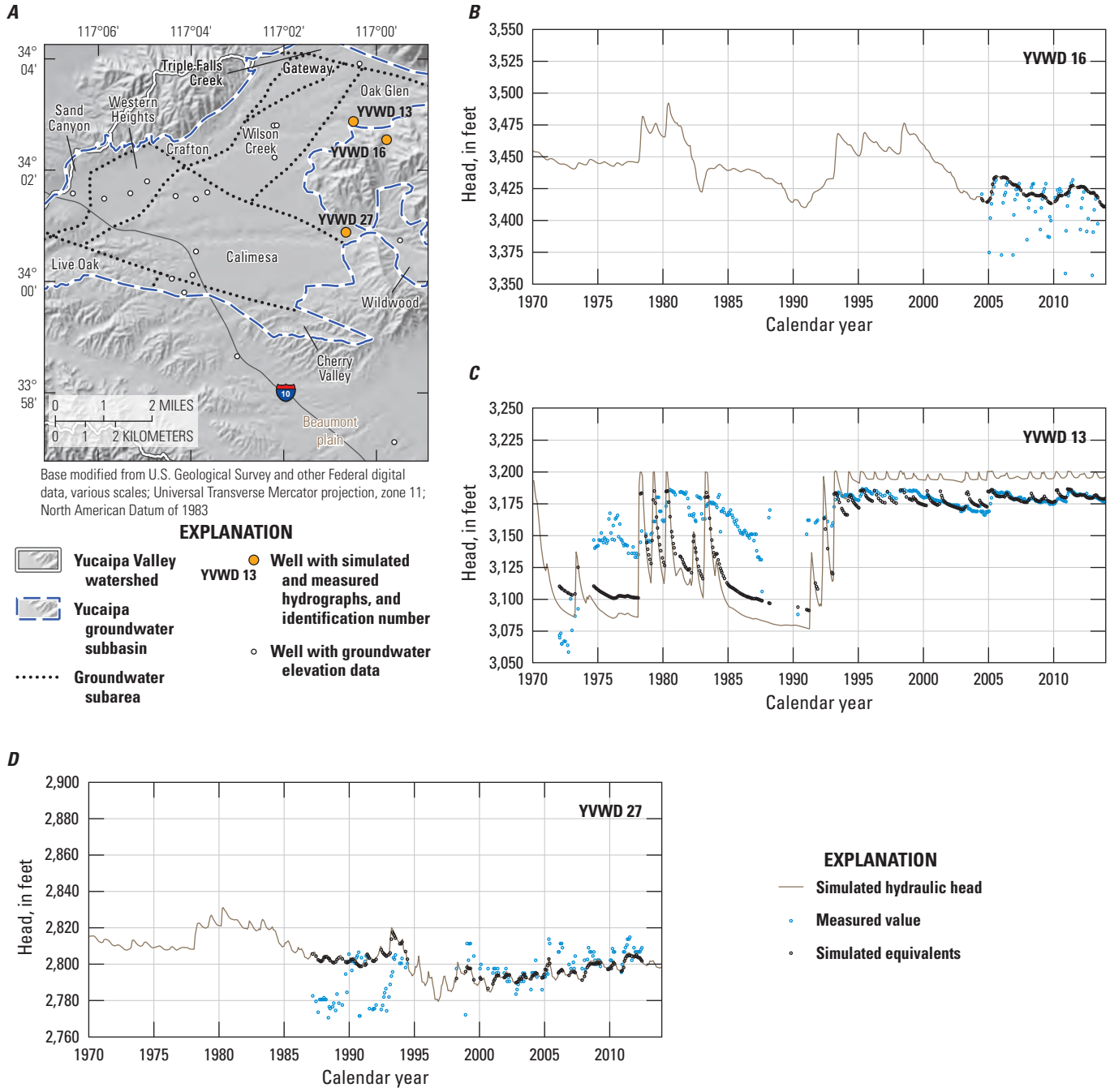

Figure B30. Comparisons of simulated hydraulic heads and measured groundwater-level elevations at select wells in the Oak Glen groundwater subarea, Yucaipa Integrated Hydrologic Model, Yucaipa Valley watershed, San Bernardino and Riverside Counties, California. *A*, Well locations; *B*, YVWD 16; *C*, YVWD 13; and *D*, YVWD 27.

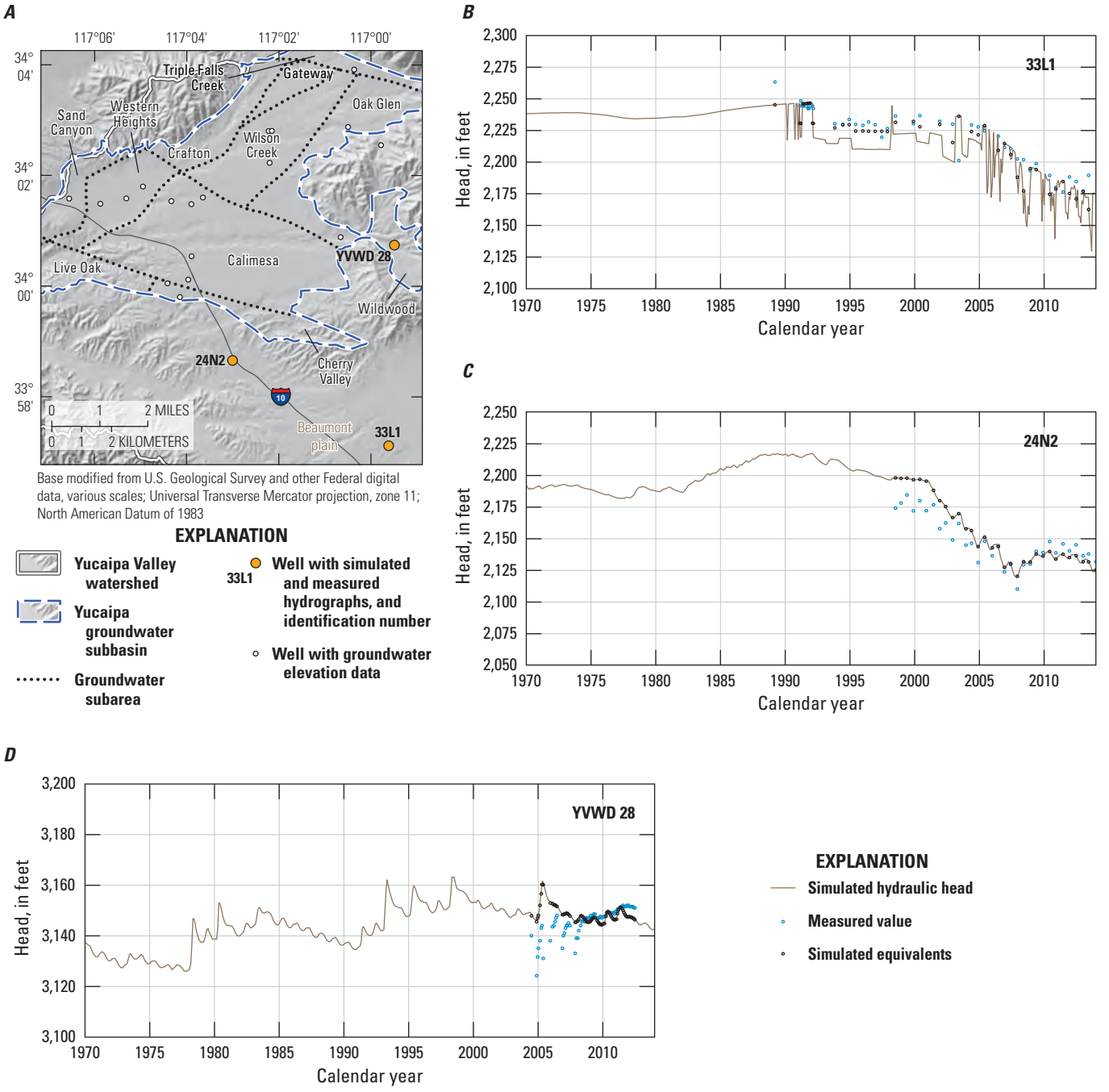

Figure B31. Comparisons of simulated hydraulic heads and measured groundwater-level elevations at select wells in the Beaumont plain and Wildwood groundwater subarea, Yucaipa Integrated Hydrologic Model, Yucaipa Valley watershed, San Bernardino and Riverside Counties, California. *A*, Well locations; *B*, 33L1; *C*, 24N2; and *D*, YVWD 28.

Simulated Hydrologic Budget

The water budget of the YIHM includes components for the surface water and groundwater systems (fig. B32). The model domain is divided into 12 subareas (fig. A3*C*), and groundwater budget components are reported for each subarea. Water budgets are provided for the entire model domain followed by the water budgets for the unsaturated zone and the groundwater model (saturated zone).

Integrated Model Budget

The simulated annual hydrologic budget for the YIHM for 1970–2014 is presented in figure B32*A*. The major source of inflow into the YIHM system is precipitation. The average annual inflow from precipitation is 78,400 acre-feet per year (acre-ft/yr), which is equivalent to 12.0 in/yr. Other sources of inflow include anthropogenic return flow recharge from agriculture, septic tanks leakage, and municipal water system leakage, and MAR at the Wilson Creek and Oak Glen Creek spreading basins for 2002–14. The major outflow component is total ET, which is the sum of ET from the soil, unsaturated and saturated zones, evaporation from impervious surfaces, sublimation from the snowpack, and interception evaporation from the tree canopy and low-lying vegetation. The average annual outflow from total ET is about 60,400 acre-ft/yr (about 9.2 in/yr, 76.7 percent of the total basin-wide precipitation). Groundwater pumping is the second largest outflow component, with an average annual pumping rate of about 15,800 acre-ft/yr (2.4 in/yr). The average surface outflow is about 1,250 acre-ft/yr (0.19 in/yr).

Total storage change is the sum of storage change of water on the land surface (snow cover, interception storage, stream channels, and water bodies) and in groundwater (the soil zone, unsaturated zone, and saturate zone). Total storage change is computed as the difference between inflow and outflow over a specified period; a total storage change of −705 acre-ft/yr was simulated for 1970–2014 using the YIHM. In the YIHM, storage changes of water on the land surface were considered negligible compared to changes in groundwater storage. The cumulative storage change for the entire YVW (fig. B32*A*) indicates that for the wet climatic periods of 1978–83 and 1991–94, the basin experienced an increase in storage. After 1994, a large portion of the gained storage was depleted as a result of dry and variable climatic periods from 1999 to 2014 (see fig. A5 in chapter A).

Groundwater Budget

The subsurface groundwater system consists of two components: the unsaturated zone (UZ) and the saturated zone (SZ). Inflow into the UZ came mainly from water percolating from the overlaying soil zone; outflows occurred as recharge into the SZ. Figure B32*B* shows the annual budget components for the UZ. The average annual infiltration rate into the UZ was 23,300 acre-ft/yr (3.53 in/yr), while the average rate of recharge into the SZ was about 23,100 acre-ft/yr (3.5 in/yr). The difference between infiltration and recharge accounted for storage change.

The budget of the saturated groundwater system is summarized in figure B32*C*. During the wet climatic periods 1978–83 and 1991–98, the cumulative groundwater storage increased to about 150,000 and 180,000 acre-ft, respectively; groundwater storage decreased during the dry and variable climatic period 1999–2014. Major inflow sources included direct recharge from precipitation on inter-channel areas, anthropogenic recharge, and infiltration of streamflow (positive stream leakage) in stream channels. Major outflow components included groundwater pumping, lateral groundwater outflow, and groundwater ET that occurred where there was shallow groundwater and dense vegetation cover. The following section provides more details about storage changes and budget components for the 12 primary subareas.

Groundwater Budgets for Subareas

Groundwater budgets are summarized for the 12 subareas that are important for the management of water resources in YVW. Figures B33–B38 show the groundwater budget and the cumulative storage changes for the period 1970–2014 for the Calimesa, Western Heights, Triple Falls Creek, Gateway, Crafton, Wilson Creek, Oak Glen, Live Oak, Wildwood, Cherry Valley, Sand Canyon, and Smiley Heights subareas. The three climate patterns of interest to this groundwater storage analysis (see fig. A5 in chapter A) were (1) the wet climatic periods 1978–83 and 1991–98, (2) the dry climatic periods 1984–90 and 1999–2002, and (3) the dry and variable climatic period 2008–14, when the State of California imported substantial amounts of water. The wet climatic periods resulted in groundwater storage gains in all subareas except the Western Heights and Sand Canyon subareas. Figure B33*A* shows that Calimesa subarea experienced a storage gain during the wet climatic period 1978–83. Groundwater storage in the Western Heights subarea (fig. B33*B*) declined substantially during 1970–98. Storage changes in the upgradient shallow subareas, Triple Falls Creek (fig. B34*A*), Gateway (fig. B34*B*), Crafton (fig. B35*A*), Wilson Creek (fig. B35*B*), and Oak Glen (fig. B36*A*) seemed to fluctuate more in response to annual climate changes compared to the Calimesa (fig. B33*A*) and Western Heights (fig. B33*B*) subareas, which were buffered from climatic changes by a relatively thick unsaturated zone.

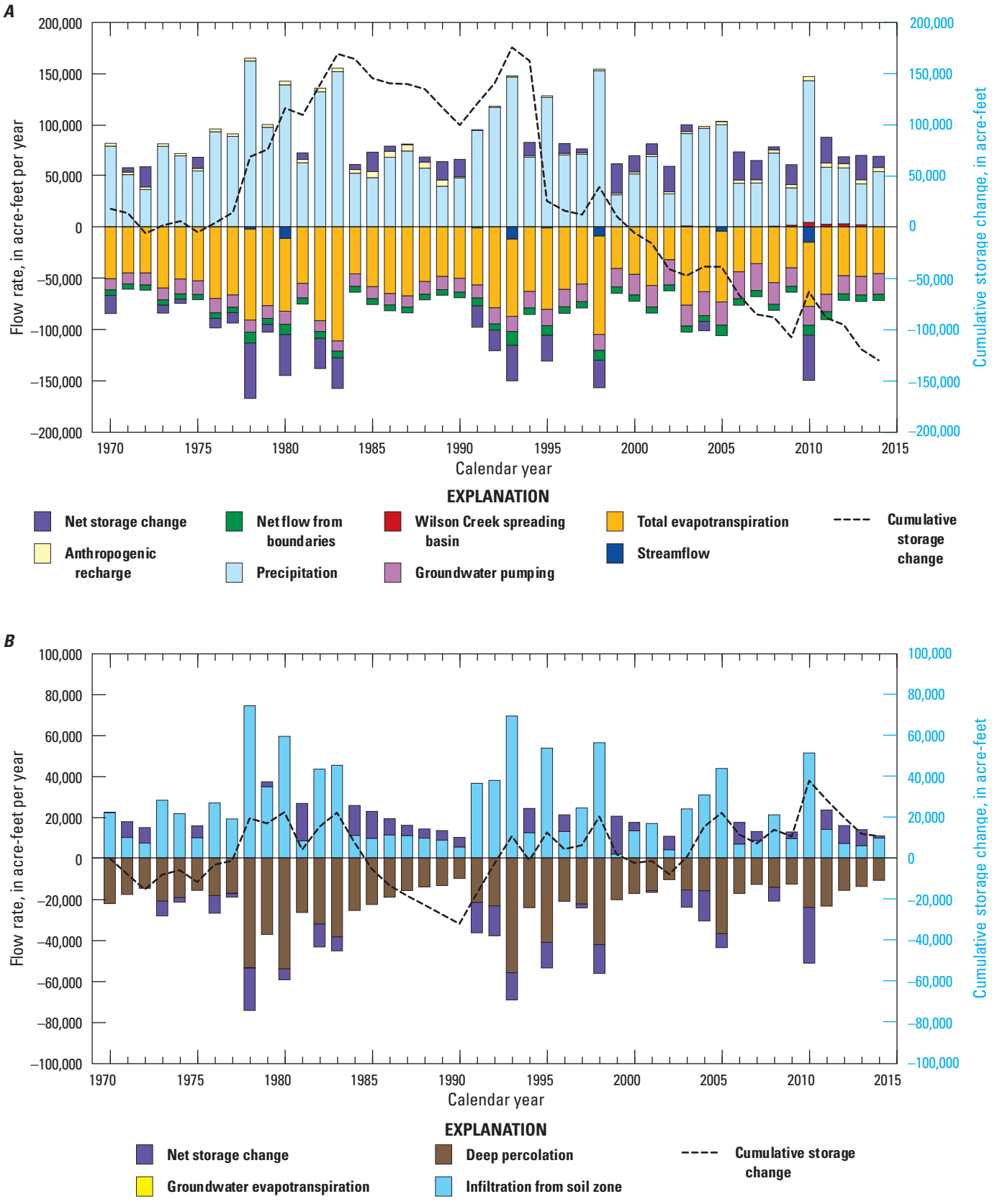

Figure B32. Water-budget components and cumulative storage changes for *A*, the Yucaipa Integrated Hydrologic Model (YIHM); *B*, the unsaturated zone component of the YIHM; and *C*, the groundwater model component of the YIHM (saturated zone), Yucaipa Valley watershed, San Bernardino and Riverside Counties, California.

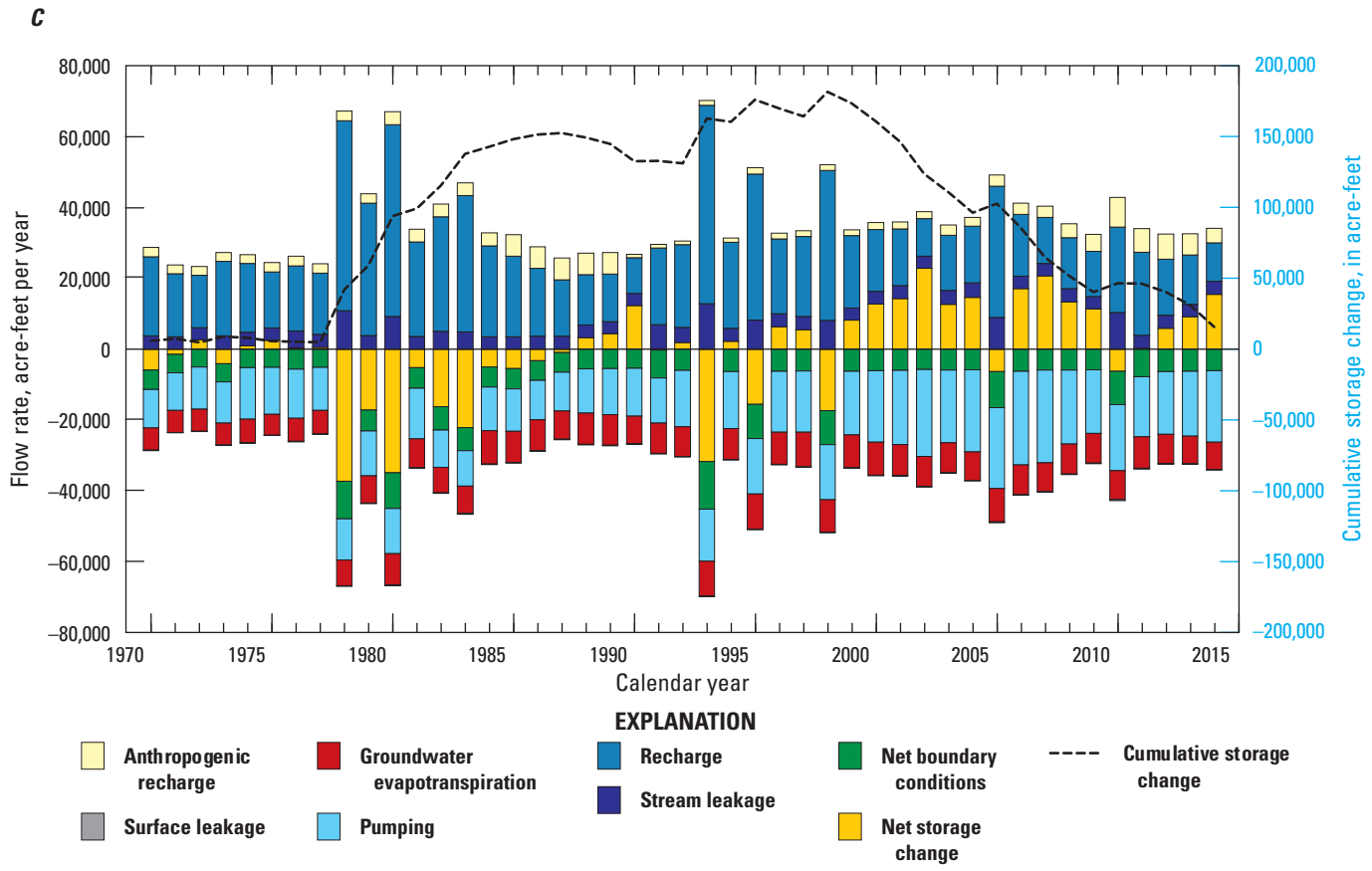

Figure B32.—Continued

The 1991–98 wet climatic period was followed by a generally dry and variable period that continued through 2014 and caused groundwater storage depletion during the period 1999–2007. After 2007, some groundwater upgradient subareas (for example, Gateway, Crafton, Wilson Creek, and Oak Glen) experienced an increase in groundwater storage over the period 2008–14, despite the dry conditions that prevailed during most of that period. The increase in groundwater storage can be explained by the reduction in groundwater pumping that followed the importing of water from northern California and the application of MAR at the Wilson Creek and Oak Glen Creek spreading basins. The total amount of imported water during the period 2002–14, which was used to augment the municipal water supply as a substitute to local groundwater pumping, was about 51,000 acre-ft (about 3,900 acre-ft/yr). The total volume of water recharged at Wilson Creek and Oak Glen Creek spreading basins was about 18,000 acre-ft (about 1,400 acre-ft/yr) during the same period.

Calimesa, Triple Falls Creek, Live Oak, Wildwood, and Smiley Heights all showed some increase in cumulative storage between 2008 and 2014, but the 2014 storage values were still lower than the 2008 values. Despite the increase in storage that occurred in some subareas during the 1998–2014 period, analysis of the simulated groundwater budget indicated that the Western Heights, Sand Canyon, and Cherry Valley subareas had some storage losses but at a smaller rate than through previous periods; however, storage gains that occurred in the upgradient subareas and the Calimesa subarea could eventually contribute to storage gains in the Western Heights subarea. Results of budget analysis for subareas indicated that reductions in groundwater pumping, importation of water from northern California, and application of MAR at the Wilson Creek and Oak Glen spreading basins either increase cumulative storage or decrease the rates of cumulative storage depletion in the Yucaipa subbasin.

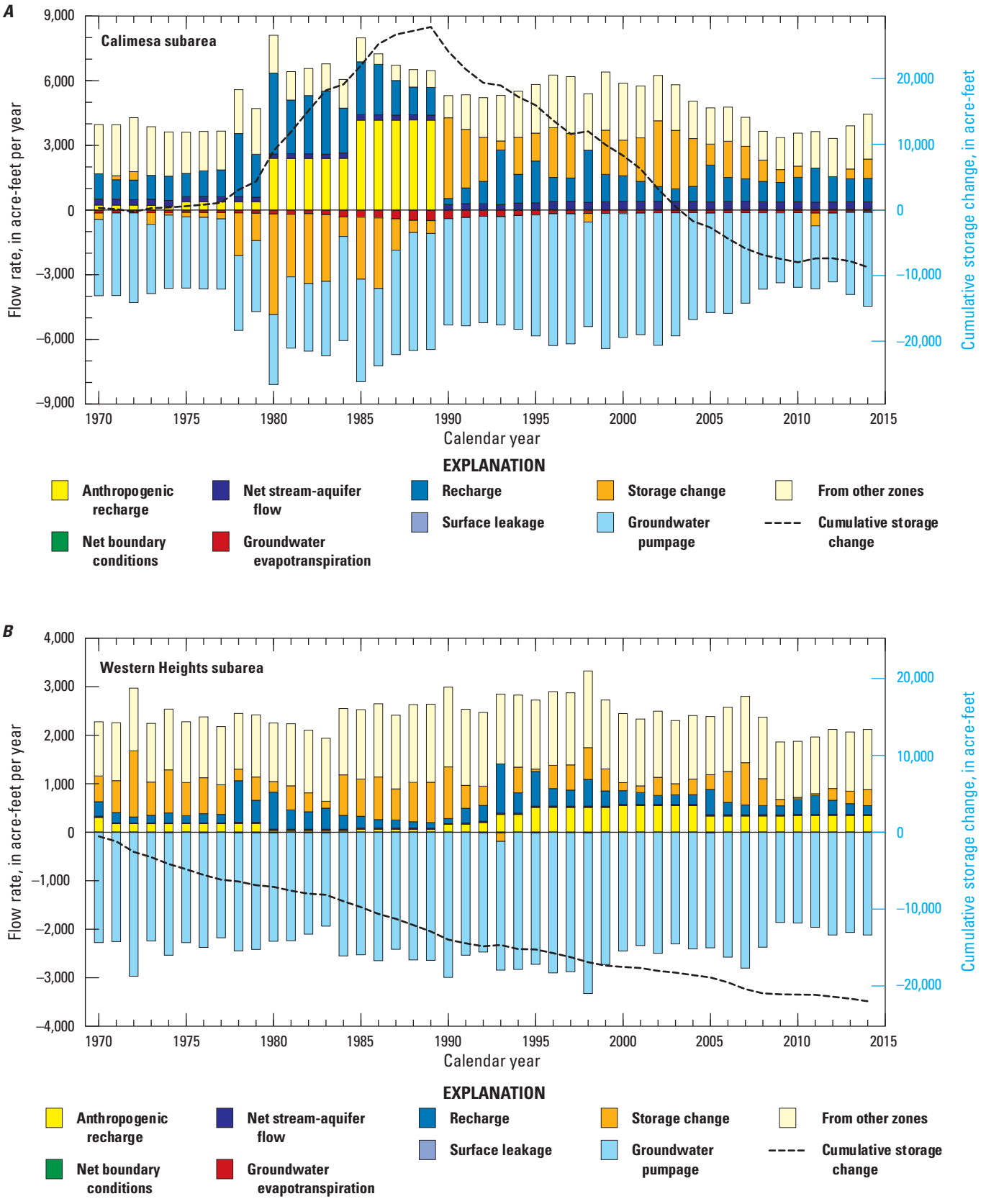

Figure B33. Flow rates for groundwater budget components and cumulative storage changes in *A*, Calimesa and *B*, Western Heights groundwater subareas in the Yucaipa Integrated Hydrologic Model, Yucaipa Valley watershed, San Bernardino and Riverside Counties, California.

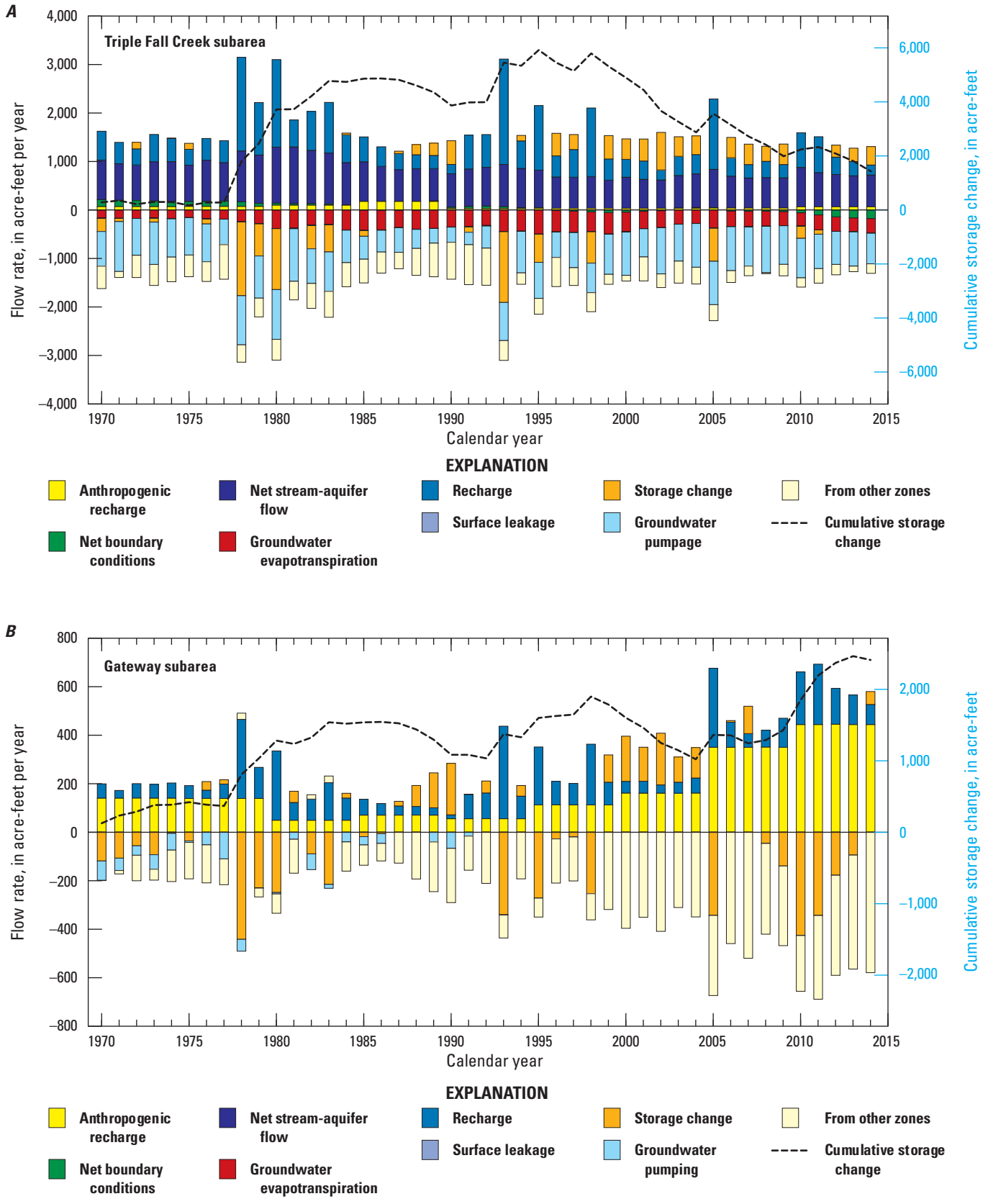

Figure B34. Flow rates for groundwater budget components and cumulative storage changes in *A*, Triple Fall Creek and *B*, Gateway groundwater subareas in the Yucaipa Integrated Hydrologic Model, Yucaipa Valley watershed, San Bernardino and Riverside Counties, California.

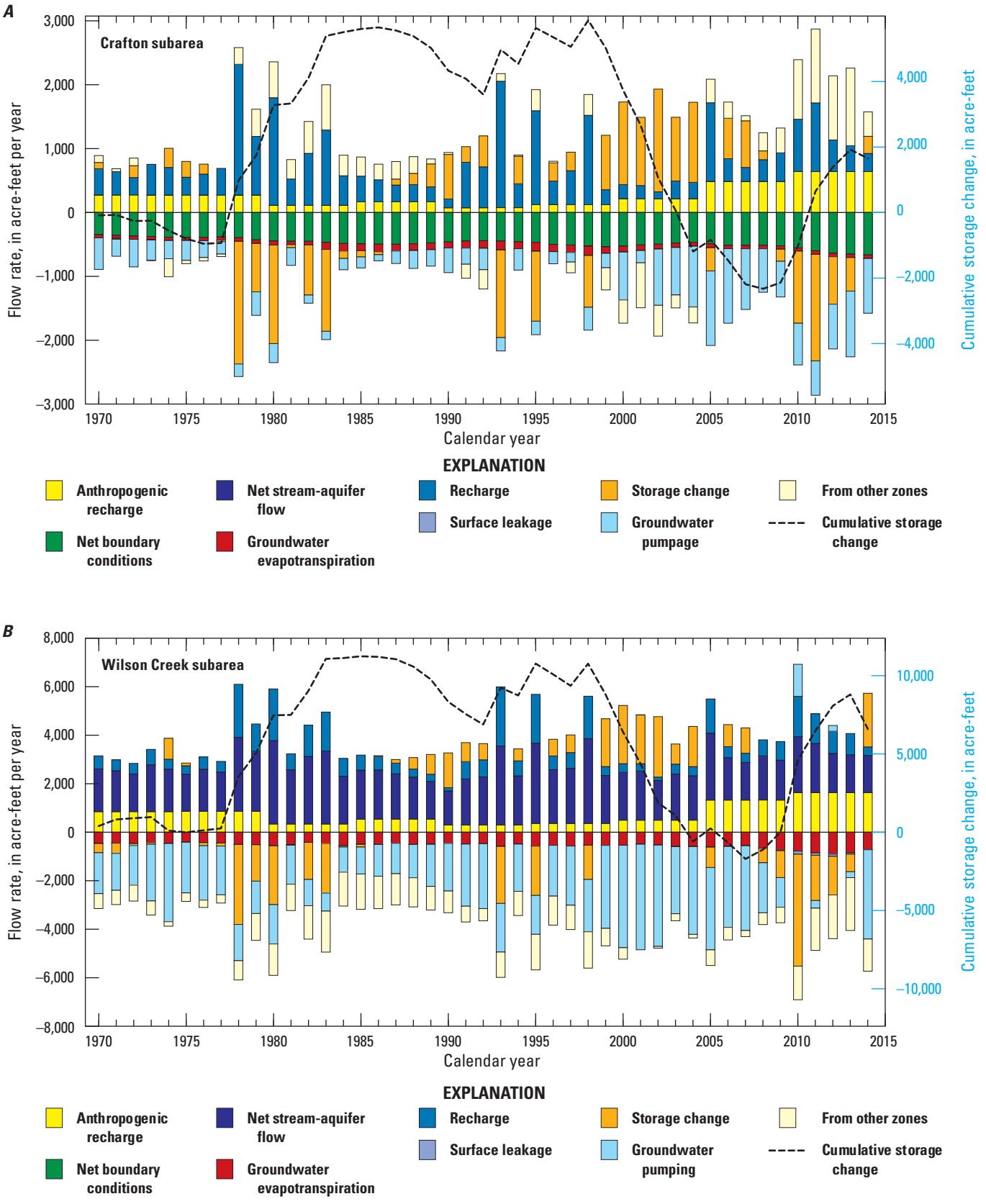

Figure B35. Flow rates for groundwater budget components and cumulative storage changes in *A*, Crafton and *B*, Wilson Creek groundwater subareas in the Yucaipa Integrated Hydrologic Model, Yucaipa Valley watershed, San Bernardino and Riverside Counties, California.

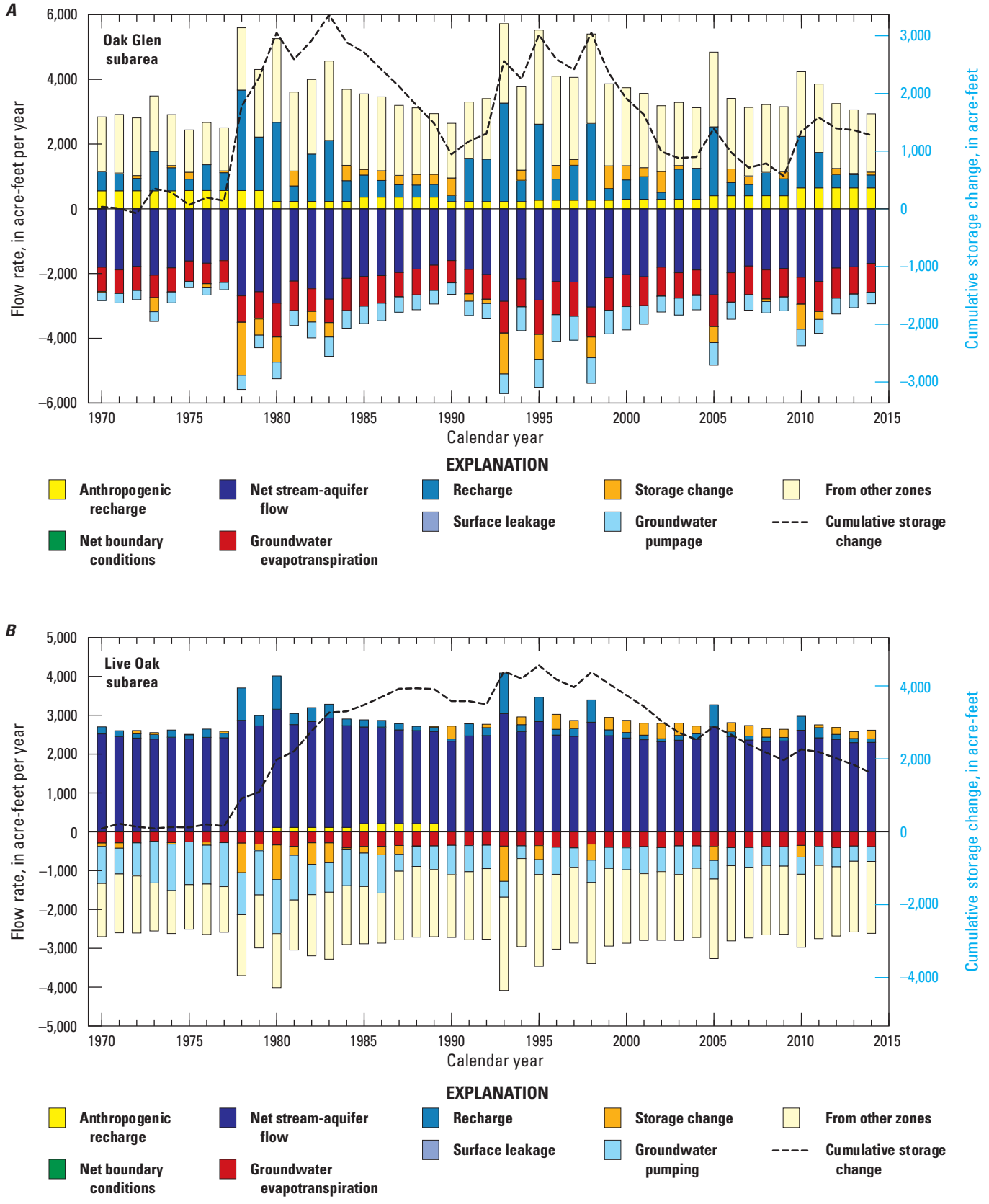

Figure B36. Flow rates for groundwater budget components and cumulative storage changes in *A*, Oak Glen and *B*, Live Oak groundwater subareas in the Yucaipa Integrated Hydrologic Model, Yucaipa Valley watershed, San Bernardino and Riverside Counties, California.

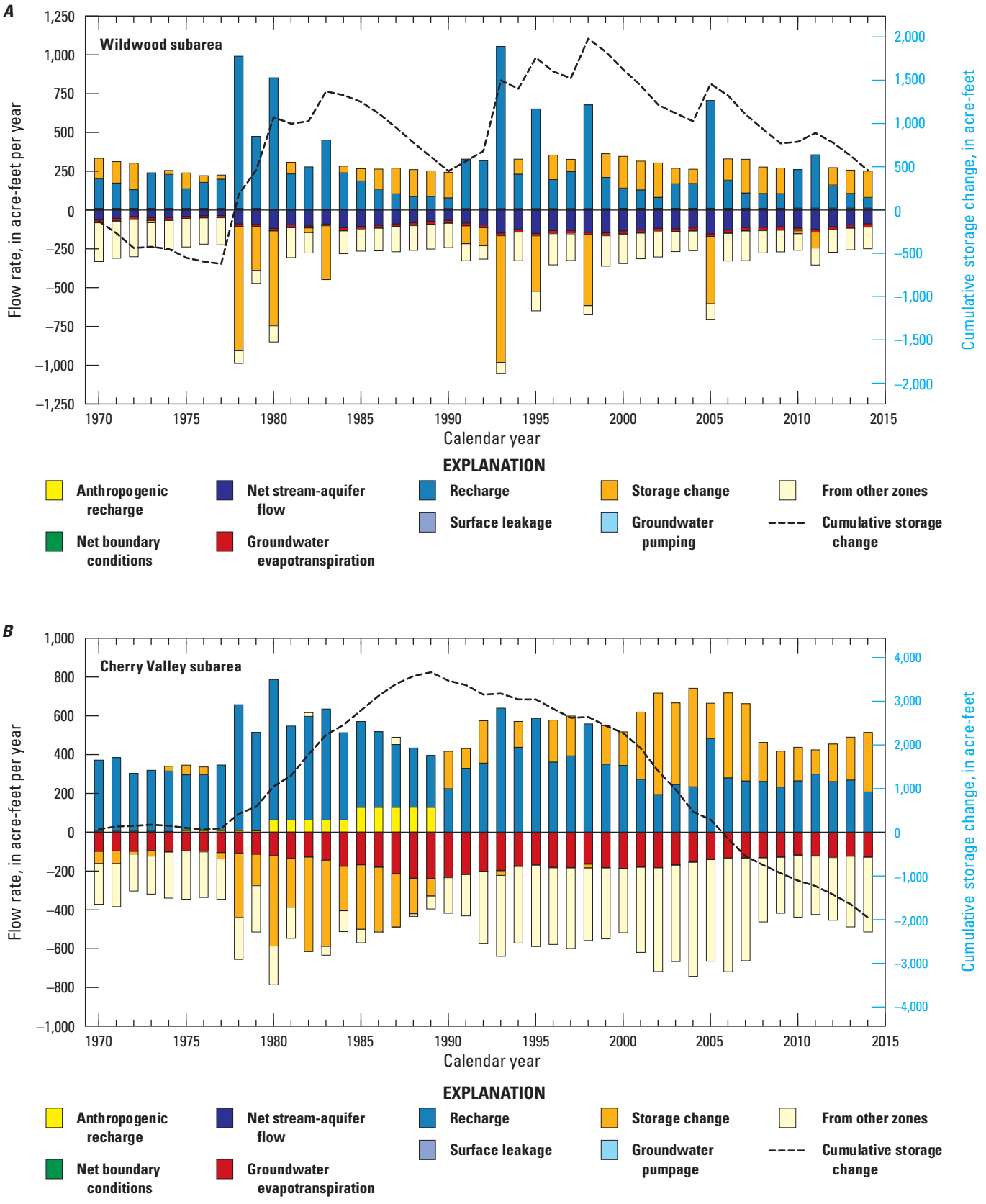

Figure B37. Flow rates for groundwater budget components and cumulative storage changes in *A*, Wildwood and *B*, Cherry Valley groundwater subareas in the Yucaipa Integrated Hydrologic Model, Yucaipa Valley watershed, San Bernardino and Riverside Counties, California.

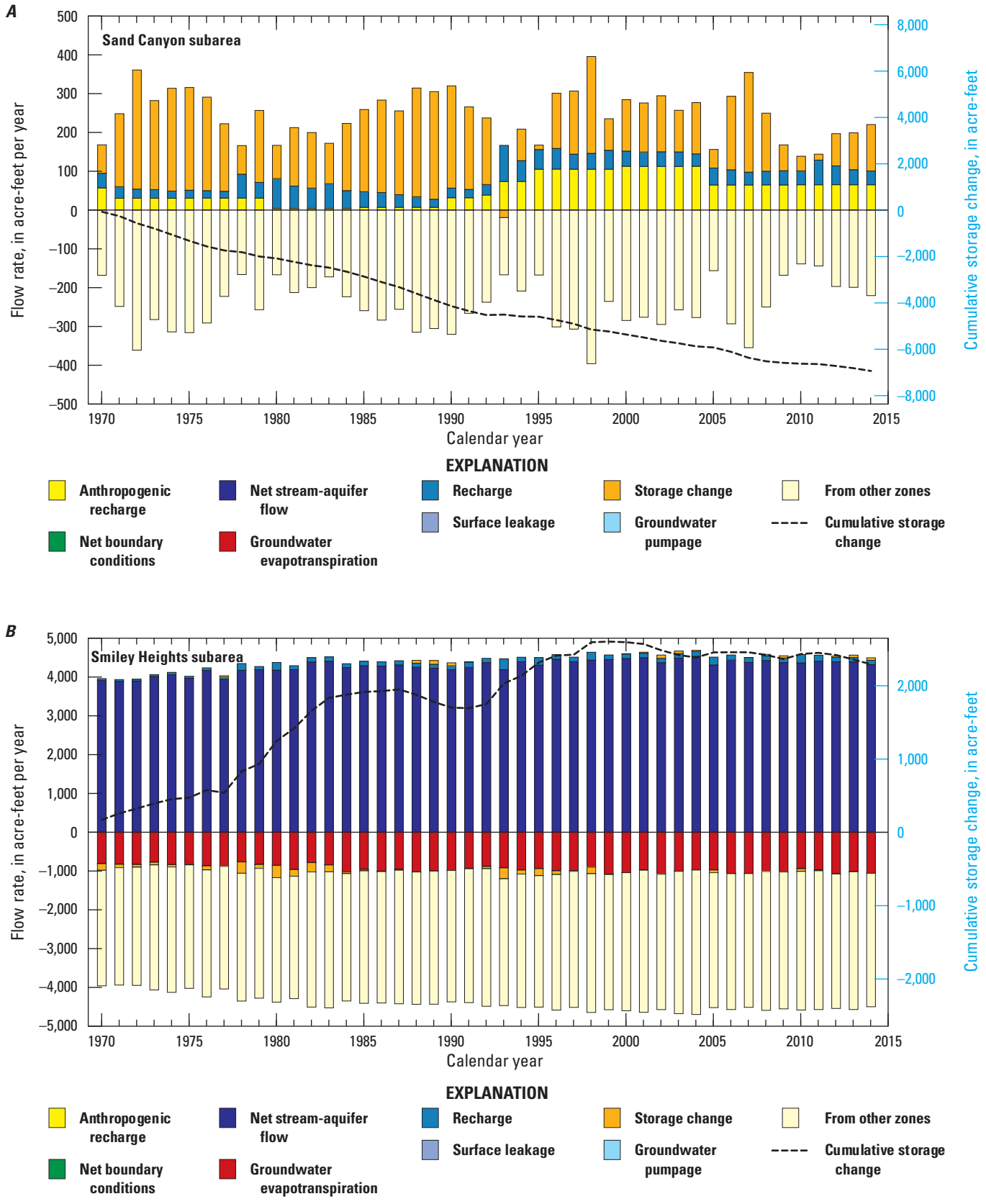

Figure B38. Flow rates for groundwater budget components and cumulative storage changes in *A*, Sand Canyon and *B*, Smiley Heights groundwater subareas in the Yucaipa Integrated Hydrologic Model, Yucaipa Valley watershed, San Bernardino and Riverside Counties, California.

Model Limitations

Hydrologic models are numerical approximations of complex natural systems that are inherently uncertain. Model uncertainty can be algorithmic, structural, and parametric (Kennedy and O'Hagan, 2001). Algorithmic (or numerical) uncertainty results from the discretization of space and time domains of naturally continuous hydrologic processes. This type of uncertainty is unavoidable but can be controlled by choosing spatiotemporal discretization that is numerically feasible, meets needed management scale, and is consistent with available data. Therefore, the YIHM cannot be used to examine hydrological processes at spatial or temporal scales that are smaller than the cell size and the length of the time step. Users of the YIHM must also consider the limitations imposed by the daily time step used in YIHM; sub-daily variations in storm intensity that usually need to be considered for simulating peak flows and flooding events are not represented accurately in the YIHM.

Structural uncertainties result from errors or misrepresentations of hydrologic processes by the governing equations. For example, GSFLOW simplifies the numerical solution of flow in the unsaturated zone using a kinematic wave approximation implemented in the UZF1 package (Niswonger and others, 2006). Consequently, the YIHM is incapable of simulating unsaturated flow beneath a perched aquifer system in which a saturated zone is embedded in a bigger unsaturated zone. Instead, UZF1 parameters can be estimated in a way that mimic the effect of a perched aquifer on recharge rate and arrival time. Care must be taken when using the model to evaluate the effects of new MAR projects on the regional groundwater-flow regime. The presence of localized clay lenses in the unsaturated zone can limit, delay, or redirect recharge to the saturated zone.

Parametric uncertainties result from misrepresenting variability and uncertainty of model inputs. Parameter uncertainties are reduced during model calibration by conditioning model input to measurements; however, uniquely estimating unknown model parameters is difficult. The uncertainties and errors in measurements used in model development and model calibration affect model predictions. One major limitation of YIHM is the uncertainty in the available streamflow records caused by several onstream retention ponds and urban runoff generated from outside the study domain (appendix B2). Small calibration weights were assigned to streamflow measurements to limit possible propagation of uncertainty from streamflow measurements to calibrated model parameters. As a result, recharge and hydraulic conductivity could not be uniquely calibrated. Although the calibrated conductivity field was evaluated to ensure its general agreement with available pumping test data, reliable streamflow data are indispensable in constraining the partitioning of precipitation into infiltration, evapotranspiration, and runoff.

The meteorological data input to the PRMS model were available for only one location outside of the model domain, leading to uncertainties in the spatial distribution of climate stresses. The spatial distribution of climate stresses is derived based on PRISM data (PRISM Climate Group, 2013), which are model outputs with their own uncertainties. Additionally, the available precipitation record has some missing data gaps that add to model data uncertainty.

Summary and Conclusions

The U.S. Geological Survey (USGS), in cooperation with the San Bernardino Valley Municipal Water District, developed a fully integrated surface-water and groundwater hydrologic model to evaluate the surface-water and groundwater resources of the Yucaipa groundwater subbasin (Yucaipa subbasin), a 35-square mile (mi^2) area of a semiarid inland valley southeast of the City of San Bernardino, California. The Yucaipa Integrated Hydrologic Model (YIHM) was developed to better understand and quantify the hydrologic system of the Yucaipa subbasin and to quantify the effects of historical and potential water resource development induced by changes in climate and human-related activities. The coupled Groundwater and Surface-water FLOW model (GSFLOW) was used to develop the integrated groundwater and surface-water interactions model for Yucaipa Valley watershed (YVW), a 121 mi^2 watershed that encompasses the Yucaipa subbasin.

The developed YIHM incorporated data about the hydrologic, climate, geologic, and landscape conditions of the YVW during 1947–2014 and was calibrated and applied for the period 1970–2014. The YIHM was used for a continuous daily simulation of the hydrologic system, with an emphasis on hydrologic processes of the land surface (including plant canopy, impervious surfaces, soil zone, and streams) and the subsurface defined by the upper soil layer and the root zone. The YIHM simulated (1) potential evapotranspiration (PET); (2) evapotranspiration (ET); (3) overland-flow processes; (4) interflow processes in the soil zone; (5) recharge; (6) groundwater discharge and losses; and (7) streamflow using hydrologic response units (HRUs), groundwater reservoirs, and stream segments. The hydrologic system was controlled mainly by daily climate stresses, such as precipitation and temperature; human impacts also were important factors that affected the hydrologic system, most notably groundwater withdrawals and managed aquifer recharge (MAR).

The YIHM was calibrated using measured solar radiation, potential evapotranspiration, average streamflow, and transient groundwater-level data. The calibration was implemented using Parameter Estimation software (PEST), the Ensemble Smoother, and trial-and-error approach to estimate a large set of input parameters required to simulate the integrated hydrologic system. Model fit was evaluated using hydraulic-head residual errors at 259 wells with transient groundwater-level data. A reasonable match between the simulated and observed hydraulic heads was achieved throughout the 3,580 feet (ft) elevation difference between the lowest and the highest groundwater-level measurements. The calibrated hydraulic conductivity field was evaluated using data from multiple pumping tests, and the calibrated specific yield was evaluated using available site-specific published data. Parameters lacking site-specific data were evaluated using published literature data. Calibration results indicated the greatest sensitivity to parameters controlling stream leakage and conductivity of faults and barriers that dissect the groundwater system. Sensitivity of the streambed conductivity of Wilson Creek and Oak Glen Creek demonstrated how flood-control structures enhanced stream seepage into the Yucaipa groundwater system.

The YIHM was used to simulate the daily hydrologic budget for the integrated hydrologic system (surface and subsurface systems) and for 12 groundwater subareas during the period 1970–2014. The major budget components for the YIHM included precipitation, evapotranspiration, groundwater pumping, and managed aquifer recharge. The basin-wide mean precipitation for the YIHM study area for 1970–2014 was 12.0 inches per year (in/yr; 78,424 acre-feet per year; acre-ft/yr), and 9.2 in/yr (60,446 acre-ft/yr; 76.7 percent of the total basin-wide precipitation) was returned to the atmosphere by ET. The average recharge into the saturated groundwater zone was estimated to be 3.5 in/yr (23,100 acre-ft/yr). The basin-wide mean of groundwater pumping for 1970–2014 was estimated to be 15,800 acre-ft/yr. About 51,000 acre-ft of water was imported by the State of California into the YVW during the period 2002–14 to augment the municipal water supply as a substitute to local groundwater pumping; the total volume of water recharged at Wilson Creek and Oak Glen Creek spreading basins was about 18,000 acre-ft (about 1,400 acre-ft/yr) during the same period. The simulated mean change in water storage (average of differences between inflows and outflows) in the integrated hydrologic system for 1970–2014 was about –705 acre-ft/yr.

The simulated water budget for groundwater subareas showed that Calimesa, Triple Falls Creek, Live Oak, Wildwood, and Smiley Heights groundwater subareas showed some increase in cumulative storage, but the 2014 storage values were still lower than the 2008 values. Some upgradient groundwater subareas, such as Wilson Creek, Gateway, Crafton, and Oak Glen, experienced storage gains from 2008 through 2014 despite the dry climatic conditions that occurred in 2011–14. Imported water from northern California and enhanced MAR activities during 2008–14 reduced demands for water and caused decreases in groundwater pumping. The calibrated model showed that the imported water increased groundwater-level elevations by more than 150 ft in some areas in upgradient groundwater subareas (such as Wilson Creek and Gateway) during 2008–14. These simulation results were supported by groundwater-level measurements in this region and during the same period. Some groundwater subareas such as Western Heights, Cherry Valley, and Sand Canyon showed steady decline from 2008 to 2014, but the rates of decline where lower than the previous period.

In general, hydraulic heads and budgets simulated using the YIHM indicated the importance of climate stresses (precipitation, temperature, and evapotranspiration), groundwater pumping, and managed aquifer recharge to the overall hydrologic system. The developed YIHM can be used to improve understanding of the hydrologic processes in YVW and to simulate future management scenarios with different climatic and anthropogenic changes.

References Cited

Abimbola, O.P., Mittelstet, A.R., Gilmore, T.E., and Korus, J.T., 2020, Influence of watershed characteristics on streambed hydraulic conductivity across multiple stream orders: Scientific Reports, v. 10, no. 3696, 10 p. [Available at https://doi.org/10.1038/s41598-020-60658-3.]

Allander, K.K., Niswonger, R.G., and Jeton, A.E., 2014, Simulation of the Lower Walker River Basin hydrologic system, west-central Nevada—Using PRMS and MODFLOW models: U.S. Geological Survey Scientific Investigations Report 2014–5190, 93 p. [Available at https://doi.org/10.3133/sir20145190.]

Alzraiee, A.H., Cromwell, G., and Engott, J.A., 2022, GSFLOW model to evaluate the effect of groundwater pumpage and climate stresses on the integrated hydrologic system of the Yucaipa subbasin, Yucaipa Valley watershed, San Bernardino and Riverside Counties, California: U.S. Geological Survey data release, https://doi.org/10.5066/P9K540DV.

Anderson, M.P., and Woessner, W.W., 1992, Applied groundwater modeling—Simulation of flow and advective transport: San Diego, Calif., Academic Press, Inc., 381 p.

California Department of Water Resources (DWR), 1967, Specific yield and storage determination for the Bunker Hill-San Timoteo ground water investigation: Southern District Technical Information Record Study Code No. 1335-5-A11, 15 p.

California Department of Water Resources, 2016, California's groundwater, working toward sustainability: California Department of Water Resources Bulletin 118, Interim Update 2016, accessed May 23, 2018, at https://www.water.ca.gov/Programs/Groundwater-Management/Bulletin-118.

California Irrigation Management Information System, 2017, Spatial Report: Sacramento, Calif., California Department of Water Resources and University of California at Davis, accessed September 26, 2017, at https://cimis.water.ca.gov.

Cooper, H.H., Jr., and Jacob, C.E., 1946, A generalized graphical method for evaluating formation constants and summarizing well field history: Transactions – American Geophysical Union, v. 27, no. 4, p. 526–534 [Available at https://doi.org/10.1029/TR027i004p00526.]

Cromwell, G., and Matti, J.C, 2022, Geology and hydrogeology of the Yucaipa groundwater subbasin, San Bernardino and Riverside Counties, California: U.S. Geological Survey Scientific Investigations Report 2021–5129, 54 p., https://doi.org/10.3133/sir20215129.

Doherty, J., 2015, Calibration and uncertainty analysis for complex environmental models: Watermark Numerical Computing, Brisbane, Australia, 227 p., ISBN: 978-0-9943786-0-6.

Doherty, J., and Hunt, R.J., 2009, Two statistics for evaluating parameter identifiability and error reduction: Journal of Hydrology (Amsterdam), v. 366, no. 1–4, p. 119–127. [Available at https://doi.org/10.1016/j.jhydrol.2008.12.018.]

Drost, B.W., Ely, D.M., and Lum, W.E., II, 1999, Conceptual model and numerical simulation of the ground-water flow system in the unconsolidated sediments of Thurston County, Washington: U.S. Geological Survey Water-Resources Investigations Report 99–4165, 106 p., https://doi.org/10.3133/wri994165.

Duwelius, R.F., 1996, Hydraulic conductivity of the streambed, east branch Grand Calumet River, northern Lake County, Indiana: U.S. Geological Survey Water-Resources Investigations Report 96–4218, 37 p., accessed at https://doi.org/10.3133/wri964218.

Eckis, R., 1934, Geology and ground-water storage capacity of valley fill, South Coastal Basin Investigation: California Division of Water Resources Bulletin 45, 273 p.

Ely, D.M., and Kahle, S.C., 2012, Simulation of groundwater and surface-water resources and evaluation of water-management alternatives for the Chamokane Creek basin, Stevens County, Washington: U.S. Geological Survey Scientific Investigations Report 2012–5224, 74 p. [Available at https://doi.org/10.3133/sir20125224.]

Evensen, G., 1994, Sequential data assimilation with a nonlinear quasi-geostrophic model using Monte Carlo methods to forecast error statistics: Journal of Geophysical Research, v. 99, no. C5, p. 10143–10162. [Available at https://doi.org/10.1029/94JC00572.]

Fienen, M.N., D'Oria, M., Doherty, J.E., and Hunt, R.J., 2013, Approaches in highly parameterized inversion—bgaPEST, a Bayesian geostatistical approach implementation with PEST—documentation and instructions: U.S. Geological Survey Techniques and Methods, book 7, chap. C9, 86 p., https://doi.org/10.3133/tm7C9.

Gardner, M.A., Morton, C.G., Huntington, J.L., Niswonger, R.G., and Henson, W.R., 2018, Input data processing tools for the integrated hydrologic model GSFLOW: Environmental Modelling & Software, v. 109, p. 41–53. [Available at https://doi.org/10.1016/j.envsoft.2018.07.020.]

Geoscience Support Services, Inc., 2014, Recharge investigation of the Yucaipa Groundwater Basin: Draft Report, 338 p.

Geoscience Support Services, Inc., 2015, Historical annual change in groundwater storage capacity—Yucaipa Groundwater Basin: Draft Report, 577 p.

Harbaugh, A.W., 2005, MODFLOW-2005—The U.S. Geological Survey modular ground-water model—The ground-water flow process: U.S. Geological Survey Techniques and Methods, book 6, chap. A16, variously paged, https://doi.org/10.3133/tm6A16.

Hay, L.E., Leavesley, G.H., Clark, M.P., Markstrom, S.L., Viger, R.J., and Umemoto, M., 2006, Step wise, multiple objective calibration of a hydrologic model for a snowmelt dominated basin: Journal of the American Water Resources Association, v. 42, no. 4, p. 877–890. [Available at https://doi.org/10.1111/j.1752-1688.2006.tb04501.x.]

Henson, W.R., Medina, R.L., Mayers, C.J., Niswonger, R.G., and Regan, R.S., 2013, CRT—Cascade routing tool to define and visualize flow paths for grid-based watershed models: U.S. Geological Survey Techniques and Methods, book 6, chap. D2, 28 p., https://doi.org/10.3133/tm6D2.

Huntington, J.L., and Niswonger, R.G., 2012, Role of surface-water and groundwater interactions on projected summertime streamflow in snow dominated regions—An integrated modeling approach: SW AND GW INTERACTIONS ON STREAMFLOW: Water Resources Research, v. 48, no. 11, 20 p., https://doi.org/10.1029/2012WR012319.

Hsieh, P.A., and Freckleton, J.R., 1993, Documentation of a computer program to simulate horizontal flow barriers using the U.S. Geological Survey's modular three-dimensional finite-difference groundwater flow model: U.S. Geological Survey Open-File Report 92–477, 32 p., https://doi.org/10.3133/ofr92477.

Kennedy, M.C., and O'Hagan, A., 2001, Bayesian calibration of computer models: Journal of the Royal Statistical Society. Series B, Statistical Methodology, v. 63, no. 3, p. 425–464. [Available at https://doi.org/10.1111/1467-9868.00294.]

Konikow, L.F., Hornberger, G.Z., Halford, K.J., and Hanson, R.T., 2009, Revised multi-node well (MNW2) package for MODFLOW ground-water flow model: U.S. Geological Survey Techniques and Methods, book 6, chap. A30, 67 p., https://doi.org/10.3133/tm6A30.

LANDFIRE, 2001, Existing vegetation type layer, LANDFIRE 1.0.5: U.S. Department of the Interior, U.S. Geological Survey, accessed March 27, 2017, at https://landfire.cr.usgs.gov/viewer/.

LANDFIRE, 2014, Existing vegetation type layer, LANDFIRE 1.4.0: U.S. Department of the Interior, U.S. Geological Survey, accessed March 27, 2017, at https://landfire.cr.usgs.gov/viewer/.

Markstrom, S.L., Niswonger, R.G., Regan, R.S., Prudic, D.E., and Barlow, P.M., 2008, GSFLOW—Coupled ground-water and surface-water flow model based on the integration of the precipitation-runoff modeling system (PRMS) and the modular ground-water flow model (MODFLOW-2005): U.S. Geological Survey Techniques and Methods, book 6, chap. D1, 240 p., https://doi.org/10.3133/tm6D1.

Markstrom, S.L., Regan, R.S., Hay, L.E., Viger, R.J., Webb, R.M.T., Payn, R.A., and LaFontaine, J.H., 2015, PRMS-IV, the precipitation-runoff modeling system, version 4: U.S. Geological Survey Techniques and Methods, book 6, chap. B7, 158 p., https://doi.org/10.3133/tm6B7.

Mitchell, W.B., Guptill, S.C., Anderson, K.E., Fegeas, R.G., and Hallam, C.A., 1977, GIRAS—A geographic information retrieval and analysis system for handling land use and land cover data: U.S. Geological Survey Professional Paper 1059, 16 p. [Available at https://doi.org/10.3133/pp1059.]

Moreland, J.A., 1970, Artificial recharge, Yucaipa, California: U.S. Geological Survey Open-File Report 70–232, 44 p., https://doi.org/10.3133/ofr70232.

Niswonger, R.G., Panday, S., and Ibaraki, M., 2011, MODFLOW-NWT, A Newton formulation for MODFLOW-2005: U.S. Geological Survey Techniques and Methods, book 6, chap. A37, 44 p., https://doi.org/10.3133/tm6A37.

Niswonger, R.G., and Prudic, D.E., 2005, Documentation of the Streamflow-Routing (SFR2) package to include unsaturated flow beneath streams-A modification to SFR1: U.S. Geological Survey Techniques and Methods, book 6, chap. A13, 48 p., https://doi.org/10.3133/tm6A13.

Niswonger, R.G., Prudic, D.E., and Regan, R.S., 2006, Documentation of the unsaturated-zone flow (UZF1) package for modeling unsaturated flow between the land surface and the water table with MODFLOW-2005: U.S. Geological Survey Techniques and Methods, book 6, chap. A19, 74 p., https://doi.org/10.3133/tm6A19.

Phillips, S.P., and Belitz, K., 1991, Calibration of a texture-based model of a ground-water flow system, western San Joaquin Valley, California: Ground Water, v. 29, no. 5, p. 702–715. [Available at https://doi.org/10.1111/j.1745-6584.1991.tb00562.x.]

PRISM Climate Group, 2013, 30-year normals: PRISM Climate Group database, Oregon State University, accessed September 11, 2013, http://prism.oregonstate.edu.

Regan, R.S., and LaFontaine, J.H., 2017, Documentation of the dynamic parameter, water-use, stream and lake flow routing, and two summary output modules and updates to surface-depression storage simulation and initial conditions specification options with the Precipitation-Runoff Modeling System (PRMS): U.S. Geological Survey Techniques and Methods, book 6, chap. B8, 60 p., https://doi.org/10.3133/tm6B8.

Rewis, D.L., Christensen, A.H., Matti, J.C., Hevesi, J.A., Nishikawa, T., and Martin, P.M., 2006, Geology, ground-water hydrology, geochemistry, and ground-water simulation of the Beaumont and Banning storage units, San Gorgonio Pass area, Riverside County, California: U.S. Geological Survey Scientific Investigations Report 2006–5026, 173 p. [Available at https://doi.org/10.3133/sir20065026.]

Russo, D., and Bouton, M., 1992, Statistical analysis of spatial variability in unsaturated flow parameters: Water Resources Research, v. 28, no. 7, p. 1911–1925. [Available at https://doi.org/10.1029/92WR00669.]

Thomas Harder and Co., 2015, 2013 reevaluation of the Beaumont Basin safe yield: Prepared for the Beaumont Basin Watermaster, dated April 3, 2015, accessed June 21, 2021, at http://documents.yvwd.dst.ca.us/bbwm/documents/reevaluationbeaumont2013.pdf.

U.S. Department of Agriculture, 2016, Soil survey geographic (SSURGO) database: U.S. Department of Agriculture, Natural Resources Conservation Service, accessed November 14, 2016, at https://websoilsurvey.sc.egov.usda.gov/App/HomePage.htm.

U.S. Geological Survey, 2016, National hydrography dataset (ver. USGS national hydrography dataset best resolution (NHD) for hydrologic units (HU) 8 – 18070202 and 18070203 (published 20161105)), accessed November 11, 2016, at https://www.usgs.gov/core-science-systems/ngp/national-hydrography/access-national-hydrography-products.

U.S. Geological Survey, 2018, USGS water data for the Nation: U.S. Geological Survey National Water Information System database, accessed October 16, 2018, at https://doi.org/10.5066/F7P55KJN.

Vogelmann, J.E., Howard, S.M., Yang, L., Larson, C.R., Wylie, B.K., and Van Driel, J.N., 2001, Completion of the 1990's national land cover data set for the conterminous United States: Photogrammetric Engineering and Remote Sensing, v. 67, p. 650–662.

Western Regional Climate Center, 2011, Western Regional Climate Center: accessed April 5, 2019, at http://www.wrcc.dri.edu/.

Welter, D.E., White, J.T., Hunt, R.J., and Doherty, J.E., 2015, Approaches in highly parameterized inversion—PEST++ version 3, a parameter estimation and uncertainty analysis software suite optimized for large environmental models: U.S. Geological Survey Techniques and Methods, book 7, chap. C12, 54 p., https://doi.org/10.3133/tm7C12.

Xian, G., Homer, C., Dewitz, J., Fry, J., Hossain, N., and Wickham, J., 2011, The change of impervious surface area between 2001 and 2006 in the conterminous United States: Photogrammetric Engineering and Remote Sensing, v. 77, no. 8, p. 758–762.

Appendix B1. Calibration Using Ensemble Smoother

This appendix documents the terminology, theoretical background, and the numerical implementation of the Ensemble Smoother, which was used in the calibration of the Yucaipa Integrated Hydrologic Model (YIHM). More details about data assimilation methods (including the ensemble smoother) can be found in Evensen (1994).

Theoretical Background

A generic model G uses input parameters K to produce a prediction of states (model response) at the next time step,

$$H = G(K) \tag{B1.1}$$

where

H is an element of $R^{n_h \times 1}$,

K is an element of $R^{n_k \times 1}$,

n_h is the number of values in the model output vector, and

n_k is the number of input parameters.

The objective of calibration using the ensemble smoother is to compute the probability distribution of input parameters given a set of field measurements, that is to say, $p(K \mid H^o)$. The vector $H_o \in R^{n_m \times 1}$ represents all field measurements at all times. Conditioning model input parameters on measurements is achieved using Bayes' law:

$$P(K|H_o) = p(H_o|K)p(K)/p(H_o) \tag{B1.2}$$

where

$p(H_o|K)$ is the likelihood distribution function, which is a function of the differences between measurements and model predictions when parameter is equal to K;

$p(K)$ is the prior distribution of input parameters, and

$p(H_o)$ is a normalization term.

When the model G is linear and the model input parameters can be described using a normal distribution, the distribution $p(K|H_o)$ is also normal with mean and covariance respectively computed using the equations below:

$$\widehat{K} = K_f + \mathbf{C}_{kh}(\mathbf{C}_{hh} + \mathbf{R})^{-1}(H_o - H_f) \tag{B1.3}$$

$$\widehat{\mathbf{C}_{kk}} = \left(\mathbf{I} - \mathbf{C}_{kh}(\mathbf{C}_{hh} + \mathbf{R})^{-1}\right)\mathbf{C}_{kk} \tag{B1.4}$$

where

$\widehat{K}$ is the posterior mean of parameters given measurements (the ensemble mean of K with probability distribution $p(K|H_o)$),

K_f is the prior mean of parameters (the mean of K with probability distribution $p(K)$),

H_f is the prior mean of model simulated equivalents,

$\mathbf{C}_{kh}$ is the cross-covariance matrix of model output and model input parameters,

$\mathbf{C}_{hh}$ is the auto-covariance of model simulated equivalents,

$\mathbf{C}_{kk}$ is the prior covariance of parameters,

$\widehat{\mathbf{C}_{kk}}$ is the posterior covariance of parameters, and

$\mathbf{R}$ is the covariance matrix of measurement errors.

This formulation is widely known as Kalman Filter (Kalman, 1960). A direct use of this formulation is difficult because the condition of model linearity is restrictive and might not be valid for many models. Additionally, the covariance matrices $\mathbf{C}_{kh}$ and $\mathbf{C}_{hh}$ are computationally difficult. Evensen (1994) suggested using ensembles to approximate all probability distributions; that is, the input parameters probability function $p(K)$ is approximated using an ensemble of realizations that represent the prior knowledge about the input parameters. In this case, the prior ensemble (also called forecast matrix in data assimilation field) can be assembled using the equation below:

$$\mathbf{K}_f = [K_1, \ldots, K_N] \tag{B1.5}$$

where

N is the number of realizations in the ensemble generated from a prior normal distribution $\sim N(K_f, \mathbf{C}_{kk})$.

This prior distribution represents prior information about the unknown parameters. Each realization in $\mathbf{K}_f$ is simulated in the model to produce an ensemble of simulated equivalents (simulated reality),

$$\mathbf{H}_f = [H_1, \ldots, H_N] \tag{B1.6}$$

To use equations (B1.3) and (B1.4), the covariance matrix $\mathbf{C}_{hh}$ is approximated from the ensemble (B1.6) using the equation below:

$$\mathbf{C}_{hh} = (\mathbf{H_f} - \widehat{\mathbf{H}_\mathbf{f}})(\mathbf{H_f} - \widehat{H_f})^T/(N-1) \tag{B1.7}$$

where

$\widehat{\mathbf{H}_\mathbf{f}}$ is the ensemble mean matrix where each row has the same mean value which is the mean of the corresponding row in $\mathbf{H}_f$.

In a similar manner the matrix $\mathbf{C}_{kh}$ is computed using the equation below:

$$\mathbf{C}_{kh} = (\mathbf{K_f} - \widehat{\mathbf{K_f}})(\mathbf{H_f} - \widehat{H_f})^T/(N-1) \quad \text{(B1.8)}$$

Since the measurements themselves are prone to measuring errors, an ensemble of measurement error is generated from ~N(0, R) and added to the measurement vector:

$$\mathbf{D} = \mathbf{H_o} + \mathbf{E} \quad \text{(B1.9)}$$

where

$\mathbf{D}$ is the perturbed measurement matrix,
$\mathbf{H_o}$ is a matrix where all columns are identical and equal to measurements vector H_o, and
$\mathbf{E}$ is measuring error matrix.

In practice, it's common to assume that $\mathbf{R}$ is a diagonal matrix where diagonal values represent the variances of measurement errors. Another way to see these variances is to deal them as the inverse of the weight for the measurements.

The calibrated ensemble of model input parameters $\mathbf{K}_a$ (the update ensemble) can be computed using the equation below:

$$\mathbf{K}_a = \mathbf{K_f} + \mathbf{C}_{kh}(\mathbf{C}_{hh} + \mathbf{R})^{-1}(\mathbf{D} - \mathbf{H_f}) \quad \text{(B1.10)}$$

The updated ensemble can then be used to compute the ensemble mean, which is the best unbiased estimate of the unknown model parameters and the ensemble standard deviation, which provides a measure of parameter uncertainty.

Equation B1.4 shows that the posterior standard deviation of parameters must be less than or equal to prior sensitivity. The difference between posterior and prior standard deviations can be seen as (1) a measure of knowledge gained about parameters after assimilating measurements (for example, larger difference indicates that more knowledge is gained) and (2) a measure of parameter sensitivity (for example, smaller difference indicates the smaller sensitivity of model's simulated equivalent output to parameters).

Numerical Implementation

Calibration using the Ensemble Smoother is achieved following two steps: model forecast and parameter update. In model forecast, an ensemble of prior realizations for input parameters is generated, and each realization is simulated in the model to produce an ensemble of model responses. Input parameters can be scalar values or spatially variable parameters such as hydraulic conductivity, specific yield, and specific storage. For spatially variable parameters, the sequential Gaussian simulator in the Geostatistical Software library (GSLIB; Deutsch and Journel, 1998) is used to generate 500 realizations for correlated fields conditioned on available texture data. Scalar variables were generated from normal distributions with means equal to the best prior value, and standard deviations represent the prior variability ranges. Wider ranges of variability were used to represent larger possibilities for parameter values. The ensembles of the spatially variable parameters and of scalar parameters are augmented in a single forecast matrix (eq. B1.5), which is simulated by running the model 500 times to produce 500 sets of model outputs (eq. B1.6).

The second step is the parameters update in which equations B1.7 through B1.10 are evaluated. A Python script (Alzraiee and others, 2022) was developed to implement input parameters update. The developed script solves the data assimilation equations using two modes: Ensemble Kalman Filter mode and Squared Root Kalman Filter. The inputs to the script consist of an ensemble of model input parameters that need to be calibrated, an ensemble of simulated equivalents, actual measurements that are compared to simulated equivalents, and measurement errors associated with each measurement.

References Cited

Alzraiee, A.H., Cromwell, G., and Engott, J.A., 2022, GSFLOW model to evaluate the effect of groundwater pumpage and climate stresses on the integrated hydrologic system of the Yucaipa subbasin, Yucaipa Valley watershed, San Bernardino and Riverside Counties, California: U.S. Geological Survey data release, https://doi.org/10.5066/P9K540DV.

Deutsch, C.V., and Journel, A.G., 1998, GSLIB: Geostatistical Software Library and User's Guide, 2nd Edition. Oxford University Press, Oxford, 369 p.

Evensen, G., 1994, Sequential data assimilation with a nonlinear quasi-geostrophic model using Monte Carlo methods to forecast error statistics: Journal of Geophysical Research, v. 99, no. C5, p. 10143–10162. [Available at https://doi.org/10.1029/94JC00572.]

Kalman, R.E., 1960, A new approach to linear filtering and prediction problems: Journal of Basic Engineering, v. 82, no. 1, p. 35–45. [Available at https://doi.org/10.1115/1.3662552.]

Appendix B2. Evaluation of Streamflow Data Quality and Calibration Goodness-of-Fit

Calibration of integrated hydrological models involves adjusting model parameters controlling streamflow and evaluation of the goodness-of-fit between simulated streamflow and measured streamflow. The questionable suitability of the available streamflow measurements within the Yucaipa Integrated Hydrologic Model (YIHM) domain complicates efforts to fully calibrate the model to match the measured streamflow data. This appendix provides a detailed description of the available streamflow measurements, evaluates the streamflow measurements suitability for calibration, and compares simulated and measured streamflow.

Streamflow Measurements

Streamflow has been historically monitored by the San Bernardino County Flood Control District (SBCFCD) and the U.S. Geological Survey (USGS) at seven streamgages (chapter B, fig. B5). Five of the streamgages (S3601A, 2915, S3601C, 2800, and S3608A) are operated by the SBCFCD and are designed to measure high discharge rates to assist in flood control, with less emphasis placed on measuring lower discharge rates (see the "Surface-Water Hydrology" section in chapter A). The other two streamgages (11057000 and 11057500) are operated by the USGS and are designed to measure both high and low discharge rates. Despite the high quality of streamflow data at the two USGS streamgages, their suitability for calibrating the YIHM is affected by multiple factors that are discussed in more detail in the following section.

Factors Affecting the Quality and Suitability of Measured Streamflow Data

The measured streamflows at the seven streamgages were affected by multiple issues that could reduce data quality and (or) reduce the suitability of streamgages for use in model calibration. Issues affecting data quality included the presence of repeated values in the record (for example, streamgage 2800) and the large gaps in some of the records (2915, S3601C, S3608A, 11057000, and 11057500). Factors that affected the suitability of the data for model calibration were flood-control structures, recharge enhancement (or retention) pools, and urban runoff generated from regions outside the YIHM domain. Flood-control structures (for example, the Wilson Creek and Oak Glen Creek spreading basins fig. B2.1, panels A and D) alter natural flow in the streams and largely affect the measured high and low streamflow rates at the streamgages. A chain of cascading instream retention pools near USGS streamgage 11057000 (fig. B2.1, panel B) alters the natural streamflow by restricting streamflow and enhancing infiltration. These structures alter the streamflow rate and timing in a way that could not be simulated in groundwater and surface-water FLOW model (GSFLOW) because the actual streamflow rate is controlled by hydraulic properties of these structures that are not simulated in GSFLOW (for example, storage capacity of the structure, elevation of the overflow outlet, weir outlet elevation, and storage capacity of permeant pool).

Urban runoff that was generated from areas outside the model domain and flowed into the stream network also affected the suitability of data from the USGS streamgages for use in calibrating the YIHM. Urban runoff from the City of Redlands flows into San Timoteo Creek near USGS stations 11057000 and 11057500 (fig. B2.1*C*). The magnitude and timing of the urban inflow were unknown and may have substantially affected the observed streamflow at these streamgages. The combined effects of flood-control structures, recharge enhancement structures, and urban runoff generated from outside the YIHM domain made the discrepancies between simulated and observed streamflow unavoidable. Therefore, in YIHM calibration using Parameter Estimation software (PEST), low weights were assigned to the measured streamflow data. The following subsection discusses the goodness-of-fit between simulated and measured streamflow.

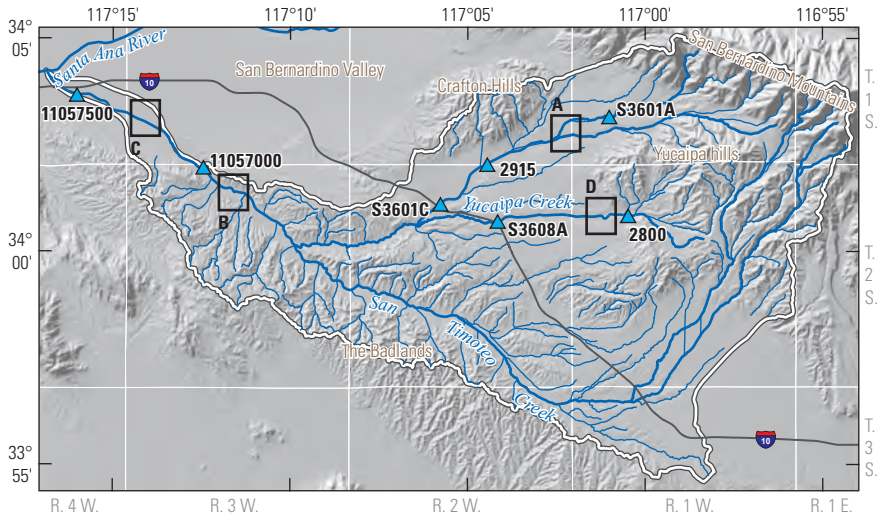

EXPLANATION

Yucaipa valley watershed

2915 Streamgage and identifier

0 1 2 3 4 MILES

0 1 2 3 4 KILOMETERS

Base modified from U.S. Geological Survey (USGS) National Hydrography Dataset (NHD, 2016) and other USGS and Federal digital data, various scales; Universal Transverse Mercator projection, zone 11; North American Datum of 1983

A

Base imagery from Google, Maxar Technologies 2021 (April, 2021)

B

Base imagery from Google, Maxar Technologies 2021 (April, 2021)

C

Base imagery from Google, Maxar Technologies 2021 (April, 2021)

D

Base imagery from Google, Maxar Technologies 2021 (April, 2021)

Figure B2.1. Locations of streamgages: *A*, Google Earth image for flood-control structures and the Wilson Creek and Oak Glen Creek spreading basins on Wilson Creek and Oak Glen Creek, respectively, *B*, instream retention pools, *C*, image showing urban runoff flows into San Timoteo Creek, and *D*, Wildwood Creek detention basins on Yucaipa Creek (imagery date April 2021; Google, Maxar Technologies 2021); Yucaipa groundwater subbasin, Yucaipa Valley watershed, San Bernardino and Riverside Counties, California.

Calibration Results at Streamgages

To reduce the impact of uncertain streamflow measurements on model calibration, lower weights were assigned to streamflow measurements. Thus, the goals of streamflow calibration were to achieve a rough match between simulated and measured streamflow and to avoid overfitting the possibly uncertain streamflow measurements. Comparison between simulated and measured monthly and annual mean streamflow at five streamgages (S3601A, 2915, S3601C, 11057000, and 11057500) are shown in fig. B2.2 and B2.3, respectively. Data quality at stations S3608A and 2800 is likely unreliable because these stations have unrealistically repeated values, and thus were not presented herein. Among the five gages presented herein, the USGS station 11057500, at the outlet of watershed, has a reasonable record that covers the period 1970–2014; however, the measured streamflow is largely impacted by factors that are not simulated by GSFLOW, such as flow control structures, recharge enhancement structures, and urban runoff from outside the study area. These factors, which affect measured streamflow at the gage, explain the discrepancy between simulated and observed streamflow. Measured streamflow during dry periods that have no base flow and evidence from aerial images (fig. B2.1*C*) show the impact of unquantified urban runoff coming from the City of Redlands.

Records of streamflow at streamgages S3601A, 2915, S3601C, and 11057000 vary in quality, with some station records containing substantial data gaps. Figure B2.2 shows a relatively reasonable match between measured and simulated streamflow. Measured monthly means at S3601A and S3601C, which are designed to measure high flows, show that the timing and rates are roughly simulated by the YIHM during periods of high streamflow. At USGS station 11057500, which has a limited record (1973–79), the simulated monthly mean reasonably matches the measured monthly mean streamflow. Measuring streamflow before and after the locations of flood-control structures and the outlets of urban runoff generated from areas outside the study domain might help quantify their impact on streamflow rates, peaks, and arrival time.

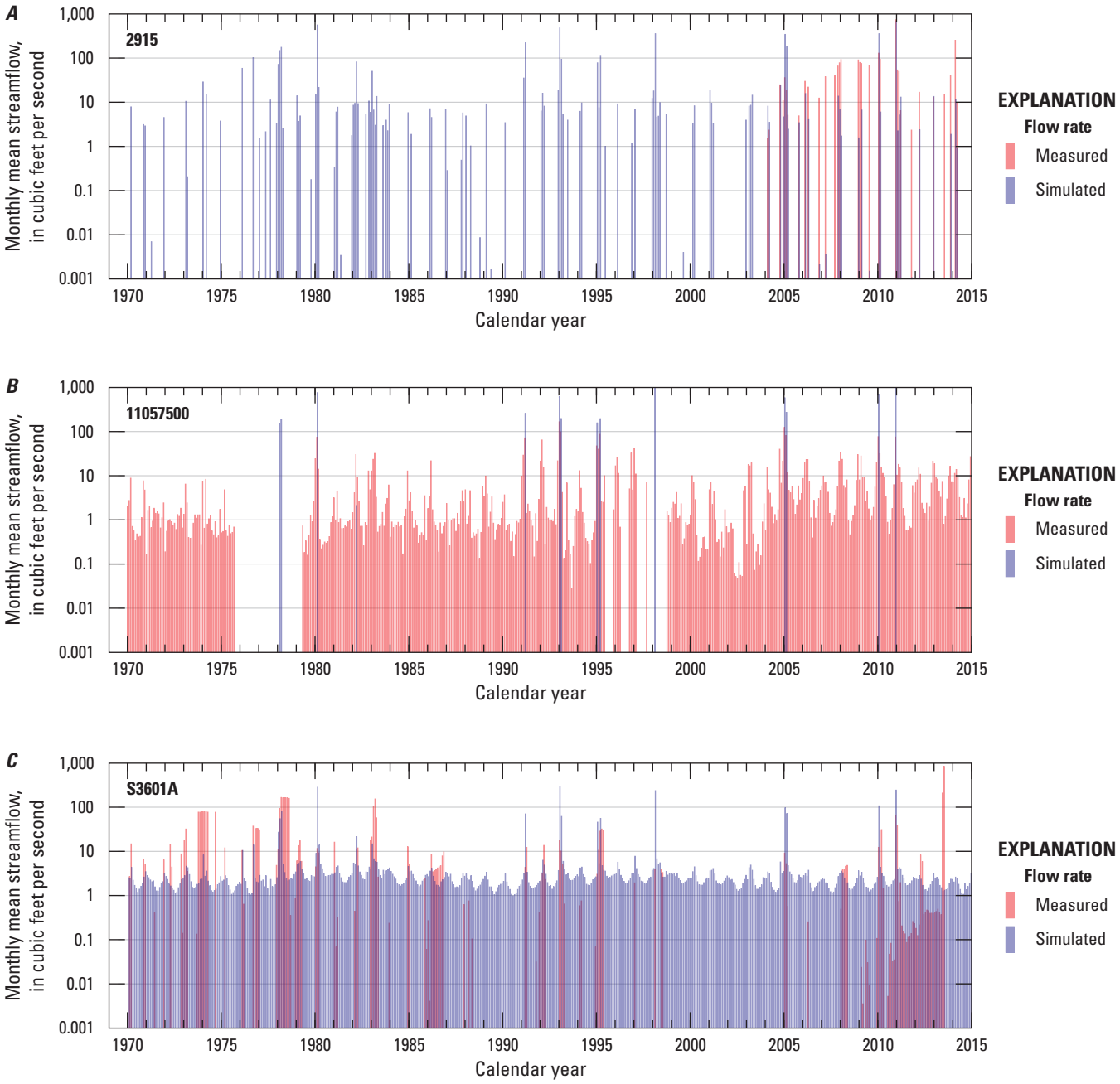

Figure B2.2. Simulated and measured monthly streamflows for years 1970–2014 using the Yucaipa Integrated Hydrologic Model (YIHM) at *A*, San Bernardino County Flood Control District (SBCFCD) streamgage 2915; *B*, U.S. Geological Survey (USGS) streamgage 11055000 (USGS National Water Information System [NWIS], U.S. Geological Survey, 2018); *C*, SBCFCD streamgage S3601A; *D*, USGS streamgage 11057000 (NWIS; U.S. Geological Survey, 2018); and *E*, SBCFCD streamgage S3601C; Yucaipa groundwater subbasin, Yucaipa Valley watershed, San Bernardino and Riverside Counties, California.

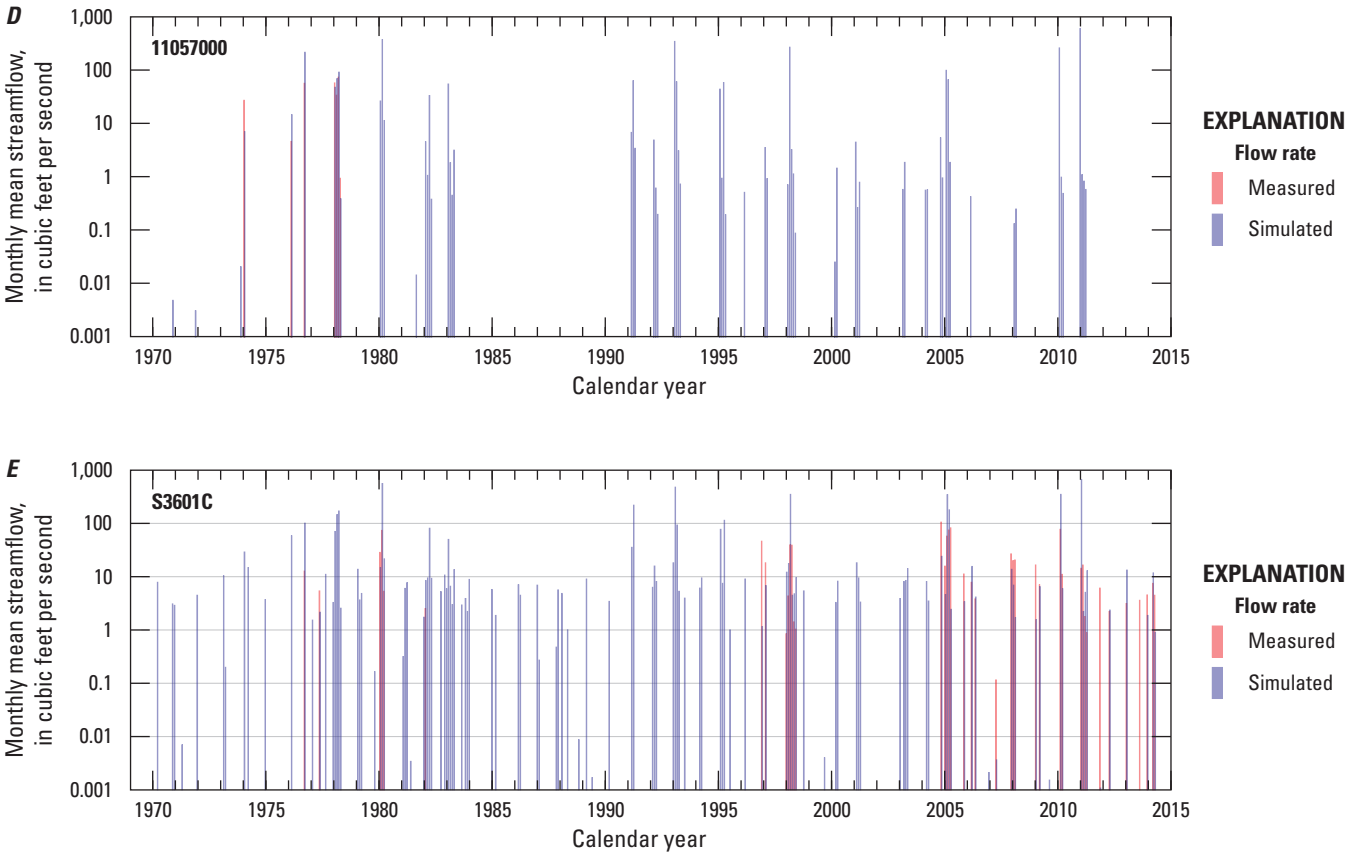

Figure B2.2.—Continued

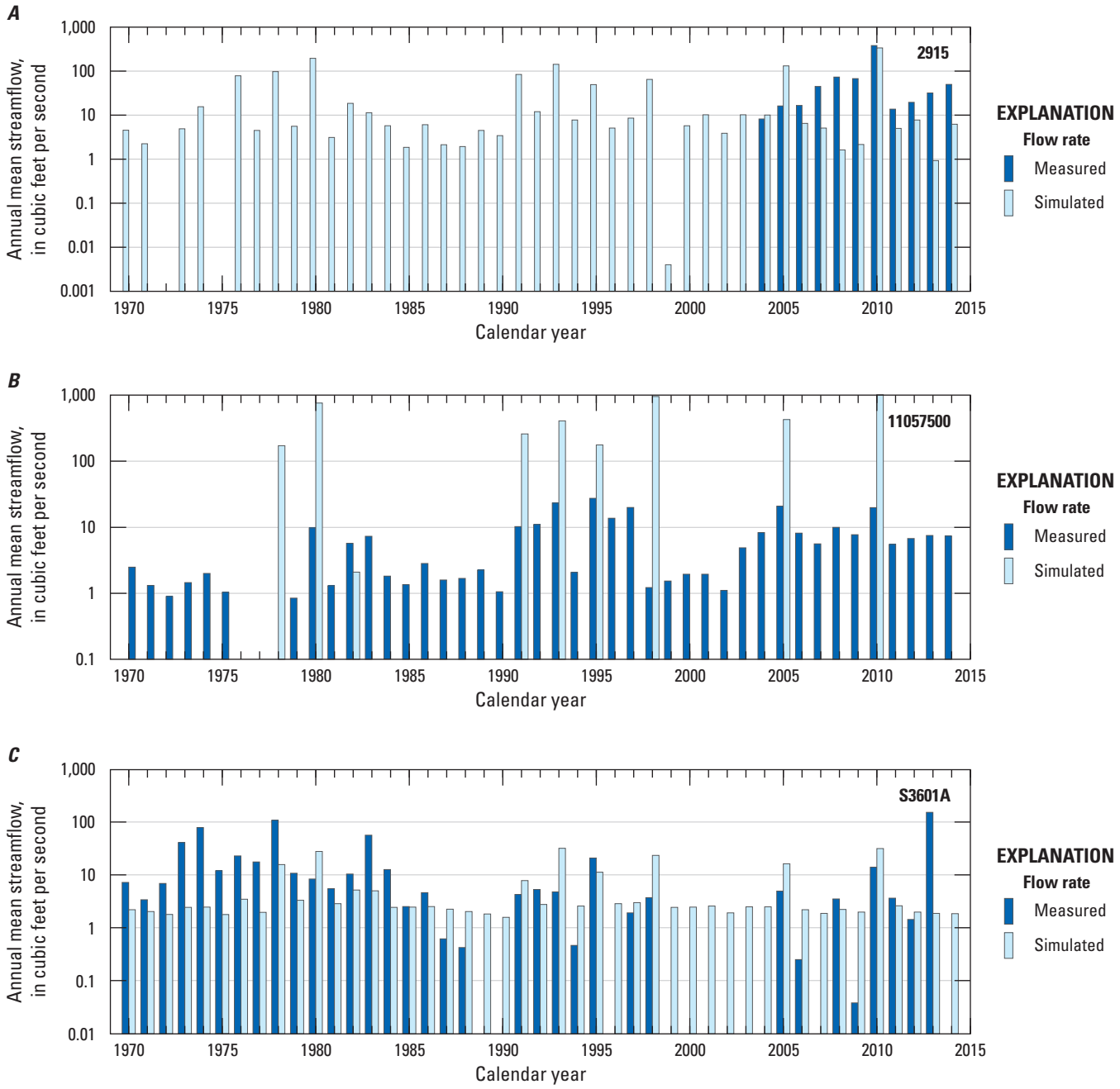

Figure B2.3. Simulated and measured annual streamflow for years 1970–2014 using the Yucaipa Integrated Hydrologic Model (YIHM) at *A*, San Bernardino County Flood Control District (SBCFCD) streamgage 2915; *B*, U.S. Geological Survey (USGS) streamgage 11055000 (USGS National Water Information System (NWIS); U.S. Geological Survey, 2018); *C*, SBCFCD streamgage S3601A; *D*, USGS streamgage 11057000 (NWIS; U.S. Geological Survey, 2018); and *E*, SBCFCD streamgage S3601C. Yucaipa groundwater subbasin, Yucaipa Valley watershed, San Bernardino and Riverside Counties, California.

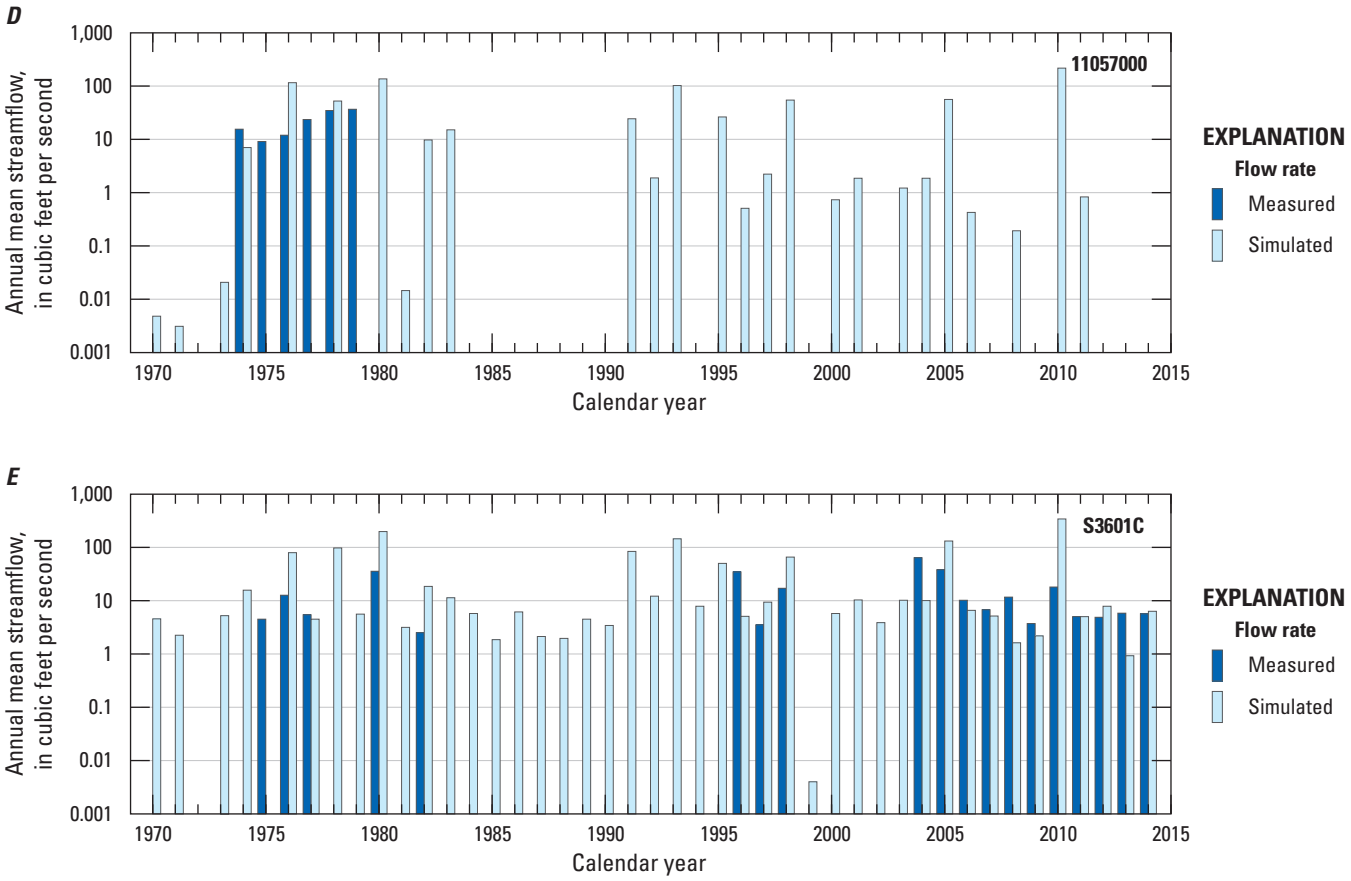

Figure B2.3.—Continued

References Cited

U.S. Geological Survey, 2018, USGS water data for the Nation: U.S. Geological Survey national water information system database, accessed October 16, 2018, at https://doi.org/10.5066/F7P55KJN.

For more information concerning the research in this report, contact the

Director, California Water Science Center
U.S. Geological Survey
6000 J Street, Placer Hall
Sacramento, California 95819
https://ca.water.usgs.gov

Publishing support provided by the

U.S. Geological Survey Science Publishing Network, Sacramento Publishing Service Center

ISSN 2328-0328 (online)
https://doi.org/10.3133/sir20215118BB